# Optical Measurement of Random-Sized Particles In Wing Tip Wake Vortices

by

Damon J. Phillips

B.S., Morehouse College (1990)

SUBMITTED TO THE DEPARTMENT OF AERONAUTICS AND ASTRONAUTICS IN PARTIAL FULFILLMENT OF THE REQUIREMENTS FOR THE DEGREE OF

MASTER OF SCIENCE

at the

MASSACHUSETTS INSTITUTE OF TECHNOLOGY

June 1992



Signature of Author _____
Department of Aeronautics and Astronautics
May 15, 1992

Certified by _____
Professor Shaoul Ezekiel
Thesis Supervisor

Certified by _____
Dr. David Klick
Technical Supervisor
Staff, MIT Lincoln Laboratory

Accepted by _____
Professor Harold Y. Wachman
Chairman, Department Graduate Committee

# Optical Measurement of Random-Sized Particles In Wing Tip Wake Vortices

by

Damon J. Phillips

## Abstract

An evaluation was undertaken to determine how well a random size distribution of water droplets followed the flow of a wing-tip vortex when compared to control particles that are considered to be more well behaved. The control particles are called eccospheres, small glass spheres (from 5 μm to 125 μm) of about one-third the density of water. The investigation measures the velocity profile of the vortex using a modification of a two-dimensional flow visualization technique called Laser Streak Velocimetry (LSV), with which the velocity of light scattering particles entrained in a flow can be determined.

The LSV technique exposes particles that are entrained in a flow to a sheet of light for only a short period of time using a mechanical chopper. The distance each particle travels during this period is imaged with an ISIT camera and recorded onto a video cassette recorder. The data extraction is accomplished through image processing of the video images that contain the velocity data.

First the eccospheres and then the water droplets were dispersed into a small-scale wind tunnel and measured with the LSV system. Although the control particles followed the flow well, the water droplets displayed variance from the actual flow. Analysis of individual fields of the video tape revealed that the velocity profile of particles traveling in a unidirectional flow was not uniform.

Using a rectangular plate with an aspect ratio of 3, to simulate a wing, vortices were generated in the wind tunnel, and entrained control particles and water droplets were measured in the vortex. It was found that the water droplets did not respond as well to the vortex flow as did the eccospheres, which suggested that the random size distribution of the water droplets influenced their response to the vortex.

# Acknowledgements

One always feels a great deal of satisfaction when accomplishing a goal that involves hard work and results in growth. I must take this time to thank some of those for their invaluable advice, assistance, and support.

First, I would like to extend my deepest thanks to Professor Shaoul Ezekiel, my advisor, for teaching me how to approach, think through, and solve problems. His wisdom and perspective toward his field has been a positive effect on me for my entire matriculation at MIT. I also wish to thank Dr. David Klick, my technical supervisor, who volunteered much of his time and concern, for pointing out the way at the crucial points without pulling me through them. I extend my gratitude to Dr. William Keicher, for allowing me the opportunity to work on my research under his leadership.

There are many others who provided invaluable technical advise and assistance during this research. Special thanks must be made to all of those in Group 52, especially Bruce Duquette, Julius Sobolewski, Charlie Summers, and Joe Theriault. I extend my appreciation to those who loaned or gave me equipment or material for my experiment: Dr. Kenneth Shultz, Dave Hovey, Lorraine Prior, Larry Sweezy, and Dr. T. Y. Fan. To those who took time out to impart some of their wisdom, thank you: Prof. Sheila Widnall, Dr. Frederick Knight, Ken Lutchen, Lt. Col. Koenig, and Dr. Jim Hallock.

A big thanks to those who gave their inspiration, friendship, love and support. Mom, Dad, Dyelan, Ida Coleman, Jonathan Allen, Mary Fouser, Desiree Gosby, Kenny Grimes, Steve Isabelle, LaCreis Kidd, Renee Lesperance, Robert Lewis, Cathryn Shaw, Sheila Sullivan, and Margo Tyler.

Finally to those who motivated me to this stage: Dr. Robert Dixon, Dr. Jocelyn Jackson, Dr. Carlise Moore, and the others back at the House. To my fifth grade math teacher and to Gen. T. H., who through their words of discouragement and disbelief, provided me with an immense source of motivation.

The greatest thanks is to Him who has given so much, yet still continues to give. May God bless you all.

# Table of Contents

## List of Figures and Photographs

# Chapter 1: Introduction

In the aeronautics community, it is well known that aircraft generate turbulence in the form of wing-tip wake vortices. This occurrence is a byproduct of lift which forms spiralling, horizontal columns of turbulent air spilling off the end of an aircraft's wings (See Figure 1.1). In some cases, as the vortices from one aircraft encounter the wings of a following aircraft, the circular motion of air creates a sufficient roll moment to disturb the trailing aircraft. The problem is particularly hazardous when considering one aircraft following another on the same flight path to a runway. In this situation, the affected aircraft's altitude and orientation may be such that a roll moment applied to this aircraft is sufficient to induce loss of control. This phenomenon has been a concern for both the military and commercial aircraft industry for some time. Aircraft such as the small fighter and the executive jet are particularly vulnerable to this effect, especially those that operate in airports with a wide distribution of aircraft sizes which will include larger aircraft that generate powerful vortices. [1] Vortex detection and evaluation would be most useful during poor weather, because under these conditions all aircraft follow their instruments along the same flight path [2].

There have been many attempts to detect wing-tip vortices in the airport environment, however, many of these fall short of adequate detection and measurement. Techniques that utilize hot-wire anemometers and flying probes in the wake vortices of a leading aircraft, provide incomplete data that can be collected and analyzed only for predictive purposes. Instruments such as acoustic sensors suffer from sensitivity to normal ambient noise. The major noise sources which limit the performance of acoustic sensors in the airport environment are aircraft operations and meteorological effects such as rain hitting the antenna. Thus acoustic sensors have limited value, especially in poor weather conditions, when (as was mentioned) measurement is most useful. [2]. These and other attempts have had only partial success,

**Figure 1.1**

# STRUCTURE OF AIRCRAFT WAKE

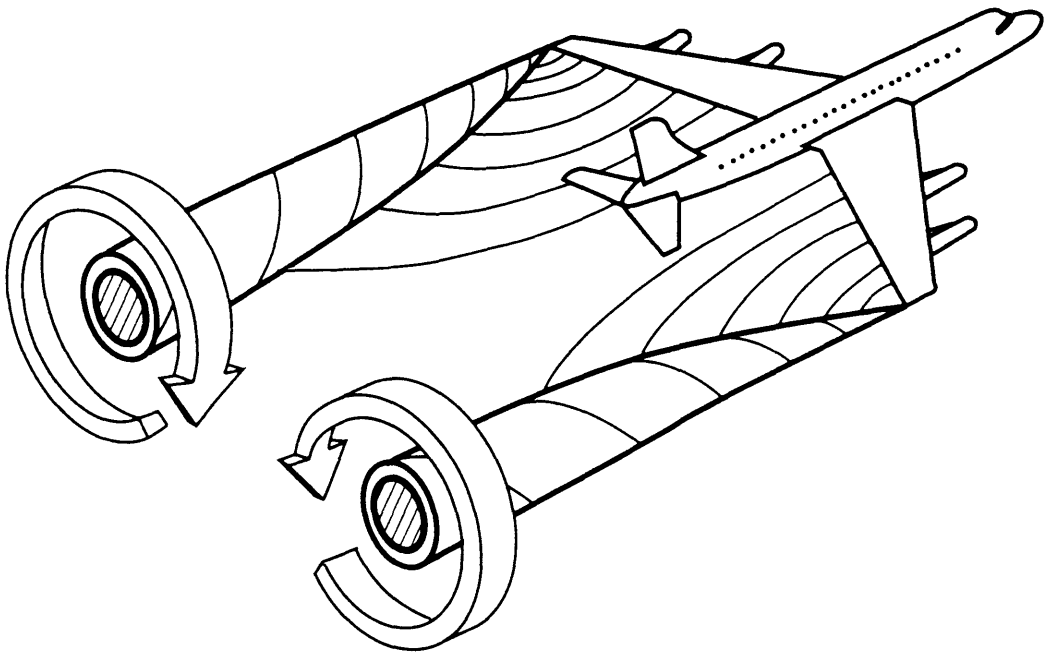

143448-1

motivating the search for other techniques for vortex measurement.

Lidar (Laser Radar) detection and measurement systems have been applied to the field of wake vortices [3]. These systems require scattered radiation from small particles entrained in the moving air to understand the motion of the air. Typically these particles are very small (on the order of microns). However, the overriding factor in determining whether a particle is properly entrained in the flow is not its size, but rather its buoyancy. In other words, the closer an object's effective density is to that of air, the better that object will follow the movement of air. Even helium balloons have been used to observe the effect of wake vortices.

There have been many lidar experiments designed to study wake vortices by placing particles (also called seeds) in the vortex in order to provide scattered light to the detector. By measuring the velocities of these particles within a vortex, it is possible to come to an understanding of the structure of the vortex, and construct its velocity profile. Realistically, scattering sources present in the airport environment vary in type and dimension due to varied weather conditions . The measured particle velocity may depend on many factors, such as vortex decay, particle size, particle evaporation, clumping, and collisions [4]. Although measurements of particles within vortices have been numerous, measurements of non-ideal particles (such as randomly-sized water droplets) are more uncommon [5].

The purpose of this investigation is to determine how well rain follows the swirling air in a vortex. This determination is important and not as straight forward as using the typically well-behaved flow seeds. Usually the flow seeds (e.g. microballons or other small monodisperse spheres) are chosen to follow the flow as well as possible. These particles are excellent for understanding the details of vortex flow, and for evaluating how well the flow compares to analytical representations. However, a realistic wake vortex radar or lidar detection system does not have the luxury of controlled, monodisperse spheres to detect and

measure. In particular, when measuring the flow of a vortex in an environment with mist or rain, a set of naturally existing flow seeds are introduced that have a wide distribution of sizes.

Flow Visualization using a laser is a well known tool in the study of small-scale air flow. The laser provides light for particles entrained in a flow to scatter as they respond to air flow. In this investigation, particles entrained in a vortex flow will be probed using a laser-based flow visualization technique. This technique is referred to as Laser Streak Velocimetry [6] and allows one to extract velocity information from particles that are entrained in a flow. Using this method, there will be a series of measurements of a variable size distribution of water droplets. The primary objective of this investigation is to determine whether the droplets respond differently to a vortex flow when compared to the response of well-behaved particles, referred to in this investigation as the control particles. Necessary for the completion of the flow seed investigation is an evaluation of the Laser Streak Velocimetry system used to make the measurements, which comprises a secondary objective for this paper.

Before any measurements are made, a brief analytical understanding of wing-tip wake vortices must be established. Thus, the investigation embarks with a brief discussion of vortices as they apply to our interests. Close attention will be given to developing an acceptable understanding of the trajectories of particles entrained within a simplified two-dimensional vortex. Of special interest will be the tangential and radial motion of particles in a vortex. The calculations in the analytical study comprise a synthesis of earlier calculations made by many of the referenced authors who have contributed valuable insight to the study of wing-tip wake vortices. When the theoretical background has been sufficiently established, the experimentation process will begin, which will test the predictions made in the calculations. The first set of experiments will determine the precision of the measurement process. These experiments will lead to the evaluation of the quality of the wind

tunnel air flow (whether it is stable enough to support vortices). Following the evaluation of the flow quality, the wing-tip vortex measurements will be made.

The data collected from the vortex measurements will be analyzed to reveal whether the randomly-sized raindrops yield a velocity profile that is similar to the profile of the control particles and respond consistently with the calculated predictions. Here there will also be an attempt to explain any discrepancies or errors. Finally, suggestions will be made as to what future directions can be taken.

# Chapter 2: Theory and Analytical Background

The objective of this chapter is to present a heuristic, single particle vortex model in order to qualitatively understand its response to being entrained in a vortex flow. The analytical discussions here will be compared to the experimental velocity measurements of particles entrained in a wing-tip vortex flow. Since the structure and stability of a wing-tip vortex relies heavily on how uniform and laminar the air that encounters a wing is, the model of the vortex will begin with an analysis of a particle entrained in a one-dimensional flow. This one-dimensional analysis will aid in the understanding of the trajectory of an entrained particle before it encounters the wing which generates the vortex.

After one-dimensional flow is discussed the single particle model will be developed, based largely upon the referenced work of earlier research. Since the primary concern is with qualitative results, estimations and assumptions will be made. The objective is to simplify the calculations without jeopardizing the integrity of the argument.

Once the basic vortex model is presented, the forces that primarily affect the trajectory of a particle in a vortex will be given. The forces that will be concentrated on are the radial forces, and the forces due to gravity and buoyancy. In order to understand the effect of these forces more clearly, they will be compared to the influence of the vortex which compels a particle to maintain circular motion, whereas the forces tend to disrupt that motion. The radial forces will be considered first, then the effects of gravity and particle buoyancy will be considered.

It is not necessary to make the vortex model more complex. The qualitative understanding is achieved from the analysis is sufficient. Furthermore, the solution that best describes the flow of particles in a vortex is non-trivial. It requires a statistically complex analysis, defining the environment of the vortex and the particle(s) as a stochastic process, to be solved by applying the mathematics of Brownian motion (Harrison, 1985). The solution

involves a well characterized particle or set of particles. In addition it is necessary to have detailed knowledge of the structure and strength of the vortex and the system that gives rise to it.

## Assumptions

The velocity in a wing-tip wake vortex is three-dimensional (See Figure 1.1). It is best to consider the three components as a cylindrical coordinate system where the downstream component is the axis of rotation and is unidirectional, passing axisymmetrically through the core of the vortex (See Figure 2.1). The tangential component revolves around this axis and relates to the circular motion of the vortex. The third component is the radial component, which moves outward or inward with respect to the downstream axis. Typically, motion in the downstream component is constant with respect to the other two components, thus any section can be understood as locally two-dimensional. Thus, when modeling the vortex, the representation will be in a plane, where the tangential component represents the rotation flow and the radial component represent any movement with respect to the center of rotation.

The vortex structure has two primary regions; there is the core of the vortex and the region outside of the core. Figure 2.2 shows the tangential velocity of a vortex. The vortex core is bounded by the radius at which the maximum tangential velocity exists. Within the core, the velocity is not understood as well analytically [8]. It is characterized by a viscous flow which has a velocity that, once simplified, increases linearly from zero to the maximum velocity at the core, as Figure 2.2 represents. However, since the region is little understood, it will only be represented by a linear increase in the model. Outside the core the magnitude of the tangential velocity almost exactly follows a 1/r function.

The fluid that makes up the vortex will be air. It will be assumed that the air flow is both inviscid and incompressible.

## Vortex Coordinate System

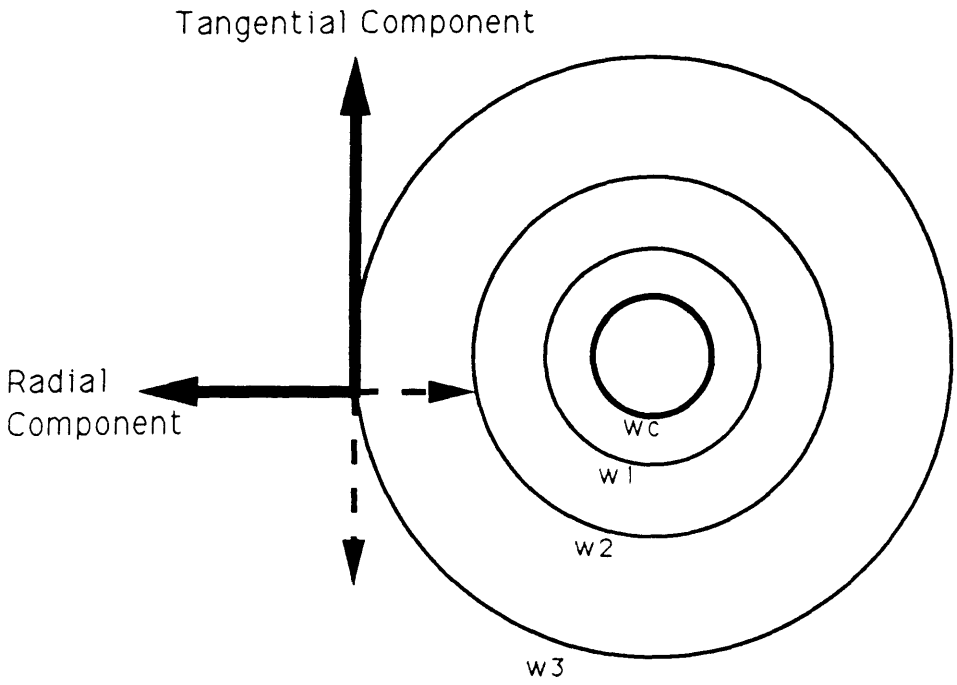


Downstream Component: Into (or out of) the Page

wc, w1, w2, and w3 are the tangential velocites at the corresponding radii, where wc is the velocity at the core and wc > w1 > w2 > w3

Figure 2.1

Relationship Between Vortex Tangential Velocity
And Vortex Radius

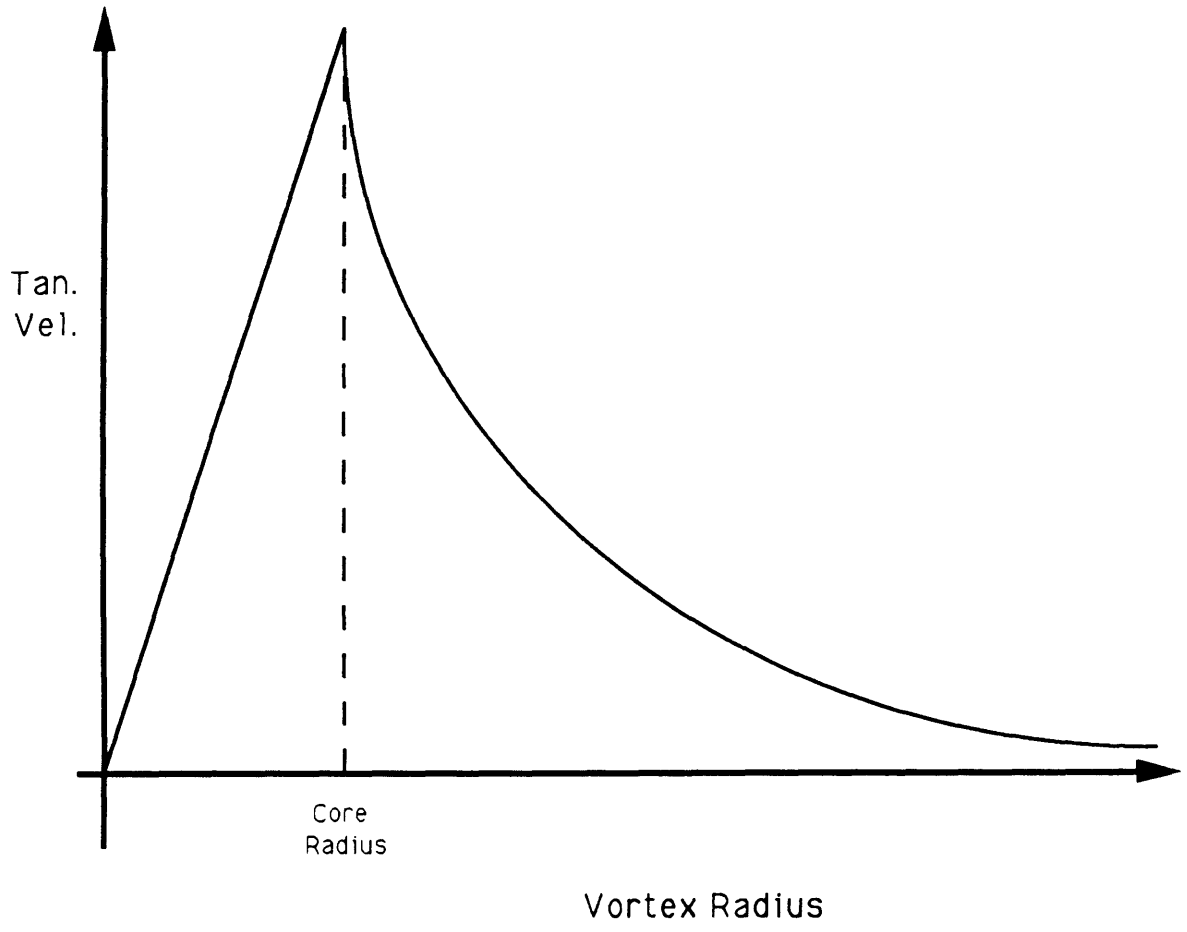


Figure 2.2

Also, the calculations will assume a steady, well-behaved flow. The physical properties of air are given below. They are selected based on 20° C and the standard pressure of 760mm Hg [the source is the CRC Handbook of Chemistry and Physics, 67th:

The density of air: $\rho_{air} = 1.204E\text{-}3\ (gm/cm^3) = \rho_f$,

The absolute viscosity of air: $\mu_{air} = 1.8E\text{-}4\ (gm/cm\ s) = \mu_f$,

The kinematic viscosity of air: $\nu_{air} = 0.1495\ (cm^2/s) = \nu_f$,

where the subscript f denotes "fluid".

All calculations will be based on the assumption that the particles under consideration are at an initial radial position r, where r is greater than the vortex core radius ($r_c$). There will be only one particle at a time in the vortex. Its location will be given at a specified radius with a radial velocity ($v_r$), a tangential velocity ($v_\theta$), and a downstream velocity ($v_d$). There are two particle types that will be compared. The first is a small, spherical water droplet, with the following physical properties:

The density of water: $\rho_{water} = 0.99823\ (gm/cm^3) = \rho_p$,

The absolute viscosity of water: $\mu_{water} = 1.002E\text{-}2\ (gm/cm\ s) = \mu_p$,

The kinematic viscosity of water: $\nu_{water} = 1.004E\text{-}2\ (cm^2/s) = \nu_p$,

where the subscript p denotes "particle". The second particle is referred to as a control particle. The control particle is to be used in the vortex measurements as a solid or hollow particle that theoretically responds to the flow more closely than does a droplet of water. The typical density of a control particle will be considered to be ~0.3.

## 2.1 Particle Entrainment in One-Dimensional Flow

In this section a brief, but important, treatment will be given of the response of a particle that is introduced to a unidirectional flow. Since the structure of a vortex is dependent upon the flow of the air through the tunnel and over the wing, it is important to know how well a particle follows the tunnel flow before the wing is encountered. This analysis will facilitate this understanding.

A stable vortex requires a laminar flow in which the velocity of each streamline is uniform. The speeds of the tunnel are to be low (from 1 m/s to 3 m/s in a 1 foot tunnel), since laminar flow tends to be associated with lower speeds. Thus, given a low speed tunnel, the question is addressed as to the response of a particle immersed in this flow.

Once a particle is introduced to the flow, there is a period of acceleration before it reaches the terminal velocity of the flow that motivates it. To show this relationship, the simplified equation below for a small particle released in one-dimensional flow at time t=0 with zero velocity is [7],

$$v = w\,(1 - \exp(-Kt)), \qquad [2.1]$$

where,

w = velocity of the air,
v = velocity of the particle,

and

$$K = \{(9\nu_f(\rho_f))/(2r_p^2(\rho_p))\}$$
$$= (8.11E\text{-}4)/(r_p^2).$$

So, if $v_\theta = 99\%(w_\theta)$ is the particle's terminal velocity, the time required for the accelerated particle to reach that velocity is

$$t_{(99\%)} = (4.61/K) = (5681.35)\,(r_p^2) \text{ seconds}$$

For a water droplet with a radius of 100 μm, $t_{(99\%)}$ = 0.142 seconds, and for a 10μm and 1 μm particles time times are 1.42E-3 seconds and 1.42E-5 seconds respectfully. For a control particle of with a density of ~0.3, the three times for acceleration are 0.043 seconds (100 μm), 4.3E-4 seconds (10 μm), and 4.3E-6 (1 μm). The typical well-behaved particle has a lower density than water, and thus has a faster acceleration time.

These values are significant. Although this result is difficult to interpret at this stage, we can express our result in terms of a velocity profile of uniform flow, with particles entrained. If the flow is moving at 1 m/s, it will require a 100 μm water droplet 14.2 cm to reach the flow's velocity. This does give some insight as to the necessary distance (in one-dimension) required for a particle to accelerate to its terminal velocity. Given that there are water droplets larger than 100 μm (one can note by eye that some particles are nearly a millimeter in size), it is quite feasible to imagine a velocity profile of water droplets at different stages of their acceleration, each at various velocities less than or equal to the velocity of the air flow. This produces a non uniform velocity profile, and will result in each particle responding to the vortex differently once they reach the wing.

Although these calculations are based on motion in one-dimension, the results do suggest that most particles, especially the water droplets, will never accelerate to the true tangential velocity of the vortex. Since an entrained particle in a vortex is acted on by air that is rotating, it is constantly changing directions, always accelerating in the direction of the flow at the particular instant. Given this, one is presented with the case in which the particle in a vortex will not have exactly the same speed as the air that entrains it. All of this information is critical since it is necessary to understand the problem of measuring the vortex flow by measuring the particle's velocity.

In order to compensate for the velocity lag of a particle in a vortex, it will be advantageous to state our calculation results based on three particle tangential velocities:

$v_\theta = 90\%\ (w_\theta)$,

$v_\theta = 95\%\ (w_\theta)$,

and

$v_\theta = 99\%\ (w_\theta)$,

where

$v_\theta$ is the particle tangential velocity,

and

$w_\theta$ is the vortex tangential velocity,

whether the calculations are for water droplets or control particles.

Therefore, our brief study of one-dimensional flow demonstrates the possibility that the use of random sized water droplets could result in a non uniform velocity profile. It is possible to encounter a set of water droplets, each traveling at different speeds when the vortex is encountered. Each droplets would respond to the vortex differently. The particles traveling at the speed of the flow would be the most likely to follow the rotational flow of the vortex. It is appropriate then, to develop a model for the wing-tip vortex, to understand particle entrainment within its flow.

## 2.2: Analytical Expression of the Wing-Tip Vortex

Finally, the model of a vortex with an entrained particle can be presented. Here, based on the work of other researchers, the two-dimensional vortex is given, with the assumptions stated earlier in this chapter. The discussion is initiated by the definition and expression of $\Gamma$, the circulation of the vortex. Using the circulation, which is a function of the wing that generates the vortex, the tangential velocity component of a vertex can be derived. At this point the particle is introduced, and a treatment of the effect of the radial forces, as well as the gravity and buoyancy, will be given. Small particles in a low speed flow corresponds to a low Reynolds number, which allows the use of

the expression of Stokes' drag force to equate the influence of the rotating air of the vortex to a force. This representation allows for the tendency of a particle to be affected by the circular flow of a vortex to be compared with the effect of the other forces. The representation will be given in terms of force diagrams.

## Circulation

Our investigation of wing-tip vortices is not driven by what type of wing to use for vortex generation. Therefore, for the sake of easing the necessary aerodynamic calculations, the wing with the simplest of geometries, the rectangular plane, will be used exclusively. $\Gamma_w$, the circulation of the wing, is related to rotational flow and, for the rectangular wing, is an elliptic function of the wingspan [9,10] or

$$\Gamma_w = \Gamma_w(y) = \Gamma_o(1 - (y/s)^2)^{(1/2)} \quad ; \; 0 < y < s, \qquad [2.2]$$

where,

y is the distance along the wing from wing center,
s is the wing half-span,

and

$\Gamma_o$ is the circulation, with units: (cm^2)/s.

Note further that $\Gamma_w(0) = \Gamma o_w$ is the circulation maximum (a constant) and is referred to as the wing root circulation [11]. Also, at the wing-tip there is no circulation ($\Gamma_w(s) = 0$) and thus no lift.

Now, the vortex generated by the wing has its own circulation, $\Gamma_v$, which is a function of the vortex radius or

$$\Gamma_v = \Gamma_v(r).$$

Kelvin's theory states for an inviscid flow, $\Gamma_w(y)$ is coupled to $\Gamma_v(r)$ [12], which is a relationship of importance that will soon become relevant as the circulation associated with the wing span is

coupled to the circulation of the vortex. This enables one to calculate the tangential velocity of the vortex. The coupling is based on an approach presented by Brown (1973),

$$\Gamma_v = \Gamma_v(r(y)) = \Gamma_o(1- (3r/s)^2), \qquad [2.3]$$

where r is expressed as a function of y since the direction of the derivation begins with the knowledge of the wing(length expressed by y) and procedes to the understanding of the vortex (radius expressed by r). Using the coupling relationship, the differences between the circulation values for the wing and vortex will be ignored, by dropping their associated subscripts and using $\Gamma(y)$ for the circulation in either case.

Data, provided by Schlichting (1979), shows the circulation for an elliptic load (See Figure 2.3)., Schlichting's data are expressed is terms of a dimensionless lift distribution $\gamma(\eta)$ that takes the same form as $\Gamma(y)$ in Equation 2.2,

$$\gamma(\eta) = \gamma_o(1-\eta^2)^{(1/2)}, \qquad [2.4]$$

where

$$\eta = y/s; \quad 0 \leq \eta \leq 1,$$

and where $\gamma(0)$ is proportional to $\Gamma(0)$ $(= \Gamma_o)$.

$\gamma(\eta)$ relates to $\Gamma(y)$ according to the following expression

$$\gamma(\eta) = \Gamma(y)/(bw_a), \qquad [2.5]$$

where

$w_a$ is the downstream air speed,

and

b is the wing span.

Rectangular Wing & the Dimensionless Load Distribution

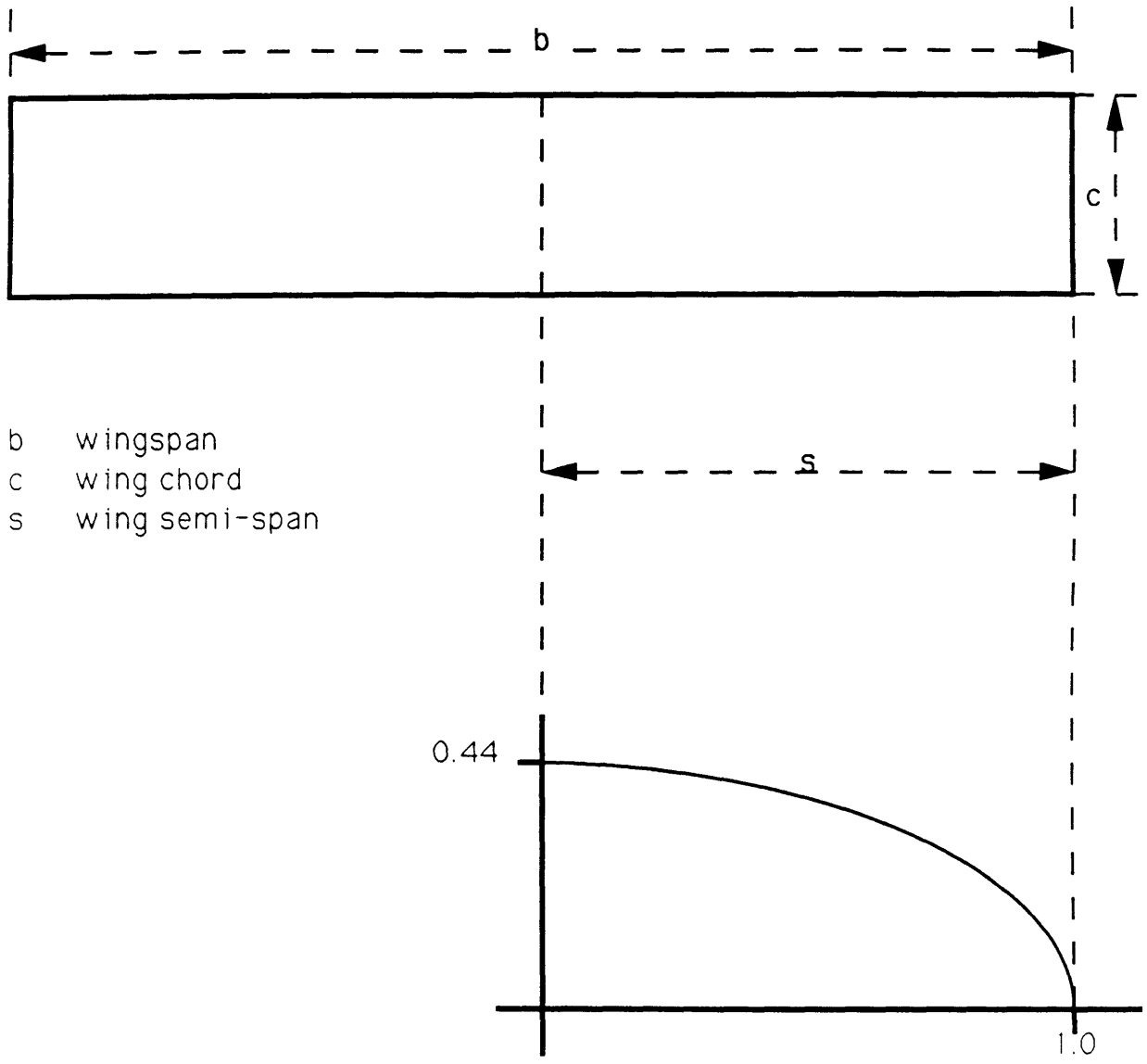


Figure 2.3

The method of the extended lifting-line theory, has been developed from the lifting-line theory of one of the pioneers of vortex studies, Prandtl. It gives the lift distribution (via the circulation distribution) over the wing span from which the total lift, rolling moment, and induced drag can be obtained.

Schlichting's distribution data are for a rectangle wing with an aspect ratio ($\Lambda$) of 6 (Figure 2.3). The aspect ratio is given by

$$\Lambda = b^2/A = b/c$$

where

b is the wing span,
c is the wing chord,
and
A is the wing area, which for a rectangle is simply (b)(c).

However, for the experiments in this investigation, the wing will have an aspect ratio of 3. Although Schlichting does not present distribution data for $\Lambda = 3$, its value can be extrapolated from available data for $\Lambda = 6$, 9, and 12. Let us choose c = 4 cm and b = 12 cm (or s = b/2 = 6 cm), so that
$\Lambda = 6$.

According to the extended lifting-line theory, when $\Lambda = 3$, for a rectangular wing with an angle of attack of $\alpha = 1$ radians (or 57.3°),

$$\gamma(0) \simeq 0.42,$$

The effect of angle of attack on the lift distribution ($\gamma$) is seen through the expression for the lift coefficient ($c_l$) since $\gamma$ is directly proportional to the lift coefficient. The rectangular wing has a linear relationship between the lift coefficient and angle of attack,

$$c_l = 2\pi\alpha;\ 0 \leq c_l < \pi^2,\ \text{since},\ 0 \leq \alpha < \pi/2.$$

Furthermore, the lift distribution and lift coefficient are defined such that when $\gamma(0)$ , $c_l = 2\pi$. In our experiments, there will be more of an interest in the angle 35°. Using the linear relationship between $c_l$ and $\gamma$:

when $\alpha = 35°$, $\gamma(0) \simeq 0.26$.

Assuming a wind tunnel downstream airspeed of 100 cm/s (which is in the vicinity of the velocity expected), and an angle of attack of $\alpha = 35°$, the dimensionless lift distribution is used to solve for $\Gamma_o$,

$$\gamma(0) \simeq 0.26 = \Gamma_o/(bw_a) = \Gamma_o/[(12)(100)],$$

Thus,

$$\Gamma_o = 310.$$

## Tangential Velocity of a Vortex

From Betz's model, which assumes an inviscid flow, there is a similarity with the derivation of a free vortex in fluid mechanics [5, 9] The actual vortex tangential velocity is a function of the distance from the vortex center (the radius),

$$w_\theta = \Gamma(r)/2\pi r.$$

Betz states,

$$w_\theta = (\Gamma_o/2\pi r)[[6(r/b) - 9(r/b)^2]^{(1/2)}], \text{ for } 0 < r \leq r_c, \qquad [2.6a]$$

and

$$w_\theta = \Gamma_o/(2\pi r), \text{ for } r \geq r_c. \qquad [2.6b]$$

where the radius of the core ($r_c$), is defined as the location of the maximum velocity. Please note though that this approximation is undefined at a radius of zero, where it goes to infinity. Spreiter and Sacks have given an linear estimation of the tangential velocity for $0 < r \leq r_c$, (which also agrees rather well with experimental data) that was alluded to earlier in Figure 2.2:

$$w_\theta = (\Gamma_o r/2\pi r_c^2), \text{ for } 0 < r \leq r_c. \qquad [2.6c]$$

If an assumption is made, for the sake of obtaining a qualitative feel for the maximum tangential velocity, that $r = r_c = 2$ cm, both equation 2.6b and 2.6c give

$$w_{\theta\,(max)} = 310/(2\pi(2)) = 24.64 \text{ cm/s}.$$

However, this value for $r_c$ is only for preliminary calculations in order to arrive at an understanding of typical results. For our final analysis (Chapter 6), $r_c$ will be measured.

## Radial Forces in a Vortex

Measurements have revealed that many particles traveling in orbital motion about a vortex center tend to spiral out radially [4,7]. These particles are dominated by a centrifugal force. Not all particles are dominated by this force however, some particles will be drawn toward the core of the vortex by a centripetal force. It is also possible for a particle to maintain a constant radius [7]. In order for this last condition to occur, the centripetal and centrifugal forces that act radially on a particle in a vortex must balance.

The centrifugal force (Figure 2.4) is the radial force that sends a particle away from the center of the vortex. It is the force that accompanies any particle traveling in a circular, or orbital motion about a center. The centrifugal force is a fictitious force that is introduced as a convenience when describing circular rotation. It is actually the inertia of the particle as the particle

Centrifugal Force:

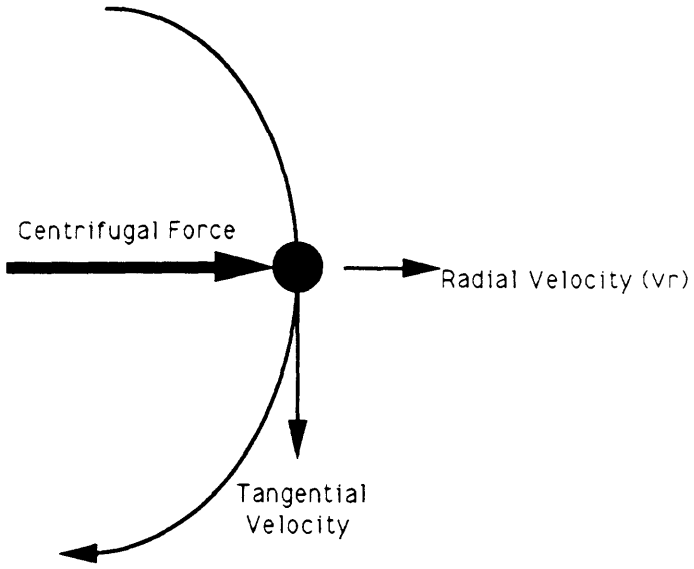


Centrifugal Force within a vortex:

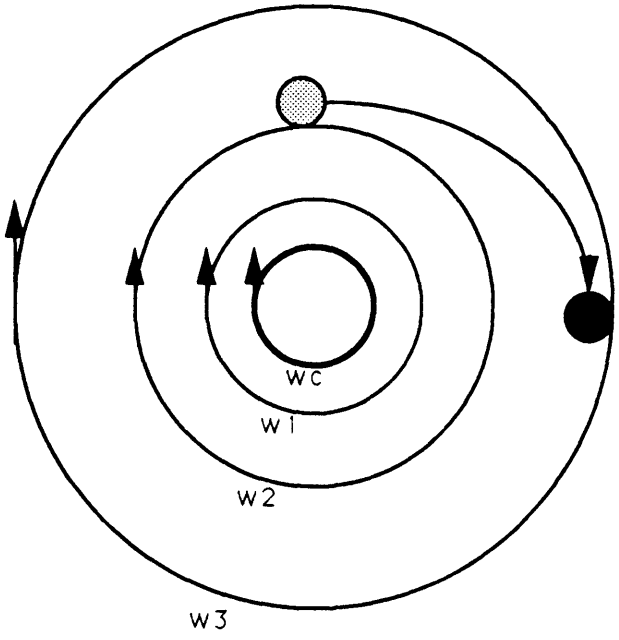


wc, w1, w2, and w3 are the tangential velocites at the corresponding radii, where wc is the velocity at the core and wc > w1 > w2 > w3

Figure 2.4

resists the continuous change of direction needed for rotation. It is a function of the particle's mass, tangential velocity, and distance from the center.

The centripetal force, (Figure 2.5) which opposes the centrifugal force, is analogous to the phenomenon of lift. It is due to the radial gradient of the vortex tangential velocity. The velocity in a vortex has a maximum at the vortex core and approaches zero as the radius increases [5] (Figure 2.2). This velocity gradient of the vortex gives rise to a force that can be understood as a pressure difference between the two sides of a particle in a shear flow. In a vortex, the associated lift force is directed toward the core, moving up the velocity gradient, to the region of lowest pressure (the motion is sometimes described in terms of a diffusive process [4]).

A subset of smaller particles is drawn to the core by the centripetal force, while relatively larger particles spiral out from the effect of the centrifugal force, which tends to overcome the effects of the centripetal force. Still, some of the particles added to vortices tend to accumulate at a radial position where the centrifugal and centripetal forces reach an equilibrium with respect to the particle, and the particle moves with a constant radius.

With this in mind, the equations relating the forces that give rise to the radial component of a particle's motion are listed below; using these one can arrive at an understanding of the radial component of a particle in a vortex. The centrifugal force [4],

Centrifugal Force ($C_{out}$):

$$C_{out} = m_p [(\rho_p - \rho_f)/\rho_p] \ (v_\theta^2/r); \qquad [2.7]$$

where,

$m_p$ is the particle mass,

$\rho_p$ is the particle density,

$\rho_f$ is the fluid density,

$v_\theta$ is the particle tangential velocity,

and

Centripetal Force:

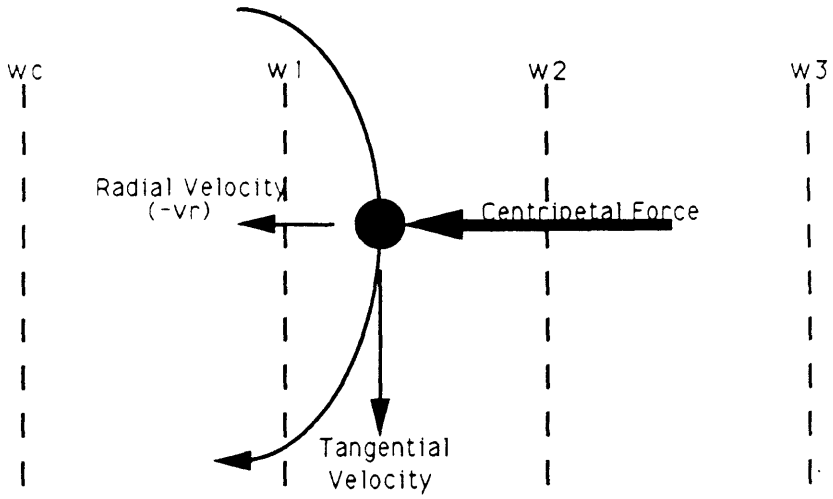


The force acts toward the direction of increasing velocity

Centripetal Force within a vortex:

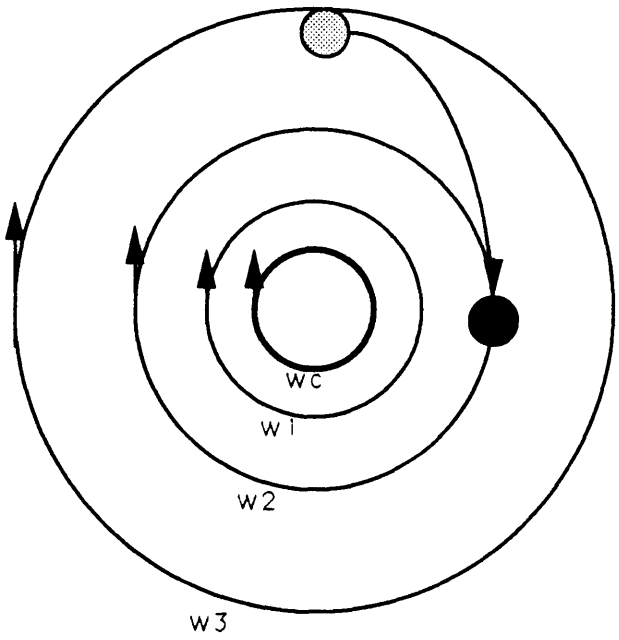


wc, w1, w2, and w3 are the tangential velocites at the corresponding radii, where wc is the velocity at the core and wc > w1 > w2 > w3

Figure 2.5

r is the distance from vortex center to particle.

There is also the centripetal, or lifting force as given by Saffman (1965),

Centripetal Force ($C_{in}$):

$$C_{in} = (32.2)(r_p)^2 \rho_f (w_\theta - v_\theta) [v_f |dw_\theta/dr|]^{(1/2)} ; \qquad [2.8]$$

where,

$r_p$ is the particle radius,

$w_\theta$ is the vortex tangential velocity,

and

$v_f$ is the fluid kinematic viscosity.

Given the above forces there are the three possible conditions that were introduced at the opening of this chapter, including the equilibrium condition for a particle that maintains a constant radius.

Condition I: $C_{out} > C_{in}$ (outward force),
Condition II: $C_{out} < C_{in}$ (inward force),
and
Condition III: $C_{out} = C_{in}$ (circular orbit, constant radius).

There is now enough information to calculate the radial forces that act upon a particle that is entrained in a vortex flow. Referring to Equation [2.2] for the "centripetal" force, the velocity gradient, $|dw_\theta/dr|$, is calculated from Equation [2.6b] in order to determine the force at a point outside of the core radius:

$$dw_\theta/dr = -\Gamma_o/(2\pi r^2); \quad |dw_\theta/dr| = \Gamma_o/(2\pi r^2); \quad r \geq r_c$$

It is necessary to estimate the value $(w_\theta - v_\theta)$ in Equation [2.8]. In many discussions it is assumed that $v_\theta = w_\theta$, i.e. the particle is traveling at the exact same speed as the air of the vortex, in which case the "centripetal" force is zero. Based upon the earlier one-dimensional flow discussions on particle acceleration and terminal

velocity in Section 2.1, an analysis will be made for the cases when $v_\theta = 90\%\ (w_\theta)$, $v_\theta = 95\%\ (w_\theta)$, and $v_\theta = 99\%\ (w_\theta)$. Using the results presented from the calculation of the tangential velocity, we find that

For $v_\theta = 90\%\ (w_\theta)$, $v_\theta = 22.18$ cm/s, $(w_\theta = 24.64$ cm/s).

For $v_\theta = 95\%(w_\theta)$, then $v_\theta = 23.41$ cm/s, and

And for the case when $v_\theta = 99\%(w_\theta)$, then $v_\theta = 24.39$ cm/s.

The experimental measurements will be analyzed in order to observe the radial displacement of particles in the experiments to gain more of a perspective of how the calculated radial velocity translates to an observed difference. Realistically, there may not be the opportunity to witness a measurable difference in the radial displacement as a function of particle density, but the images will be analyzed with any displacements recorded in order to address the possibility.

Gravity and Buoyancy

Each particle is constantly subject to the forces of gravity and buoyancy, which act opposite to each other along the vertical direction. When acting on a particle, the greater of the two depends on the density of the particle and the medium it is immersed in. There is, then, a resultant force that acts along the vertical. This resultant force will act on each particle under consideration, and influence the trajectory of the particle entrained in the vortex fluid flow. The force due to gravity $\mathbf{F_g}$ is given by

$$\mathbf{F_g} = -m_p g\mathbf{k} = -(\pi/6)(d_p^3)\rho_p g\mathbf{k},$$

where

$d_p$ is the particle diameter,

$g$ is the gravity = 980 cm/s$^2$,

and

$-\mathbf{k}$ is the directional vector, pointing down,

where the sign denotes the direction of the vector along the vertical (negative denotes down). The force due to buoyancy, which is due to the volume of air displaced by a particle, takes a similar form,

$$\mathbf{F_b} = (\pi/6)(d_p^3)\rho_f(g)\mathbf{k}$$

So that our resultant force ($\mathbf{F_r}$) is expressed as

$$\mathbf{F_r} = -(\pi/6)(d_p^3)g(\rho_p - \rho_f)\mathbf{k} \qquad [2.9]$$

or in scalar form,

$$F_r = (\pi/6)(d_p^3)g(\rho_p - \rho_f); \quad \rho_p > \rho_f$$

which points down along the vertical. Using the constants stated earlier in this chapter, $F_r$ is calculated, with respect to the particle diameter, $d_p$, where the particle is a spherical water droplet entrained in air,

$$F_r = (511.601)d_p^3.$$

Given all of the forces that have been considered as candidates to influence the motion of the particle, there is a need to relate the forces acting on particles to the velocities of the particles. To link the velocity of a particle to the force acting on it, the force defined as Stokes' drag force is enlisted. The expression of drag relates the force on a particle of a specified size in a flow of given viscosity, to its velocity. This force is based on Stokes' flow, which

corresponds to the low Reynolds numbers associated with a small particle immersed in a moving fluid. In using this expression there is an assumption that a force presents an equivalent drag force on a particle that results in the particle moving at a velocity v.

Stokes' Drag (D):

$$D = 6\pi \mu_f r_p (v) ; \qquad [2.10]$$

where,

$\mu_f$ is the fluid viscosity,

and

v is the particle velocity.

Using the previous calculations for the centrifugal force ($C_{out}$) and the centripetal force ($C_{in}$), a comparison is first made with the direction that the radial forces to that of $F_r$, by treating it as a force with a radial and a tangential component in the vortex coordinate system (See Figure 2.6). The top half of Table 2.1 compares the magnitude of the forces associated with a particle in a vortex with the equivalent force caused by the 22.18 cm/s tangential velocity. The calculations are for three water droplet diameters that represent different orders of magnitude: 1 μm, 10 μm, and 100 μm at a radius of 2 cm.

For a control particle, the influence of the radial forces are similar, but not as significant since the control particle's density at ~0.3 is much lower than water's. The bottom half of Table 2.1 gives the calculated data for a control particle influenced by the tangential, radial, gravitational and buoyant forces at the same tangential velocity and radius. For either particle, Table 2.1 shows that small particles, on the order of 1 μm, will only be minimally affected by the forces that would cause the particle to vary from its circular orbit. However, by the time the particle size reaches 100 μm, the water particle is more affected by gravity than by any other force. In this case, we would not expect the water droplets of this size or larger to be entrained in the vortex flow.

Primary Forces that Influence Particles in Vortices

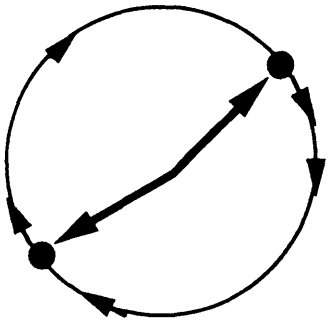

"Centrifugal" Force

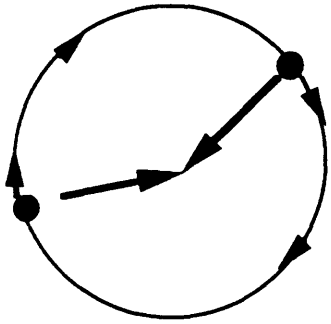

"Centripetal" Force

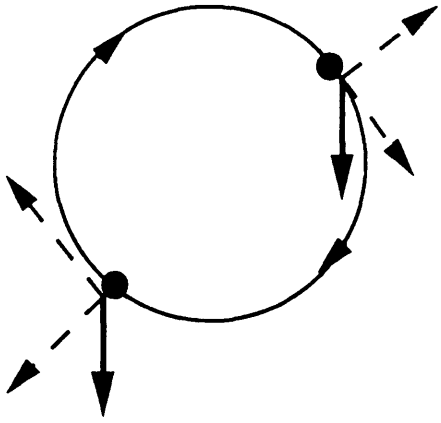

Gravity and Buoyancy

Figure 2.6

## Table 2.1: Magnitude of Forces Acting on a 100 μm Water Droplet and a 100 μm Control Particle

Water Droplet:

Units: g (cm)/$s^2$

| Diameter | Tangential | Centrifugal | Centripetal | $F_a+F_b$ |
|---|---|---|---|---|
| 1 μm | 3.76E-6 | 1.28E-10 | 3.24E-10 | 5.12E-10 |
| 10 μm | 3.76E-5 | 1.28E-7 | 3.24E-8 | 5.12E-7 |
| 100 μm | 3.76E-4 | 1.28E-4 | 3.24E-6 | 5.12E-4 |

Control Particle:

Units: g (cm)/$s^2$

| Diameter | Tangential | Centrifugal | Centripetal | $F_a+F_b$ |
|---|---|---|---|---|
| 1 μm | 3.76E-6 | 3.85E-11 | 3.24E-10 | 1.53E-10 |
| 10 μm | 3.76E-5 | 3.85E-8 | 3.24E-8 | 1.53E-7 |
| 100 μm | 3.76E-4 | 3.85E-5 | 3.24E-6 | 1.53E-4 |

The 100 μm control particle is still largely dominated by the tangential force which keeps the particle in a circular orbit. However, it is on the same order as the gravitational pull. This constant force downward would cause an entrained particle to follow a path around the core that would be more elliptical than circular.

Thus, from the circulation of a wing, the tangential velocity was derived and the velocity profile of a vortex presented. Based on this model, the forces that influence a particle that is entrained in the vortex (the radial forces, gravity, and buoyancy) were applied to different particle sizes for each particle type. The calculations show the effects on the particles' trajectory as they attempt to follow the flow of the vortex.

In this chapter, the objective was to present a model of a wing-tip wake vortex, that included an entrained particle's response to the flow. The analysis began with understanding particle acceleration in a one-dimensional flow. Then the vortex was presented, and the forces that influence the particle were applied to the two different particle types, at sizes over three orders of magnitude. The results show that water droplets, unless very small, have difficulty maintaining the circular orbit of the vortex. At the larger particle sizes, gravity and the centrifugal force, which act radially outward, dominate the tendency for the particle to travel around the vortex core. The control particle is much less affected by the radial and gravitational forces, although at the larger diameters the gravitational force begins to compete with the circular motion such that the trajectory around the vortex core would no longer be circular.

The calculations are qualitative indicators of what the experimental observations of these particles in a vortex should reveal. Once the vortex velocity measurements are obtained, the tangential and radial velocities will be calculated in the same manner and evaluated to determine the agreement between the analytical and experimental results. Before the evaluation begins however, the measurement system will be explained, in addition to the experimental procedures used to generate the data.

# Chapter 3: Laser Streak Velocimetry

In order to obtain velocity measurements, there must be an assurance that there is an effective method that will give valid data. During this chapter, a technique called Laser Streak Velocimetry (LSV) [6] will be introduced and described as an excellent method for measurement particles entrained in vortices. The discussion is motivated by presenting the specifics of the velocity measurements that are required. Then the LSV technique of measuring the velocity of particles entrained in a gaseous flow (air in this investigation) will be explained. The original technique must be modified however, to match the requirements that are unique to the measurements of this investigation. These modifications will be presented, with a discussion of how unambiguous velocity data can be extracted, and minor distortions resolved.

## 3.1: The Motivation

Assume that there is a unidirectional flow of air, flowing with a constant velocity of 3 m/s through a small transparent tunnel. Using a laser and a cylindrical lens, a sheet of light can be introduced parallel to the flow. If small particles (called flow seeds) are entrained in the airflow, they will scatter the light as they travel along the length of the sheet. The sheet is thick enough (2 mm) so that when the sheet is viewed along a line of sight perpendicular to the direction of flow, one observes a set of long streaks formed by the entrained particles. If the flow is uniform and laminar, these streamlines will be parallel.

To measure the velocity of the flow, Laser Streak Velocimetry can be utilized. One can apply one of two methods to extract the velocity of the entrained particles that give rise to the streaks. The two methods are merely two similar ways of obtaining the streak data. In both approaches the illuminated particles that flow along the light sheet are imaged by a camera. In the first method, the imaging system is a still camera with an

adjustable shutter time [6], whereas in the second, a video camera and video recorder are used with a pulsed or chopped laser beam (mechanically or acousto-optically chopped) [14]. With each of these methods, the sheet will be thick enough to illuminate the particle for a period of time longer that the exposure time. In order to insure all of the information is gathered. Each of the approaches will be examined briefly, then the second method will be explained in more detail.

## 3.2: The Original LSV Method (Still Camera)

Using a still camera with high speed film, and particles that provide sufficient illumination, one can take a time exposure of the illuminated particles as they move through the laser sheet. On the photographic film the particles appear as streaks. Not only will the streaks reveal the trajectory of the particles in the two-dimensional plane of the light sheet, but if one knows the length of the streaks and the exposure time, the average local velocities averaged over that time can be obtained. If streak length is denoted by s, the particle's average velocity by $v_a$, and the exposure time by t, then the relationship can by simply expressed by

$$s = v_a t.$$

The validity of the velocity calculated depends on how accurately one knows the streak length and the exposure time. This technique was initially developed by Sparks and Ezekiel [6] and was shown to produce results that agreed with theory very well. Unfortunately the power of the laser available for this investigation (100 mW) was observed to be too low for Polaroid photographs, even when high speed film was used. Still photographs were also taken with a 35 mm camera, but only minimal success was met, which was insufficient for indepth velocimetry.

## 3.3: The Modified (Video-Based) LSV Method

For obtaining the data with a video system, the light scattered by the traveling particles is imaged on the photocathode of an Intensified Silicon Intensified Target (ISIT) camera tube. The images of the particles passing through the light sheet are recorded by a video cassette recorder and viewed on a standard monitor. As the camera records the streaking particles, the laser is chopped at a specified periodic rate. The chopping results in pulses of light of equal length which expose the particles to light only during short time periods. This is analogous to the use of a shutter in the still camera method. The analysis of the image by the video method is more complicated, but the video method has its advantages also.

First, the ISIT is designed for detecting single photons, and thus has a higher sensitivity than the conventional still camera with high speed (low light) film. Thus particles can be imaged with light sheets from lasers that may not have sufficient power to be visualized by a still camera system. Poor illumination may also occur if the particles used are poor scatterers because of size or optical properties. An ISIT camera with a 3/4" video recorder was used to record the streak data. Although the power of the laser used in this flow visualization experiment is lower than in past experiments [6,14], the video system easily visualizes the particles as they travel along the sheet. The video technique also allows real-time display and immediate play-back, which facilitates alignment and optimization of the experiment. Using the play-back option, one is given the opportunity to easily observe the time evolution of the flow.

The video measurement system follows the standard American video electron beam scanning rate. The information on the target is sequentially read in the interlaced video scan pattern of 256 even lines and 256 odd lines (called the even and odd fields), and then stored on magnetic tape. The scan starts from the upper left corner and scans for 256 lines, each line followed

by a horizontal fly back, and at the end of 256 lines (which is called a field), there is a long vertical fly back period. Given that each line scan is 60 microseconds, the horizontal fly back 10 microseconds and the vertical fly back 1.5 milliseconds, the total time for one field is 1/60th of a second, and the time for one frame (two fields plus vertical fly back) is 1/30th of a second.

When a target emits photons toward the camera, the corresponding area on the ISIT target becomes capacitively charged. The target is images as the electron beam scans the target and "reads" off the positively charged areas. Note that the scanning electron beam does not scan all of the intensity at once; rather it leaves a fraction of the original intensity to be picked up by the next scan. Thus, the remainder of a streak can be seen , although dimmer, for more than one frame even though the particle that generated the streak has left the region of view. This phenomenon is known as the intensity or capacitive lag of the ISIT. The lag is a residual signal that is observed after the imaging tube is scanned. It is expressed as a percentage of the original signal. The lag is both a function of the capacitance and gain of the imager. It occurs as a result of the finite time it takes the electron scanning beam to remove the charge accumulated on the camera tube target. The specifications for the ISIT present lag as a percentage of initial signal output current for different values of input signal current [5]. For the signal current associated with a point source, 1/30th of a second after the point source has disappeared, the current signal is about 18% of the original intensity. In another 1/30th of a second the signal is at 3%, at which point the intensity level approaches the level of the dark current, where the point source is no longer visible. These specifications reveal that it could take a complete 2 frames or more (in the case of stronger initial signals) for a streak to completely disappear. This results in a system which images streaks over several fields, allowing the illumination of the particle along the sheet to make streaks that last several fields.

Although chopping the beam gives exposure time, and the length of the streak corresponds to the velocity, it is possible to

measure an incorrect velocity if the particle leaves the sheet early, before completing its streak. However, If the illumination period is limited to pulses of light less than 1/60th of a second, there is a significant improvement in the chances of obtaining a complete streak. For instance, a square wave chopper at 150 Hz produces a 1/300th of a second burst of light followed by a 1/300th of a second period of no light. During 1/300th of a second, the 3 m/s particle travels 1.0 cm. In this case, a scanned field will yield a series of bright dashes 1.0 cm long, separated by dark spaces 1.0 cm long, with the entire series of dashes not being over 5 cm in length in one field. See Figure 3.1 for an illustration. Whether one will see all of the dashes in a single field or frame depends on the location of the scanning beam when the particle crosses the region of view, the size of the region of view, and the intensity lag of the ISIT.

## 3.4: Correcting LSV Measurement Distortions

Now that it has been shown that there are techniques and characteristics of an ISIT video system that allow one to obtain accurate streak (velocity) data, it is necessary to discuss certain refinements that can be made to the data analysis method that would insure the recording of velocity data unambiguously. There are three possible errors in the velocity measurement that need to be discussed: Blooming, pin cushion distortion from the lens, and the possible occurrence of incomplete streaks. As discussed earlier, significant error reduction is automatically accomplished due to the scanning properties of the video system (i.e lag). However, there still exists the possibility of ambiguity in the streak measurements. Even with a fast chop rate, a particle could enter and/or leave the light sheet before being illuminated long enough for velocity data to be extracted. Also, the scanning rate could scan through a streaking particle before it completed its scan. Although if the next field were examined, the completion of the streak would be found with the original part of the streak still

## Streaks (or Dashes) Left by A Particle in a Horizontal Flow

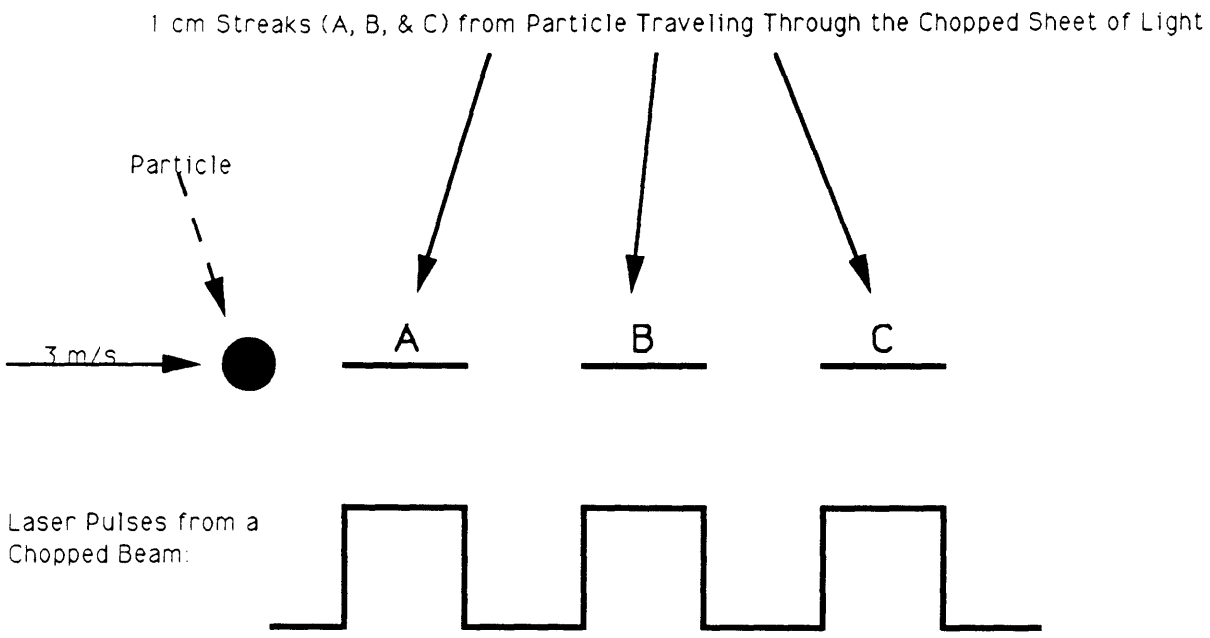


*Notes:*
*Assume 150 Hz Chop*
*Each Streak = 1 cm*

FIGURE 3.1

imaged, there could be an error if the first part of the streak is read and the length not be representation of the actual velocity

Blooming, an occurrence also noted by Sparks and Ezekiel (1976), causes a distorted blur and results in images with incorrect lengths. Another error to overcome is lens distortion that is a natural part of the ISIT camera. This distortion in the image is referred to as a pincushion effect. The result of the effect is that a streak, 1 cm in length, in the center of the image, would be measured to be continuously longer as the streak moved closer to the edge of the field of view. At the edge of the field of view, the length from the same particle would be measured to be from 1.2 to 1.6 cm. This effect makes it difficult to analyze an entire field of view of particles. Although the particles may be traveling at the same speed, the pin cushion effect will cause the velocity profile to appear non uniform.

Each of these possible errors can be reduced without much effort. The potential error caused by blooming, can be alleviated, by manually selecting the streaks to be measured. Blooming is the easiest to overcome, since it is visually well-defined, usually as an irregular spot of high intensity on the screen. If this spot appears on either end of a streak, the streak will not be measured, since the blooming may mislead the actual length of the streak. The pin cushion lens distortion effect will be compensated by mapping a square grid that is placed at the image plane of the ISIT. The process of mapping the grid is considered to be a preliminary experiment, and will be discussed further in Chapter 4.

To make sure an incomplete particle streak or dash is not measured, only those series of streaks that fit a certain criteria will be measured. As Figure 3.2 shows, given a series of at least three dashes labeled A, B, C, etc., a single dash (B) which has dashes on each of its sides (A and C) is a complete streak. A middle streak will not be subject to the particle entering or exiting the sheet, nor is it left incomplete by the scanning electron beam. This method is simply one of observation, requiring a minimum

## Unambiguous Velocity Measurement from Three Streaks

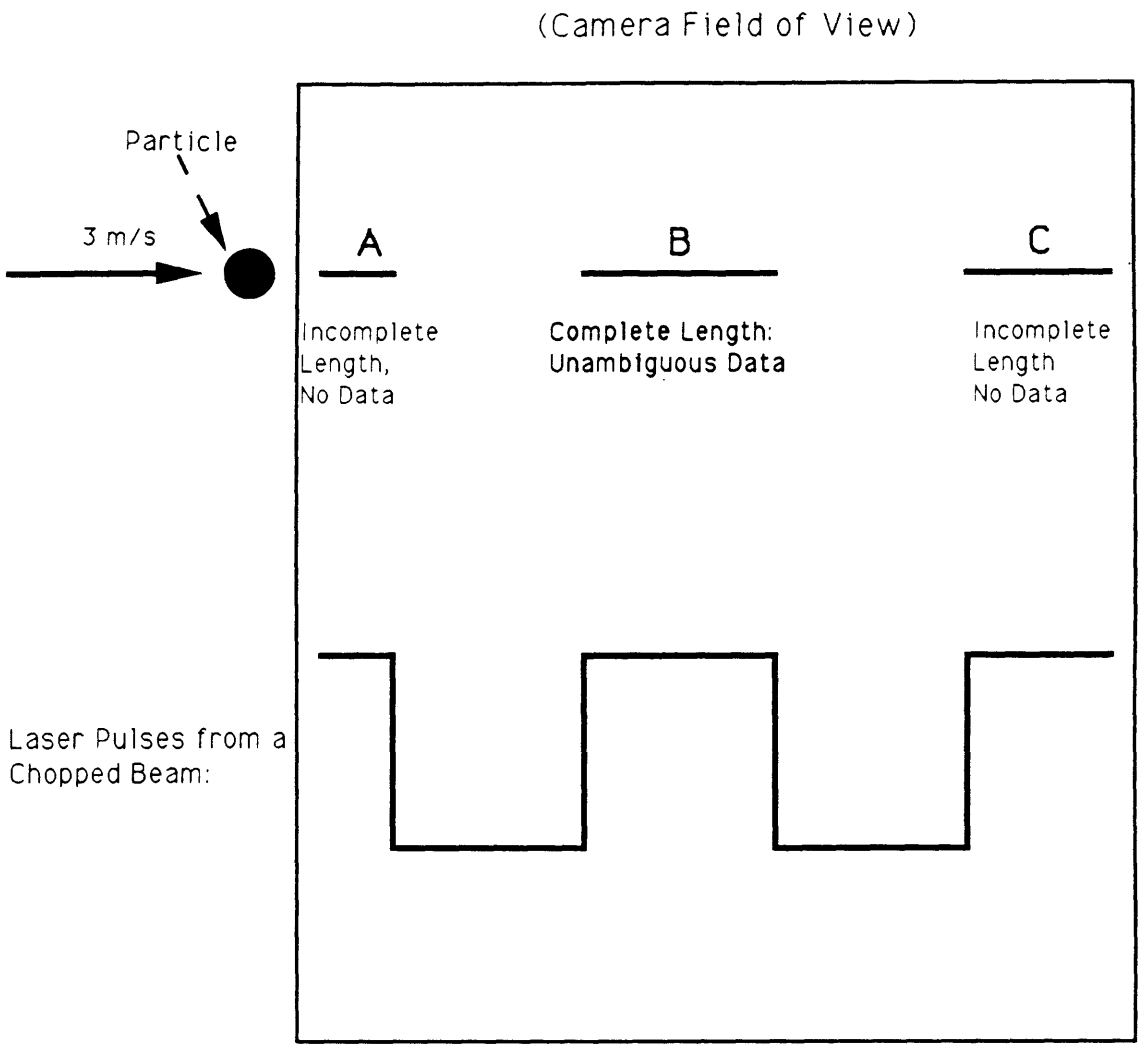


*Notes:*
*Assume 100 Hz Chop*
*Middle Streak = 1.5 cm*

Figure 3.2

of three streaks (dashes) in order to obtain the velocity data unambiguously. Preliminary data shows that there are many cases in which there are three or more dashes for the motion of one particle.

## 3.5: Streak Length Measurement

The validity of the velocity data depends upon how accurately the streak length and pulse width is measured. Streak length measurements are considerably less precise and depend on the spatial resolution of the camera and image processing system. Thus, to optimize the accuracy of the velocity data, the spatial resolution must be maximized. The laser pulse width is known precisely, and is detailed further in the next two chapters.

The images will be analyzed by an image processing system where an image (i.e. dashes) is digitized in the form of an array by a frame grabber and transferred to a computer's memory or display for further analysis. Once the image is digitized, it is available for a variety of operations. Most of these do not need to be enlisted, however. The goal is simply to obtain the length and direction of the dashes as accurately as possible. There is also a requirement for the measurement to be executed without using too much of the computer's memory since there are memory limitations and a stored image can take hundreds of kilobytes of memory to store. Thus, the processing should be effective without being complex.

It was found that measuring the distance between pixels at two different points on a digitized image is an accurate and simple method of measuring lengths. The pixels are the individual points of the digitized image array. Each pixel position is assigned an intensity value according to the original image. Using a zoom lens to reduce the ISIT's field of view, one can establish the resolution greater than two pixels per millimeter. In addition, there exists image processing software that will allow further enhancement by magnifying the original image. This allows one to find the end of the streaks more precisely, and reduce the error in streak length

measurements. Software exists or can be written to perform this measurement task, but because of the image complexity it is much more reliable to make these measurement using this system manually. Given a screen full of dashes, one can quickly find the candidates that will provide velocity data unambiguously and measure them without resorting to extensive programming or a complex software package. In order to maintain consistency, each streak that is over a specified threshold intensity is measured. The intensity value of 60 (out of 255, being the brightest) reflects a sufficient intensity threshold value. The measurement from one point to another is simply a matter of displaying the cursor position, in pixel coordinates, for each end of the streak or dash. Extracting the streak length is a matter of calculating the length between the two pixel points, then multiply by a scaling factor due to the ISIT lens.

Given the wing-tip vortex environment that must be measured, the video-based LSV model will provide excellent data. The low-light ISIT, the ability to record data continuously and in real time, the flexibility of controlling the chopping rate, and the image processing creates a LSV system that is well suited to measure particle entrainment in a vortex. Now that the measurement system has been introduced and discussed, the next step involves moving to the outlining of the experimental procedures and obtaining the measurement data.

# Chapter 4: Experimental Procedures

In this chapter, the experiments that produce the data for this investigation are introduced. The research conclusions are based on the vortex velocity data from the random-sized water droplets, as well as from the control particles. Although the most important experiments are those which involve direct measurements of the trajectories and velocities of the entrained particles, there must be a series of supporting experiments. They fall into two categories: The first category involves what is referred to as preliminary measurements, which are used to obtain values and constants that are necessary for all of the experiments that follow. There are three specific preliminary measurement procedures, the sizing of the control particles, the measurement of pulse lengths and chopping rates associated with the mechanical chopper of the video-based Laser Streak Velocimetry system, and the measurement of the scaling grid that is used to compensate for the pin cushion lens distortion caused by the ISIT. The second category comprises those experiments that are designed to evaluate the quality of the downstream flow in the wind tunnel. Since the structure, strength, and stability of a vortex depends upon the quality of the air flow over a test wing, the downstream flow through the tunnel must be understood and characterized. The wing is a rectangular plate, with dimensions that remain consistent with the dimensions used in the analytical study of Chapter 2 (Theoretical Background).

First the preliminary measurement procedures will be dicussed, followed by the flow quality and wing-tip vortex experiments. Explanations will be given of relevant procedures associated with making the observations. Then an examination will be made of those experiments designed to measure the velocity and trajectory data of particles entrained in vortices. Included in each of these discussions will be the instruments and devices used, their purpose as well as their physical position in the experimental setup. The results of each of these experiments are presented in the next chapter.

## 4.1: Preliminary Measurements

### Particle Sizing

As is known from the earlier calculations in the analytical study of particles entrained in vortices, in order to understand the trajectory of a particle within a vortex, it is necessary to know the properties of the particles, most importantly, their density and mass. There are established experimental procedures for the measurement of spherical particle sizes. Possible procedures include the derivation of particle size from Mie scattering [13], and analyzing the far-field diffraction pattern that a particle would yield on an image plane [13]. However, these experiments would require much time and effort, resulting in a digression from the topic of interest. In addition, simpler methods, possibly less accurate but not significantly so, can be utilized.

Control particles are generally manufactured with specific dimensions and properties. The fact that they are solid or hollow types of microballoons facilitates the viewing and measurement of the particles sizes with a microscope. There is a particular type of control particle, manufactured by Emerson & Cuming Composites, called eccospheres. According to the manufacturer, most of the particles (40%) have a diameter of 64-100 μm, with a typical density of 0.38 g/cc. Another category of control particle (or microballoons) that can be used in the experiment is the small spheres manufactured by Union Carbide. They have a typical diameter of approximately 40 μm and a density of about 0.3 g/cc. The advantage that the eccospheres have is that they, as hollow glass spheres, scatter more light than do the Union Carbide microballoons, which are completely solid spheres brownish-amber in color. The candidates for control particle were measured with a microscope that has spatial resolution at the micron level in order to confirm the manufacturer's specifications. The particle size data is presented in Chapter 5, as selected photographs from the microscope. It was finally decided that the Emerson & Cuming eccospheres are acceptable control particles since they are small,

scatter light well, and have a low density, suggesting that they follow the flow well. Data from the size distribution measurements of the eccospheres by the microscope are presented in the next chapter.

## Measurement of Pulse Widths and Chop Rates

Measurement of the laser pulse width was not complex, but it was essential to confirm the chopper manufacturer's (EG&G) calibration. There must be an understanding of the pulses created by sending the laser beam through the mechanical chopper. Not only is there a need to know the pulse shape, but there is equal concern about the pulse repetition frequency, and about the fluctuation in the chopping rate of the mechanical chopper. In other words, when the chopper it set to 200 Hz, how close is it to generating square pulses that are equally spaced such that the complete cycle lasts 1/200th of a second?

To answer this question the beam from a 25mW HeNe laser was be sent through the chopper and into an ultrafast photodetector (the response time was less than a nanosecond). The output of the photodetector was sent into an oscilloscope and a time interval counter. First, a signal of specified frequency was measured by these two instruments from the synchronization output of the chopper (it acts as a square wave frequency generator), then this result was compared to the output of the photodetector. The oscilloscope was used to display the waveform and the time interval counter was used to produce the accompanying numeric values. The results from each instrument should agree with the manufactuer's calibration.

Using these data found in the next chaper, the pulse shape and true cycle rate were found. With this information, the lengths of the imaged dashes can be converted to velocities with negligible loss in precision.

### Compensation of Pin Cushion Lens Distortion

Before the procedures designed to produce and understand the streak data are discussed, there still remains the fact that all of the data was subject to the pin cushion distortion that was discussed in Section 3.5. In order to correct for this effect, a grid of squares of known size was at the same image plane that the sheet of light occupies. This allowed a measurement and mapping of the distortion, using the same length measuring techniques that are used to measure the streak lengths. The distortion expands the streaks that are not at the center of the field of view. The first task in interpreting the streak lengths is correcting for this distortion. The map comprises a set of vertical and horizontal scaling factors that are correspond to the squares on the scaling grid. Each square was measured 1.3 cm x 1.3 cm. The map is a remeasurement of the squares after they have been imaged and digitized by the frame grabber. They scaling was be based on millimeters per pixel. By contructing this map, the pin cushion distortion is overcome. The scaling grid and results will be presented in the next chapter.

## 4.2: Wind Tunnel Flow Quality Measurements

The goal of these series of experiments is to arrive at a velocity profile that will aid in understanding the quality of the flow in the wind tunnel. In Chapter 2 it was stated that the air flow velocity profile that gives rise to stable vortices must be characterized by a uniform velocity profile and laminar flow. There is a concern about air flow in the rectangular test wing's region (located approximately in the middle of the tunnel's test section) since this is the air that will respond by rolling up into a vortex. In order to create vortices that are stable, it is necessary to initially have a stable flow; that is, the flow should be as uniform and constant upstream of the wing as possible. Otherwise, the wing will not produce a stable, well-behaved vortex, but rather a turbulent flow with some degree of vorticity.

The primary objective of this experiment was to determine how well the flow reflects the requirements. Preliminary experiments suggested that the horizontal velocity was not constant in time. Since that observation, modifications were made to the wind tunnel in order to improve the stability of the flow. This series of experiments will evaluate the flow with the tunnel's modifications.

Flow visualization, in general, and Laser Streak Velocimetry specifically, allows an analysis of the tunnel flow quality. An examination was made of a series of particles leaving the tunnel flow-straightening section and entering the test section where vortex measurements were conducted. Additionally, this experiment involved measuring the effects of the varying concentration of water particles that were dispersed into the flow by the atomizer. Not only does the flow visualization experiment allow determination of particle velocity variations, but there are simultaneous observations of the velocities of randomly distributed particles in the field of view. The quality of these data are dependent upon the velocity resolution, which means that it is necessary to have the ability to differentiate the velocities of two illuminated streaks with similar, but not equal lengths. The experiment was performed twice, once with the control particles, and a second time with water droplets.

Figure 4.1 is a schematic of the flow visualization and Laser Streak Velocimetry experimental setup which was used to evaluate the quality of the wind tunnel flow. The laser sheet was introduced through the open exhaust and of the wind tunnel. This particular configuration was an arrangement to study velocities and trajectories of particles as they flow down the tunnel, entrained in the moving air. The light source was a 100 mW cw Argon laser (with all spectral lines). The laser emission from a cw Argon laser is visible, blue-green light, with the principal spectral lines at 488 and 514 nm. The laser beam was transmitted through a cylindrical lens which sharply focuses the beam in the direction perpendicular to the cylinder's axis, so that the light was spread in a plane, within a sector of a certain thickness. With

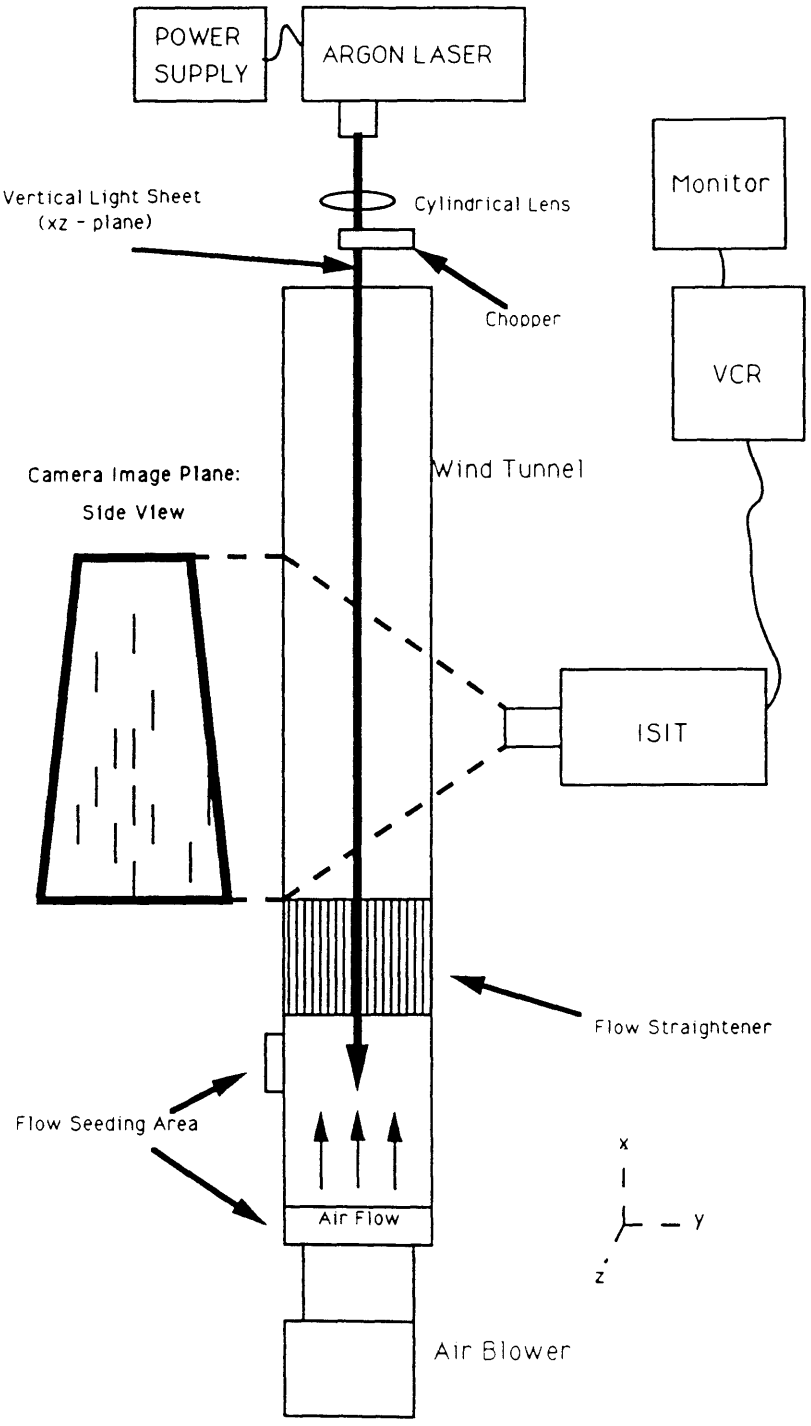


FIGURE 4.1: Wind Tunnel Measurement Setup

reference to the coordinate orientation in Figure 4.1, the beam is traveling in the negative x direction (opposite that of the flow), as a plane parallel to the xz-plane. The typical thickness of the plane of light for these experiments was small, on the order of a few millimeters (which corresponds to the natural divergence of the beam from the source), with a sector height that linearly increases as a function of the cylindrical lens's focal length (the lens was a glass rod with a diameter of 12 mm). The result was an illuminated sheet which was actually a thin slab of light.

However, as was mentioned earlier, the power of the laser in the experiments was relatively low. Similar flow visualization experiments have benefited from higher power lasers and avoided the concerns of low light imaging. This was a factor that could not be neglected. It was shown in Chapter 3 that the video LSV system can work well under these conditions. This imaging system (i.e. the ISIT camera, VCR, and Monitor) will image the projection of the volume as a two-dimensional image plane.

The thickness of the sheet of light is important. It must be thick enough to illuminate the particles traveling down the wind tunnel, but not so thick that the particle illumination leads to insufficient scattered light. In addition, if there are so many particles within a laser sheet that individual particles cannot be resolved, then the concentration of particles in the illuminated region must be decreased. The time the particle travels through the sheet should be greater than the exposure time (the shutter speed or chopping rate) of the imaging system. This is in order to insure that the exposure time measures a full event, unaffected by the particle exiting the sheet. If the sheet is too thick, there is a loss of some of the understanding of the two-dimensional particle trajectory, since now a moving particle may have enough space to travel in the third dimension. This dimension cannot be resolved by the system however, yielding an observation that may likely be misinterpreted.

The flowing air in the wind tunnel was generated by a blower located at the tunnel's opening (See Figure 4.1). Following the blower is the first section, which is responsible for

concentrating the turbulent air from the blower to the middle of the tunnel and helps to make the flow more consistent, with a uniform velocity profile distribution that will have its maximum along the axis of the cylindrical tunnel. This was accomplished with a Venturi tube, which focuses the air into a narrow orifice, then allows the air to exit through an inverted cone. This process concentrates the air in the middle of the tunnel then allows it to expand while proceeding down the tunnel, in order to give the velocity profile more of a Gaussian shape. The water droplets are introduced to the flow by an atomizer, and the control particles by a syringe. The flow straightener is made up of a collection of standard drinking straws, 1/4 inch in diameter. Both types of particles become entrained and are propelled through the flow straightener, which makes the flow from the first section more laminar.

Once the particles leave the flow straightener, they enter the test region of the wind tunnel. It was here where they encounter the plane of laser light, and consequently scatter light to the image plane of the ISIT. The task was to determine the quality of the flow leaving the straightening section of the wind tunnel and entering the testing region. A perfect flow will result (after encountering a wing) in a well-defined, stable vortex which would agree well with theory [15]. Using such a small-scale wind tunnel makes it very difficult to produce perfect conditions, the vortex may yield measurement data that reveals fluctuations in its structure due to an imperfect initial flow. However, in order to obtain a vortex stable enough to study, the variations and instabilities (i.e. acceleration and deceleration of the speed of downstream flow) must be minimal. If the flow is of poor quality, stable vortices cannot be generated. At worse, the flow could be so unstable that the vortex would break up immediately after its generation.

After the data are collected, instantaneous velocity profiles are examined, and an attempt made to determine the time dependence, if any, of the velocity profile. As long as the individual velocity profiles are uniform, and a given set of

sequentially ordered profiles do not vary greatly from each other, there should be an acceptable flow for vortex generation.

Using the video-based LSV System, the downstream flow of the wind tunnel will be analyzed by the velocities and trajectories of control particles and the water droplets as they travel down the tunnel. Each particle was measured at two chopper cycling rates. The measurement parameters are

1) Downstream Flow with Control Particles* at 200 Hz
2) Downstream Flow with Water at 200 Hz
3) Downstream Flow with Control Particles* at 75 Hz
4) Downstream Flow with Water at 75 Hz

There are advantages and disadvantages to using either cycling rate. The faster rate, 200 Hz, is more likely to create a greater number of dashes for a traveling particle than would a 75 Hz rate. For instance, a particle traveling 1 m/s over 2 cm would be imaged as four dashes if it were chopped at 200 Hz but only one and a half dashes if chopped by the 75 Hz rate. In Chapter 3 it was demonstrated that streak lengths can be obtained unambiguously from the imaged dashes if there is one dash bordered by similar dashes (whether they are complete or incomplete dashes) from the same particle. That means at least three dashes are necessary to form an unambiguous streak length measurement. The above example shows that unambiguous velocity data can be obtained from a 2 cm length only if the sheet is chopped at 200 Hz. When considering a large number of

* In these experiments the control particles were talc powder. The reasons for this are two-fold. Talc has a density low enough to accurately follow a downstream flow, and was shown to be successful as such a seed in the first Laser Streak Velocimetry experiments performed by Sparks and Ezekiel (1976). Since the particles are entrained in the flow over a length of meters and the flow is largely one-dimensional, it does not matter whether the talc or the eccospheres are used here since the density for each is low enough to respond to the flow similarly. The second reason is that there is a limited quantity of eccospheres available, and these particles must be conserved for the vortex measurements, in which the particles exact density and geometry become more important.

particles, this means that there will be more data of qualifying particles at 200 Hz than at 75 Hz.

There is also an advantage to using slower chopping rates. These produce longer streaks which tend to be easier to measure, requiring less spatial resolution than a 200 Hz chopped streak. If two streaks from a 200 Hz chop differ in length by 1 mm, the same streaks would differ in length by 2.67 mm with a 75 Hz chop. This is significant since the precision of the velocity measurements depends largely on the spatial resolution. Noting the characteristics of the faster and slower chopping rates, it was advantageous to make the measurements at both rates for a more complete understanding of the particle trajectories.

The results and anaylsis of these measurements will be presented in Chapter 5. At that point, not only will downstream velocities be measured over a period of time, but individual fields and frames will be analyzed in order to construct instatanteous velocity profiles. The velocity profiles will show whether the flow was uniform within the ISIT's field of view.

## 4.3: Vortex Velocity Measurements

Once there is a characterizization and understanding of the flow of air in the downstream direction of the tunnel, one can visualize vortices created by a rectangular wing. For these measurements the principles and techniques of Section 4.2 are preserved. However, there are many differences that make the vortex measurements unique, forcing an alteration of some of the aspects of the experimental setup in order to visualize a particle within a vortex well enough for data extraction. Before describing these physical changes, it is necessary to address the problem of obtaining video-based Laser Streak Velocimetry data from a wing-tip vortex.

Figure 4.2 shows a general schematic of the experimental setup of a vortex visualization and measurement system for the particles. As in the flow quality measurements, the 100 mW Argon laser was directed into a cylindrical lens, which was

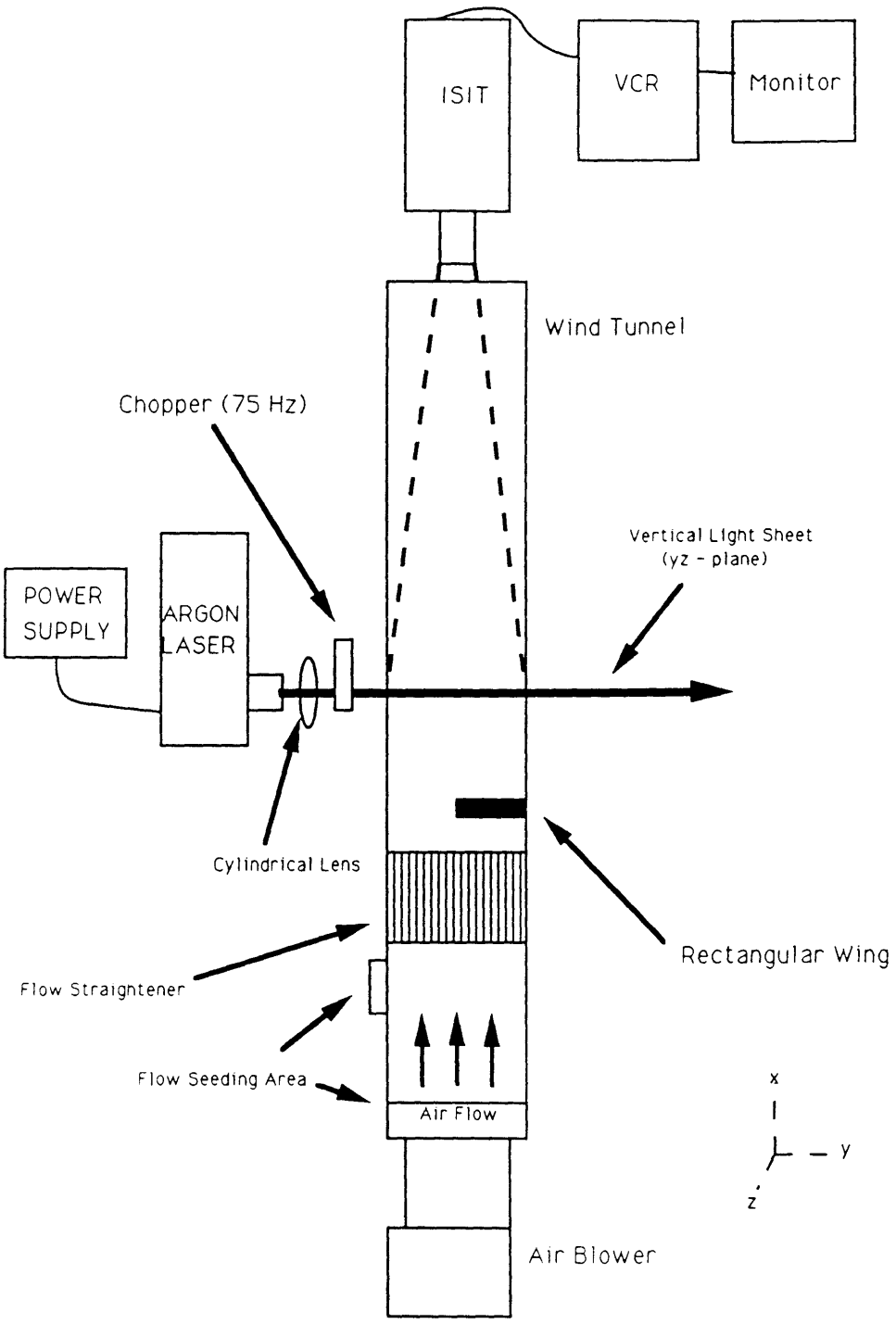


FIGURE 4.2: Wing-Tip Vortex Measurement Setup

followed by a chopper. This time, however, the sheet was oriented perpendicular to the downstream axis along the yz-plane. With this orientation, a plane exists that illuminates the tangential and radial components of the trajectory of a particle. The ISIT camera was positioned at the end of the tunnel, peering into the flow. Take note that the schematic is a bit misleading. In order to conserve paper space and reduce complexity, the scale does not reflect the actual setup. The tunnel's length was longer than presented here and the camera was oriented further back from the end of the tunnel and equipped with a zoom lens (105X) in order to view the vortices. Also the camera is covered, except for the lens, to protect it from the small particles thay may reach that distance.

Proper flow visualization of a seeded vortex will provide a two-dimensional image of the vortex, with arcing streaks left by the illuminated particles, entrained in the vortex. These arcs represent the circular, elliptical, or spiraling motion (as the case may be) of the particles in the vortex. With these images not only can one find particle velocities at different radii, but the two-dimensional image will allow determination of the vortex core (the origin is the center of the core), the vortex maximum velocity, and other elements of the vortex structure.

Once again, assume a particle moving 1 m/s downstream before entering the vortex. 1 m/s is chosen because it is known that this is only a little less than the actual tunnel velocities. Recall from Chapter 2 that while traveling through the vortex, the velocity of a particle can be understood as having three components in a somewhat cylindrical coordinate system. Ignoring the effect of gravity, they are listed in order of magnitude: 1. the downstream velocity component parallel to both the axis of the vortex and the downstream direction, 2. the tangential velocity component which is directly related to the rotational velocity of the particle spiralling around the axis of the vortex, and 3. the radial velocity which is perpendicular to and directed toward the axis of the vortex. In order to describe the concept simply while maintaining an adequate understanding, the

resultant speed was assumed constant; that is the resultant magnitude of the three components will equal the original unidirectional velocity magnitude of 1 m/s. Estimating the tangential and radial velocities for a small particle unaffected by gravity as being 50 cm/s and 5 cm/s respectively, a calculation of the downstream component yields 86.5 cm/s. One can see, then, that the sheet thickness used in the flow quality measurements, on the order of millimeters, will fail to provide good results in this measurement. A camera viewing into a 1 mm sheet will not visualize any tangential component since the downstream velocity causes the particle to enter and leave the sheet before any tangential or radial velocity can be observed. For a 1 cm thickness the 86.5 cm/s particle traverses the sheet in 0.012 seconds, in which it travels 5.8 mm tangentially and 0.6 mm radially.

A 5.8 mm streak is long enough for visualization. However, in order to obtain velocity data from the streak it must be illuminated by light pulses from the chopper. These pulses must be much shorter than the time it takes a particle to travel through the sheet (0.012 sec) in order to illuminate the particle enough times for it to be imaged as very short dashes (at least three dashes for an unambiguous measurement). Therefore, it would be necessary to chop at about 250 Hz, which produces pulses of 1/500th of a second in length. During this pulse the particle has only a tangential displacement of 1 mm, which begins to approach the limits of the spatial resolution. For the measurements a lens with a very short focal length (33 mm) was used in conjunction with the cylindrical lens. This creates a light volume with the thickness on the order of a few centimeters. The final thickness was established at approximately 3 cm. Up to this point there has been some reservation in stating the specific thickness since the lens created a linearly increasing thickness with the thickness ranging from 2.5 cm to 4.5 cm over the measurement area. Also, a cross section of the light volume along a plane perpendicular to its propagation shows that the intensity spread was a broad Gaussian distribution whose boundaries are visually unclear. A

sketch, Figure 4.3, is included which shows the volume of light for vortex measurements with respect to the tunnel and wing. The figure shows the thick laser sheet expanding in the direction normal to the airflow but parallel to the rectangular wing. The camera's line of sight is into the flow, perpendicular to the light sheet so that the image plane is focused at the sheet.

For measuring tangential movement in the vortex, there are limitations, in that the streak lengths are significantly shorter than in the previous experiments, which measured flow velocities that were greater and more unidirectional. Although there was an argument earlier for varying the rate of the chopper for the flow quality analysis, there is much more of a limitation here with the choice of pulse lengths. The total unchopped streak lengths will rarely be much greater than a centimeter, and only the particles with the fastest tangential velocities will present a streak to be imaged. Keep in mind that it is important to measure as many particle velocities as possible. A fast chop rate is not reasonable for it would make the individual streaks too small. Slower particles would only appear as bright dots. On the other hand, recall that the chop rate must be fast enough to present the moving particles as a series of dashes so that velocity data extraction becomes possible. It was found through various trials that 75 Hz was an acceptable compromise between the two restrictions on the chopping rate.

All of the vortex measurements are made with the same chopping rate of 75 Hz. There were two measurements, made with the 3 cm thick sheet oriented perpendicular to the downstream flow:

1. Vortex Flow with Control Particles (Eccospheres), with 75 Hz Chopped Beam and a Rectangular Test Wing (@ 35 degrees)
2. Vortex Flow with Water, with 75 Hz Chopped Beam and a Rectangular Test Wing (@ 35 degrees)

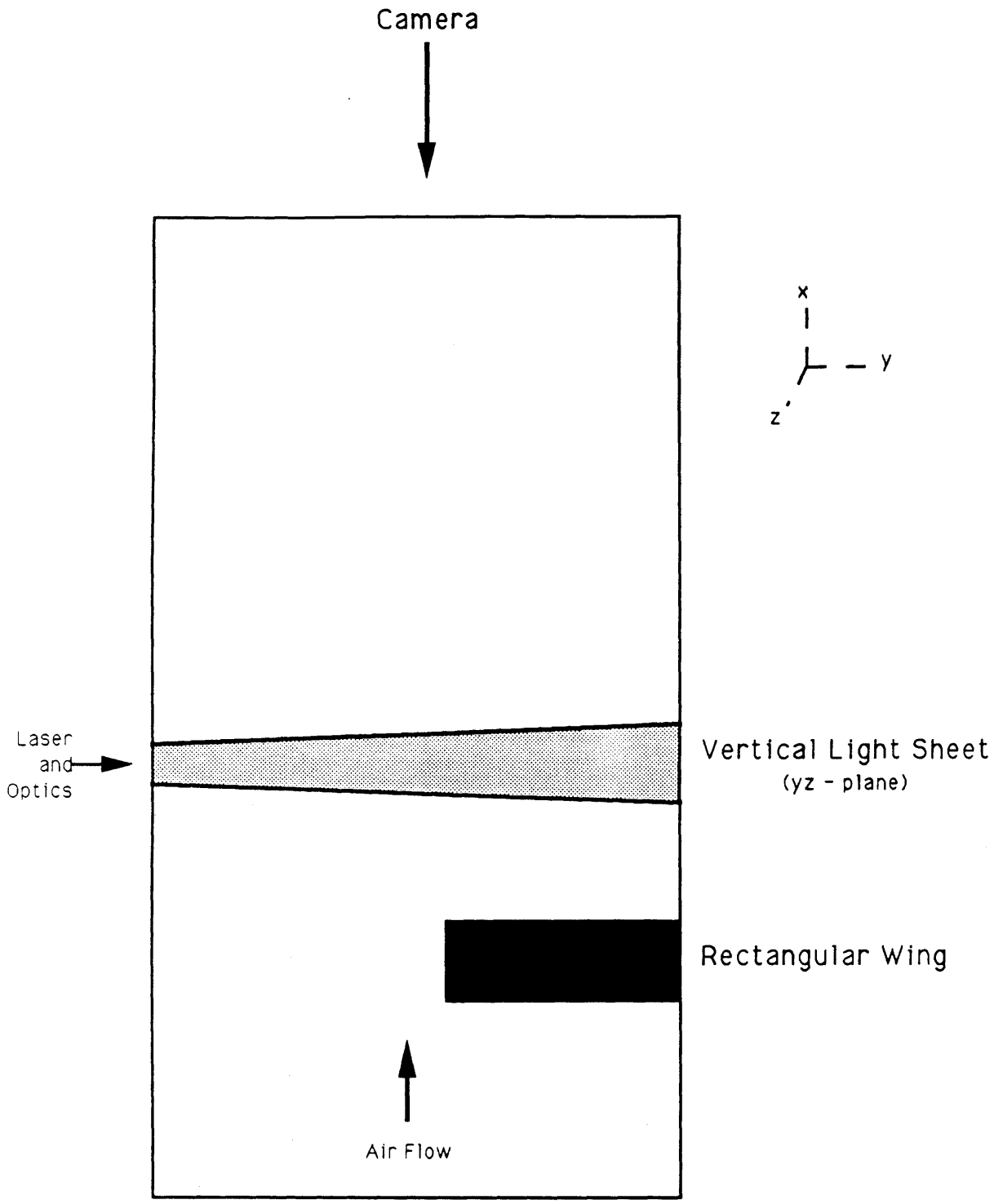
Camera
x
y
z
Laser
and
Optics
Vertical Light Sheet
(yz - plane)
Rectangular Wing
Air Flow

FIGURE 4.3

The experimental setup here was similar to that in Figure 4.1 except that the wing was placed in the flow at 35 degrees. The wing remained constant throughout the measurements in this investigation.

With the completion of these experiments and analysis of the results, it is possible to determine the velocities and trajectories of the control particles and the water droplets within vortices. The results of the preliminary and downstream measurements will be presented in the next two chapters, with an interpretation and qualitative analysis of the data. A more specific and quantitative analysis for the particles entrained in a vortex will be pursued in Chapter 6 (Vortex Data Analysis).

Therefore, the experiments are outlined that will lead to an evaluation of the response of water droplets to a vortex environment. The procedures begin with understanding the size of the control particles, and the accuracy, reliability and resolution of the chopper and digitized image of the LSV system. Once this data is known, particle entrainment in the downstream flow of the tunnel can be studied, and a characterization of the response of each particle given. With the completion of the downstream measurement, the flow will be understood well enough to measure and understand particle entrainment in vortices. The data from each of this experiments is analyzed in the next chapter.

# Chapter 5: Experimental Results

It is at this point in the investigation when the data measured in the experiments as outlined in Chapter 4 are presented. The primary objectives here are to present the results, primarily in graphical form, and perform a preliminary analysis. The bulk of the analysis will be undertaken in Chapter 6, where a determination is made as to whether there is enough evidence to suggest that water droplets respond differently from control particles in a wing-tip vortex environment. That cannot be accomplished until there is an understanding of how accurate the measurements are, since confidence in the velocity data hinges on the accuracy of the vortex measurement.

With this in mind, this chapter will first present the specifications of the control particles used in the experiment, the eccospheres. The specifications are based on information from the manufacturer, as well as on results from size measurements by microscope. A sample of the eccospheres is included in the form of photographs of the field of view of the microscope. Following the presentation of the size data and specifications, there will be an analysis of the results of the pulse length measurements in order to determine the temporal resolution of the measurement system. Then the analysis will move to calculating the spatial resolution and accuracy of the image processing technique designed for extraction of streak lengths from video images. Once this is accomplished, there will be an evaluation of the flow through the wind tunnel, without a wing by examining the data from both the 200 Hz and 75 Hz chopping rates, for both the control particles and the water droplets. It is important that results yield an expression of any instabilities and variations in the tunnel, and that the effect these anomalies may have on the structure and stability of the wing-tip vortex is evaluated. Most importantly, when the tunnel flow is analyzed, care must be taken to note the differences in the data for the two particle types, as well as the effect of the two different chopping rates. Using the results, the goal will be to attempt to isolate these two variables

(particle type and chopping rate), and understand each of these with respect to the tunnel flow. The next chapter will be devoted to understanding the vortex and how each of the flow seed types responds to it.

## 5.1: Preliminary and Supporting Experiments

### Particle Sizing

Photograph 5.1 and Table 5.1 show the microballoons (or specifically eccospheres, type R) and give their specifications. All of these specifications are acceptable for the calculations except for the data of the particle size distribution. Unfortunately the microballoons made available for the experiment are over five years old. This has potential problems since these particles are only guaranteed for a shelf life of six months. Moisture tends to cause the particles to clump together, thus giving a larger, nonspherical size distribution. It was, therefore important to take a sample of the volume of eccospheres and place them under a microscope (accuracy to 1 micron) to measure the sizes and note any clumping. The sample was taken from the middle of the volume of particles, after it had been lightly mixed. The results of the size measurements are presented graphically in Figure 5.1. This figure reveals most of the particles are between 10 and 30 microns (60.44%), smaller than the distribution stated in the specifications (where instead of sorting by number, the specifications give data based on sorting by weight). Additionally, there was no clumping found, and the data suggest that the particles fall within the size range that the calculations and predictions of Chapter 2 assumed. In fact, the measured sample yields sizes that are more promising than the manufacturer indicated since smaller particles follow the airflow more closely. The specifications given for the particles by the manufacturer will be accepted, except for the size distribution. When the calculations are performed, the sizes assumed will be consistent with the eccosphere microscope measurements.

## Photograph 5.1: Microscope Photographs of Eccospheres

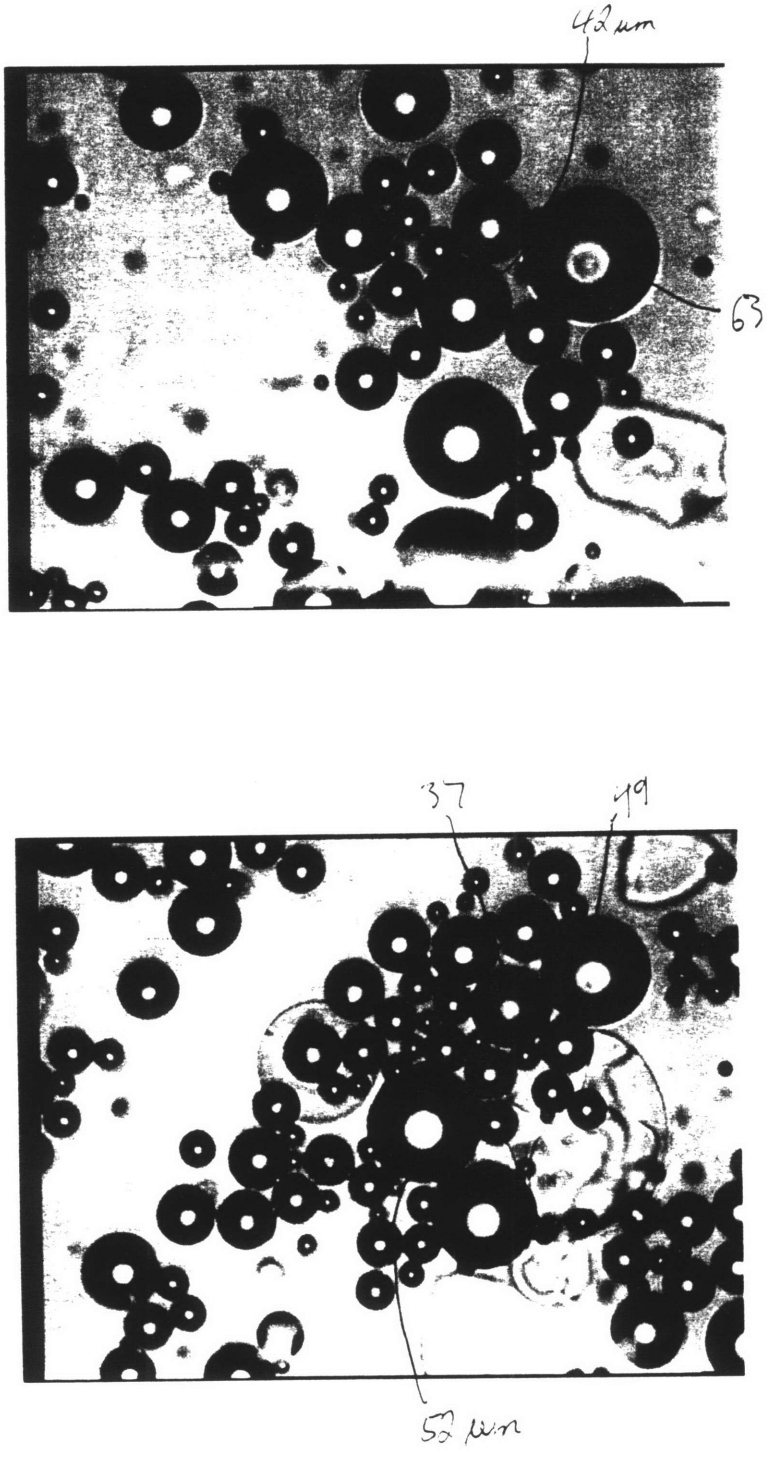

**Table 5.1 Microballoon (Eccosphere, type R) Specifications**

The True Particle Density (TPD) is the weight of a sample divided by the volume of liquid displaced by the sample. This corresponds to the weight of an average particle divided by its real volume.

TPD = 0.38 g/cc

Particle Size Range (% by Weight)

| | |
|---|---|
| Greater than 100 μm | 36% |
| 63 - 100 μm | 40% |
| 45 - 63 μm | 10% |
| Less than 45 μm | 14% |

These specifications are reproduced from data given by GRACE Syntactics, a unit of Emerson & Cuming, Inc., a subsidiary of W.R. Grace & Co.

## Figure 5.1: Histogram of Eccosphere Diameter Measurement

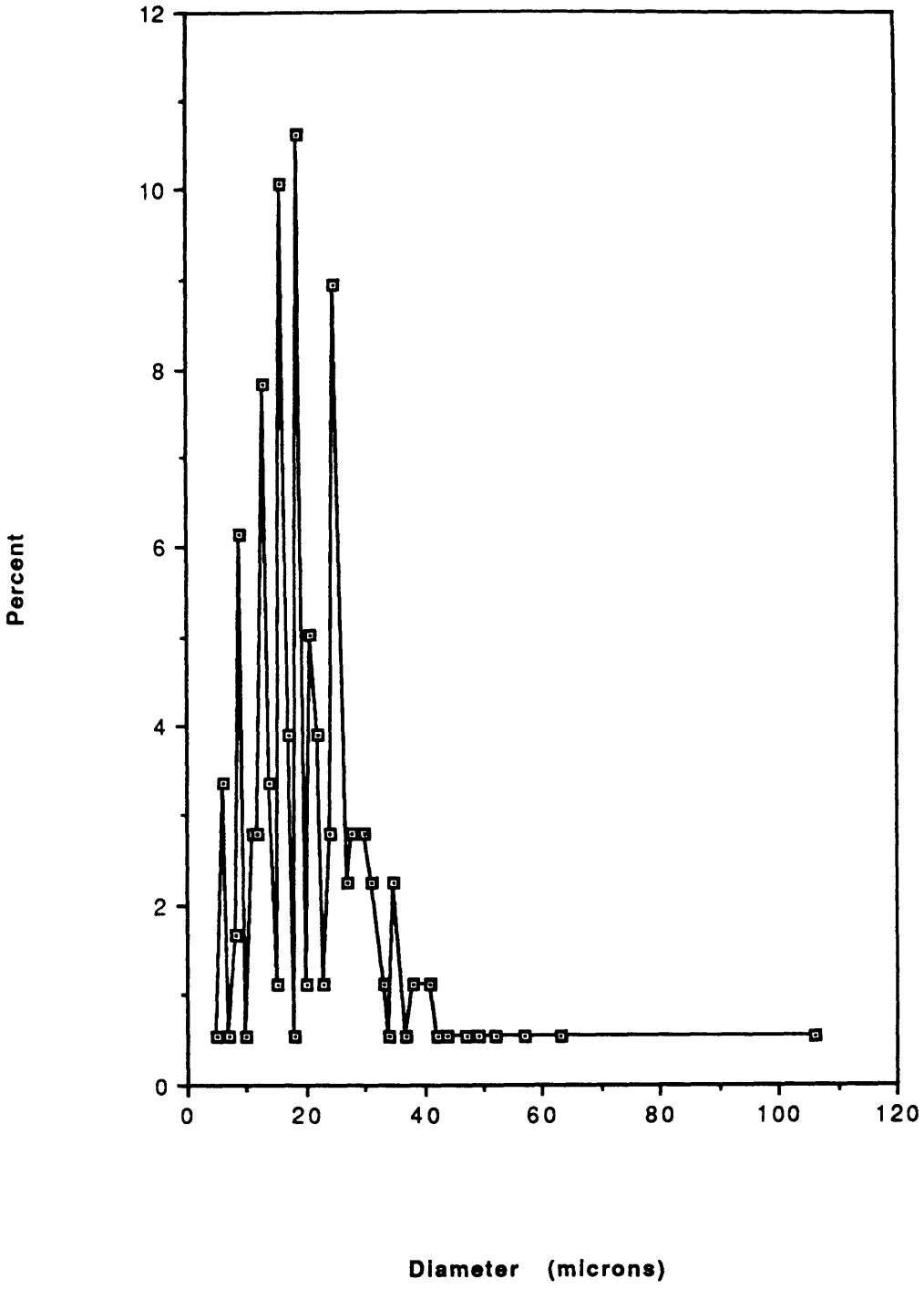

## Measurement of Pulse Widths

When examining the output of the ultrafast detector with the oscilloscope and time interval counter, it was possible to view the shape of the pulse, and the pulse repetition rate. Figure 5.2 is a schematic of the pulse signal. The pulse shape is trapezoidal, and the slope of the rise time varies with the chopping rate. The faster the chopping rate, the greater the slope of the rising pulse signal. It seems that the rise time is a function of the beam diameter interacting with the chopping wheel. The faster the wheel, the faster the full beam will be exposed to the detector. The wider the beam, the longer it will be for the full intensity to be exposed to the detector. The oscilloscope showed that the rise time for the 200 Hz chopping rate was 0.1 milliseconds while the rise time for the 75 Hz rate was 0.3 milliseconds.

Using the time interval counter, one is able to precisely examine the time interval between two events, with accuracy to nanoseconds if necessary. When examining the response from the detector is was found that the chopping rates are very stable over time, with only minor, infrequent fluctuations. Table 5.2 shows pulse width stability data for four chopping rates (200 Hz, 150 Hz, 100 Hz, and 75 Hz). Since the fluctuations are minor, rarely exceeding 1% of the indicated value, one can assume that the pulse widths are constant values.

Given these data, the temporal limits to the accuracy of the velocity measurements can be calculated. For pulse width, the full width of the half maximum (FWHM) will be used. For the 200 Hz chopped beam, the width is 2.45 $\pm$ 0.0025 milliseconds, which corresponds to 1/408th of a second or a chopping rate of 204 Hz. The fluctuations of the chopper are so small that they can be ignored. For the 75 Hz chop, the width is 6.51 $\pm$ 0.0833 milliseconds. This corresponds to 1/154th of a second or 77 Hz. Although there is more of a fluctuation here in the chopping rate, its effect is still insignificant for the low velocities that are being used in this investigation.

Pulse Lengths for 200 Hz and 75 Hz

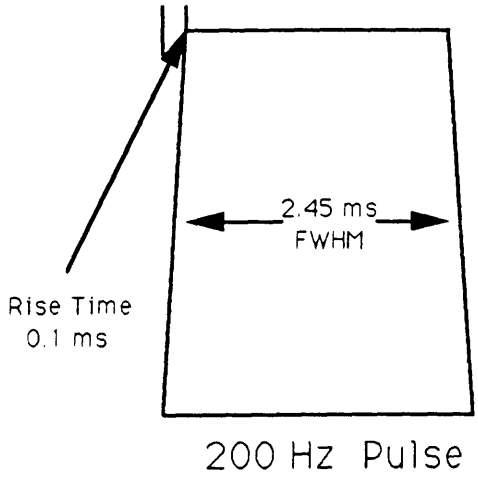


200 Hz Pulse

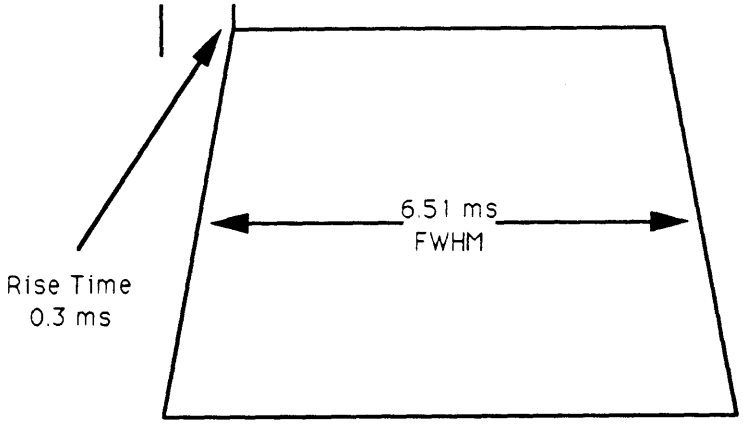


75 Hz Pulse

Figure 5.2

**Table 5.2 Pulse Width (PW) Fluctuations of the EG&G Mechanical Chopper**

| Chop Rate | Expected PW | Maximum PW | Minimum PW |
|---|---|---|---|
| 200 Hz | 5.000 ms | 5.004 ms | 4.995 ms |
| 150 Hz | 6.667 ms | 6.680 ms | 6.658 ms |
| 100 Hz | 10.000 ms | 10.020 ms | 9.990 ms |
| 75 Hz | 13.333 ms | 13.500 ms | 13.311 ms |

## Grid Mapping at the Image Plane: The Pin Cushion Effect

Photograph 5.2 shows the 1.3 cm x 1.3 cm grid that was imaged at same plane that the light sheet is usually propagated. For this image, for the downstream flow measurements, the camera was 87 cm from the grid. A 105X lens was focused at the plane of the grid. Figure 5.3 shows the pixel lengths along the vertical and horizontal axes of the grid. In this diagram one can note the expansion of the lengths as a function of the distance from the center of the field of view. The scale at the center of the screen is 70 pixels per side of the square, or 70 pixels per 1.3 cm. This ratio is to be used as the ratio to determine the spatial resolution. For the streak calculations, the length of the streak in pixels was multiplied by the ratio 1.3/Scale, where Scale is the number of pixels per side of the square for the region of the field of view where the particle was found (in the center Scale = 70). Although the examples given here are for the horizontal components, the scaling calculations were also made for the vertical component of a streak length.

## 5.2: Spatial Resolution of Streak Length Measurements

Once a video image is digitized, it is represented by a finite array of pixels. It is now in a form that can be manipulated using many of the operations of image processing. For the use of an image of dashes whose lengths are to be measured, an understanding is required of the resolution limits of the digitized image. In order to measure the streak and dash lengths. The cursor will be moved to any two locations on either end of the streak in question, then the coordinates of the two points will be recorded. The streak length is the distance between the two coordinate points. The image processing allows any section of a frame to be magnified and examined closely to facilitate greater accuracy in assuring that the cursor is positioned correctly.

## Photograph 5.2: Grid Used for Scaling and Correction of the Pin Cushion Effect

(Scale: Each Square is 1.3 cm x 1.3 cm)

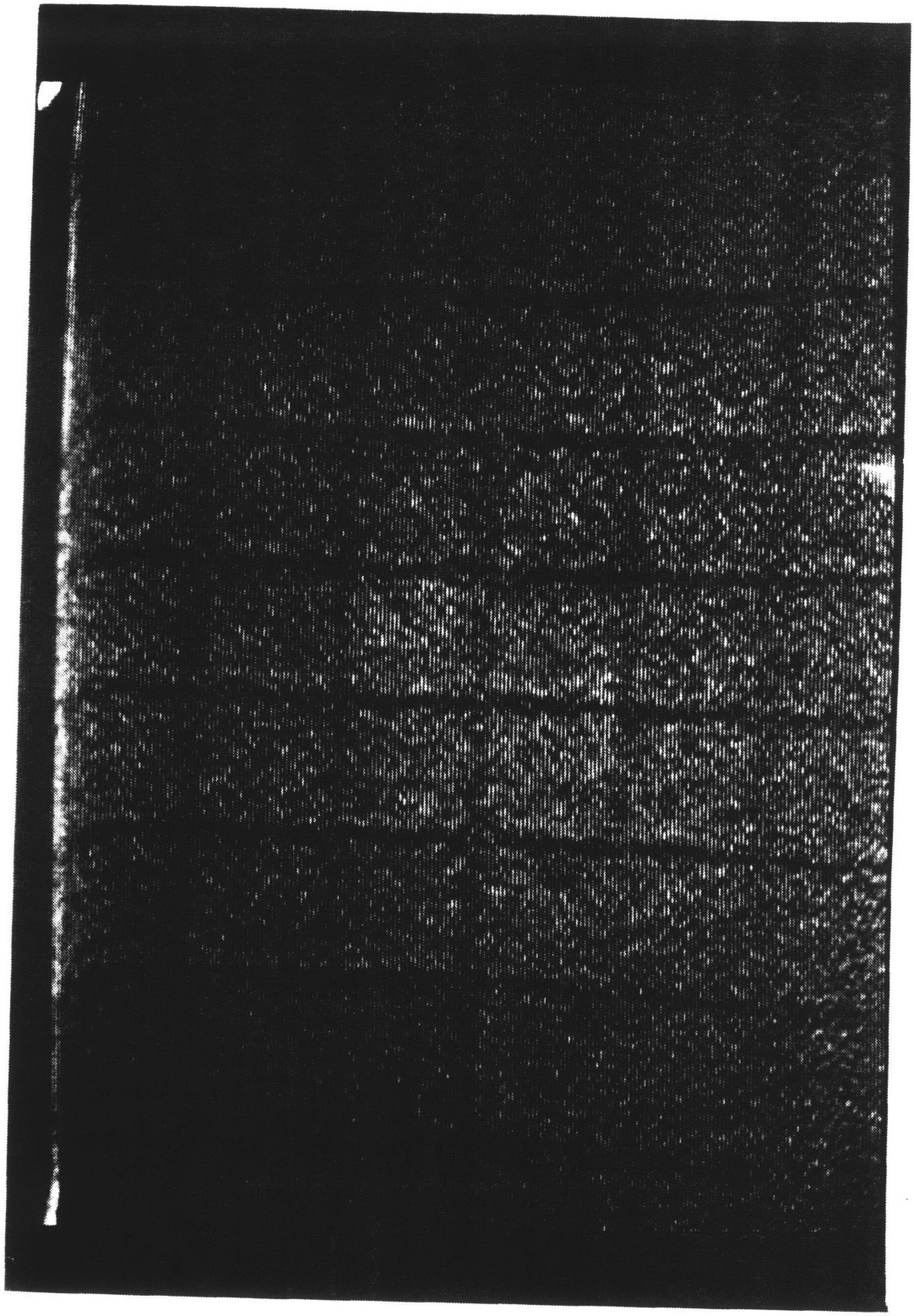

Example of the Mapping of the Scaling Grid
(See Photograph 5.2)

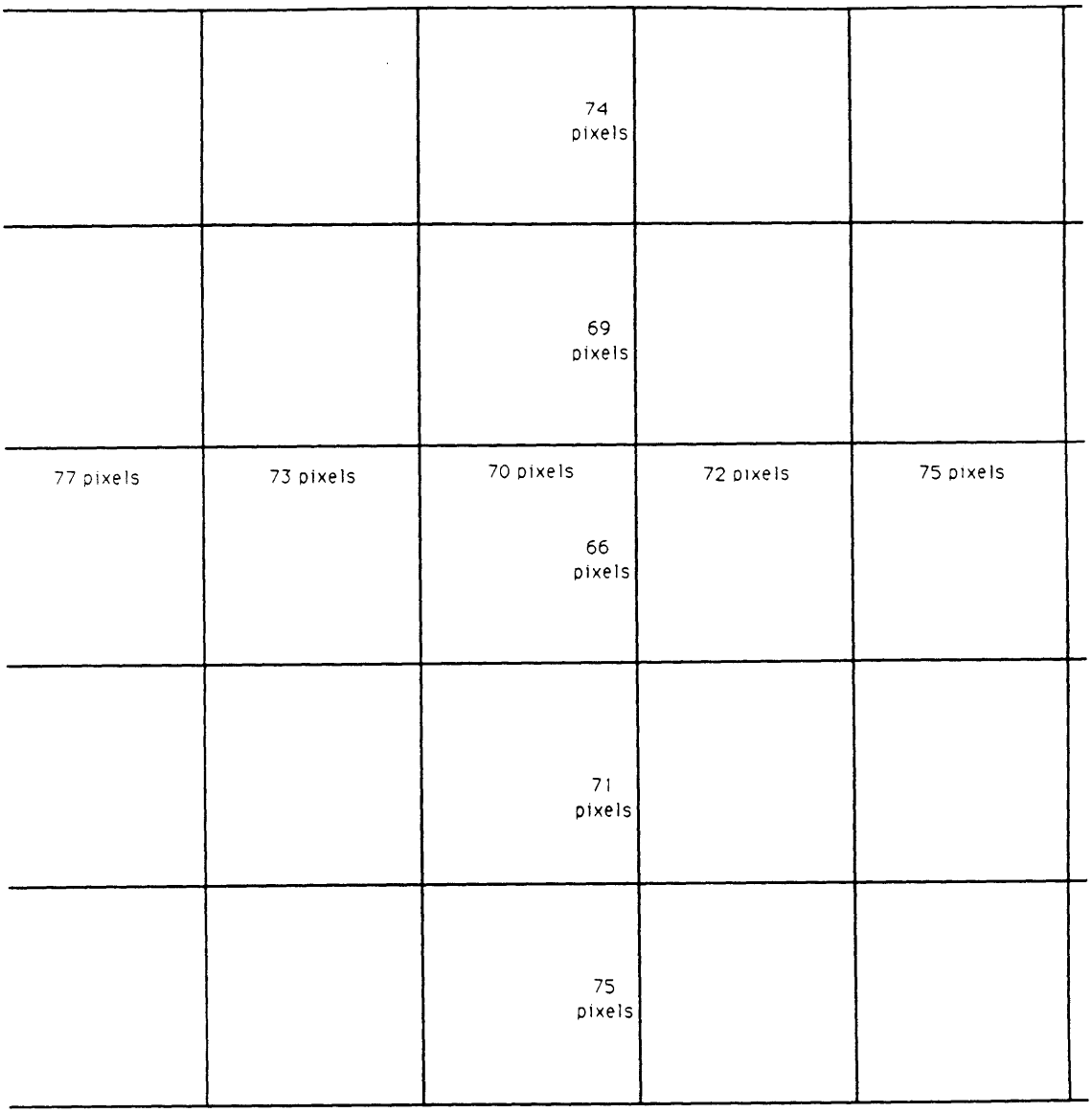


Figure 5.3

From the grid measurements, the number of pixels that are equal to 1.3 cm in the center of the field of view is 70 (horizontally). Therefore, the resolution is 70/13mm or over 5 pixels per millimeter, which satisfies the desire that this technique be an improvement over measurement by a typical ruler, which cannot measure lengths less than a millimeter. Now there is enough information from Sections 5.1 to determine the velocity resolution for each chop rate; that is, calculations can be performed to find out the velocity the length of a single pixel represents. The equation is as follows:

(1 pixel) x (1.3cm/70) / (Pulse Width) = Lowest Unit of Velocity

For 204 Hz,

(1 pixel) x (1.3cm/70) / (2.45 ms) = 7.5802 cm/s

For 77 Hz,

(1 pixel) x (1.3cm/70) / (6.51 ms) = 2.8528 cm/s

Not only do these values represent the lowest velocity that can be measured, but they also tell us that all of the velocity measurements will be expressed in units of these base values. For instance, a dash 10 pixels long from a 200 Hz chopped beam is traveling 75.802 $\pm$ 7.58 cm/s, which equates to a precision of 5%. But the fractional precision improves as the velocity increases. A 100 pixel length dash translates into a 758.02 $\pm$ 7.58 cm/s particle. Here the possible error is much less, at 0.5 %. Hence, one can expect that the data extracted from the streaks at 75 Hz will be more precise than at 200 Hz, but both should yield the same value.

## 5.3: Downstream Flow Measurements at 200 Hz

Photographs 5.3 and 5.4 show a control particle in successive fields (1/60th of a second each). The laser is being chopped at 200 Hz, although the pulses are actually 1/408th of a second long. As was stated in Chapter 3, the LSV visualizing and measurement system provides ample information for velocity extraction. It was calculated that this particle is traveling at 148.2 cm/s. Each dash is 3.63 mm long in real space, although the zoom lens on the ISIT camera magnified the image. To understand the flow, 100 particles were measured in the same way. The results are presented in Figure 5.4, a histogram of the downstream velocities of the control particles. Figure 5.5 presents a histogram of the water droplets and Figure 5.6 presents a combined histogram of both particles. During the measurements, an error of1 pixel was estimated. For the 204 Hz pulse, this equates to a possible error of 7.58 cm/s.

Initially there is a concern over the range of velocities measured. The average velocities and ranges for the control particles and the water droplets are tabulated below:

Control Particles

Fastest Particle: 212.24 cm/s
Slowest Particle: 96.80 cm/s
Average Particle Velocity: 148.60 cm/s

Water Particles

Fastest Particle: 216.03 cm/s
Slowest Particle: 94.25 cm/s
Average Particle Velocity: 151.78 cm/s

By examining the velocity histograms, it was found that the downstream velocities of each particle type were similar. Figure 5.6 suggests from its distribution that the particle types both follow the flow equally well. There are differences however. The control particle histogram has a defined peak with 26% of the

**Photograph 5.3: Control Particle with 200 Hz Laser Chop; Field 1 of 2**

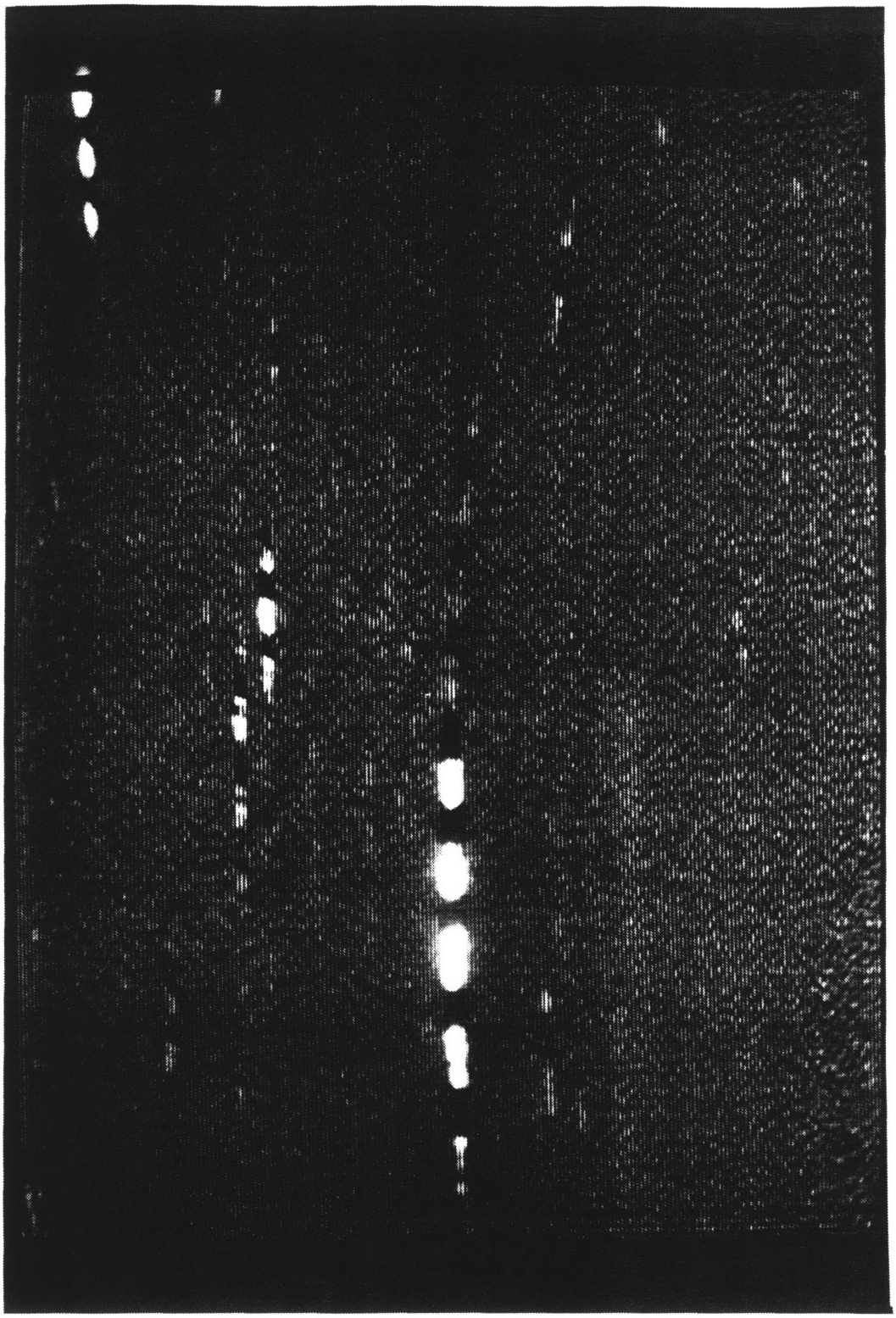

**Photograph 5.4: Control Particle with 200 Hz Laser Chop; Field 2 of 2**

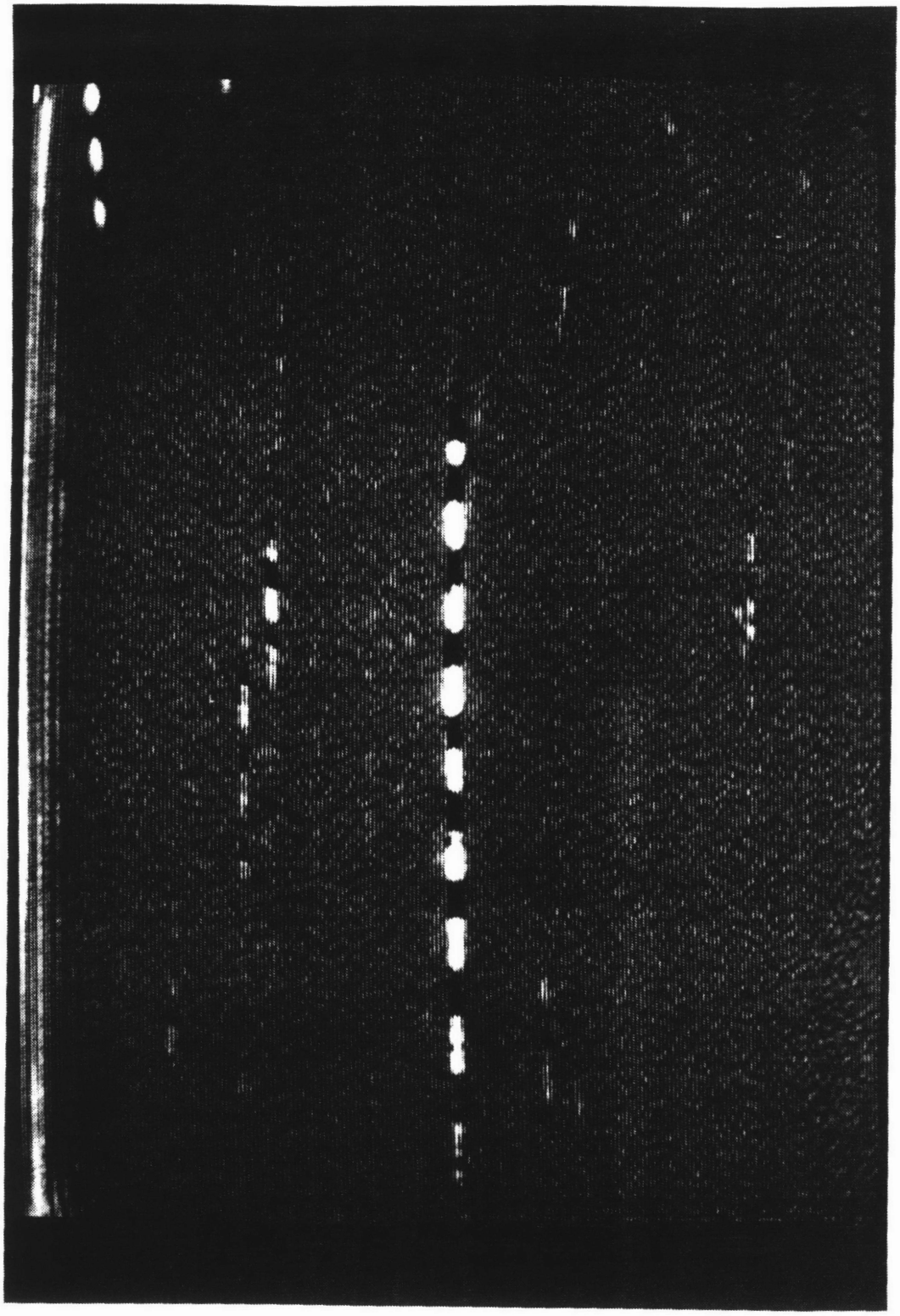

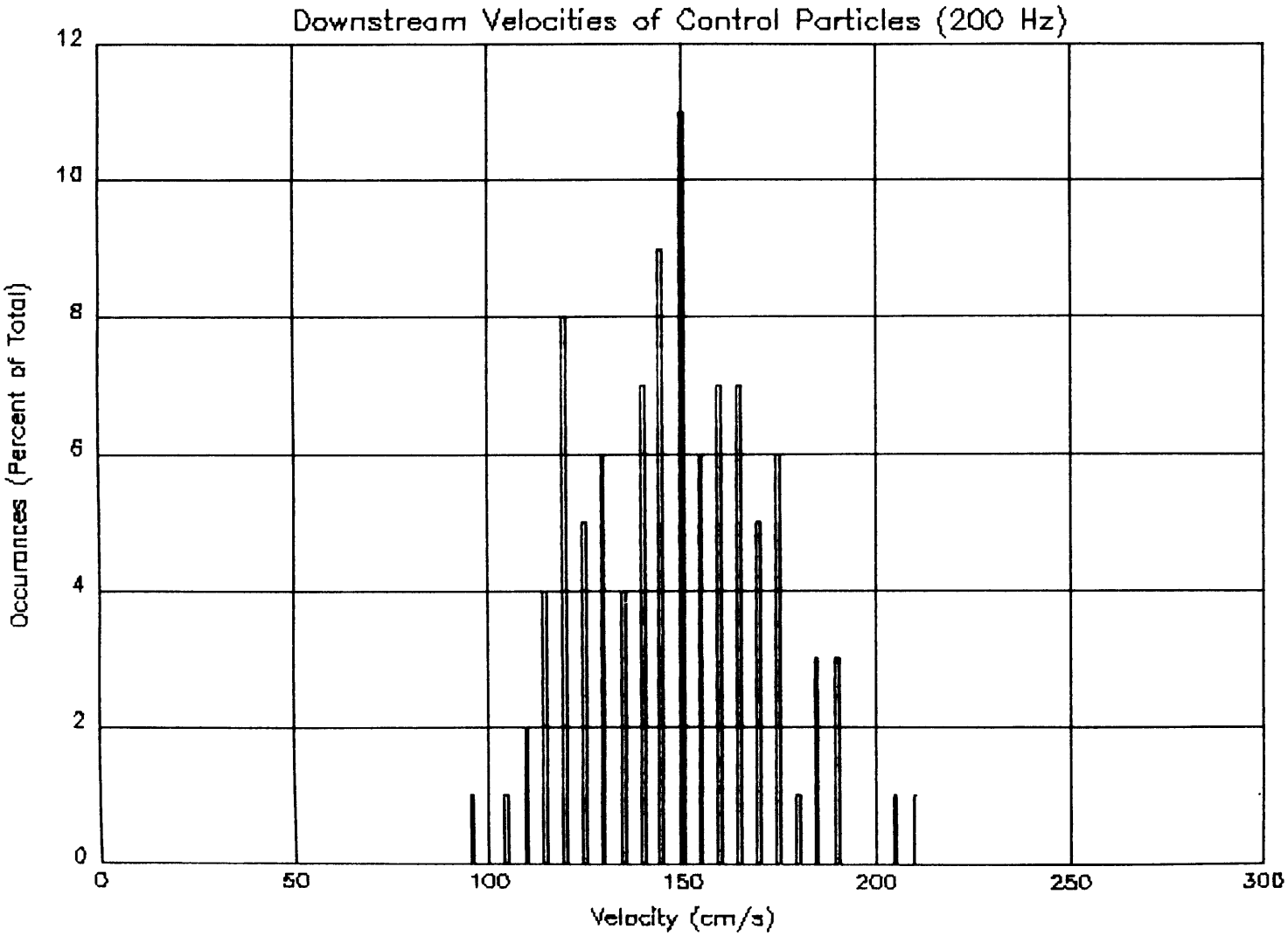
Downstream Velocities of Control Particles (200 Hz)
Occurances (Percent of Total)
12
10
8
6
4
2
0
0
50
100
150
200
250
300
Velocity (cm/s)

**Figure 5.4**

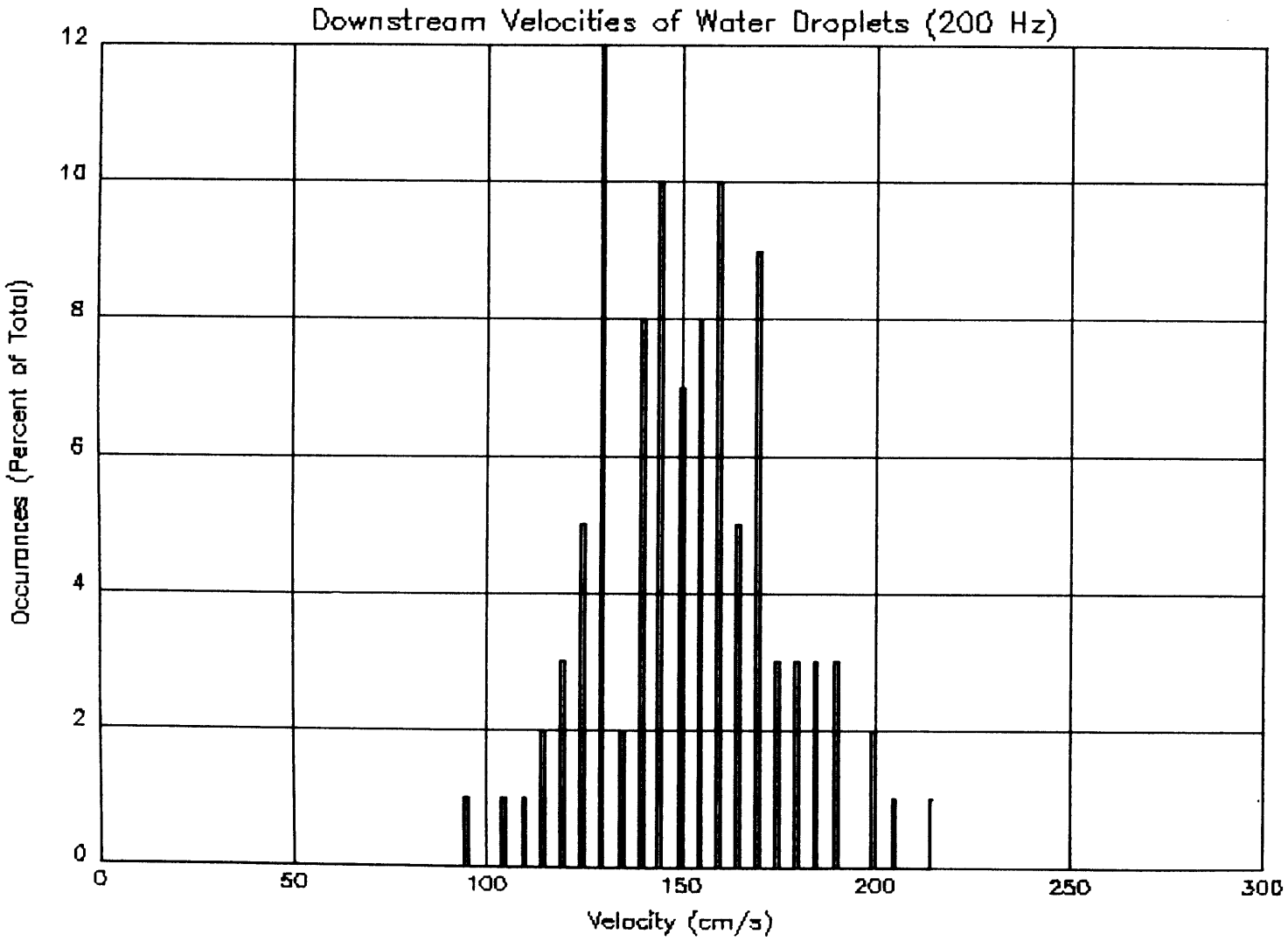
Downstream Velocities of Water Droplets (200 Hz)
Occurances (Percent of Total)
12
10
8
6
4
2
0
0
50
100
150
200
250
300
Velocity (cm/s)

**Figure 5.5**

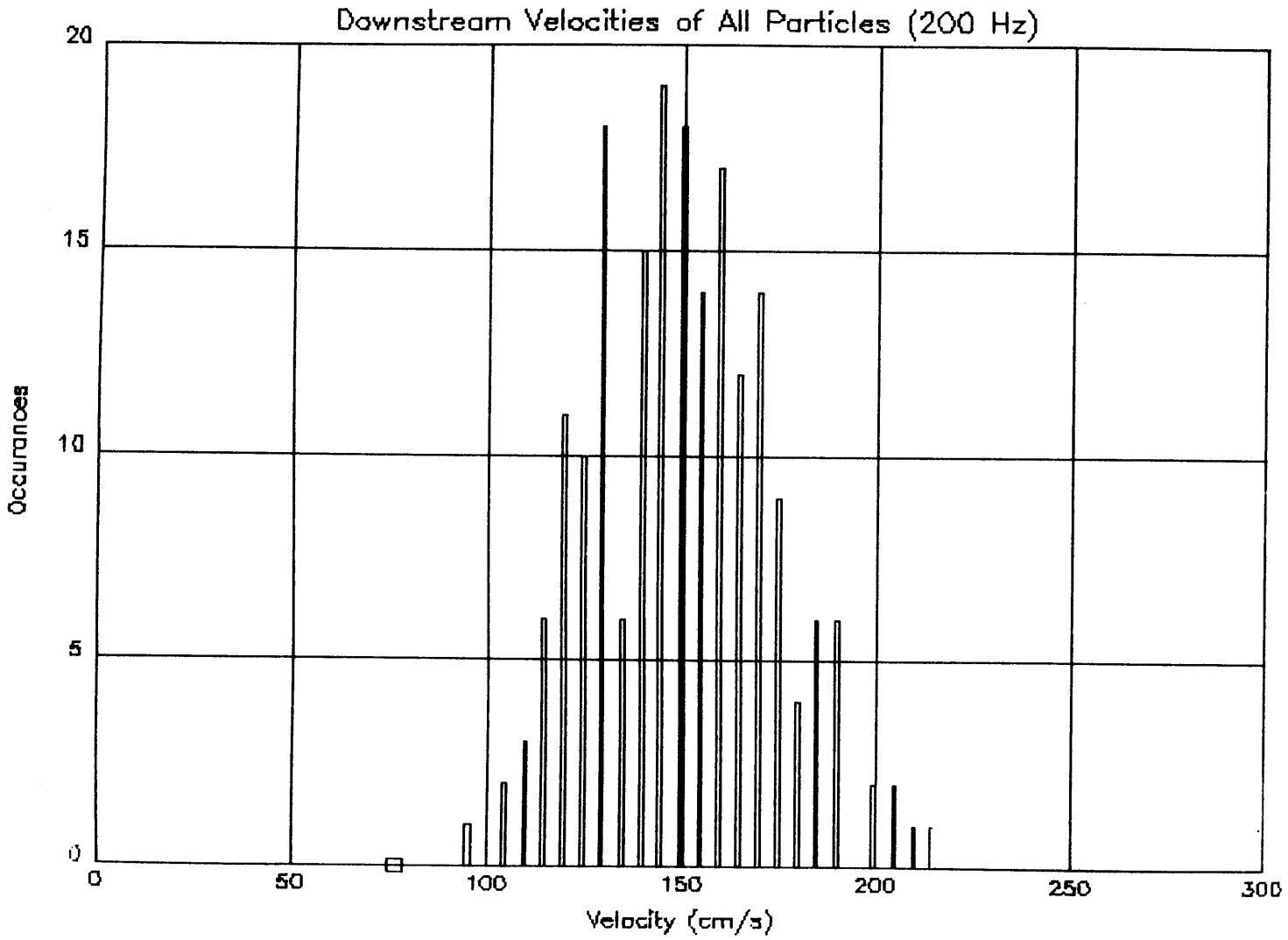
Downstream Velocities of All Particles (200 Hz)
Occurances
20
15
10
5
0
0
50
100
150
200
250
300
Velocity (cm/s)

Figure 5.6

particles traveling from 145 cm/s to 155 cm/s. The FWHM of the distribution was approximately 55 cm/s (87% of the particles fall within this width). This variance suggests that the wind tunnel will not be capable of supporting a stable vortex. However, upon frame by frame examination it is found that the control particles are traveling at the same velocity for each frame. A typical image had particle velocities of 117.9 cm/s, 117 cm/s, 121.6 cm/s, 125.3 cm/s, 120.3 cm/s, 132.7 cm/s and 117.9 cm/s. The velocity range here within the field of view is 14.8 cm/s, or about two pixels. The velocity does not remain constant over a period of time, but it is uniform, maintaining a given velocity for a few seconds before a velocity change is measured.

The water droplets seemed to flow similarly overall, but there were some differences. The histogram is less broad, with a FWHM of 40 cm/s and 64% of the particles falling within that width. The smaller width may be due to the inertia of the water droplets, presumably greater than that of the control particles. In other words, a water droplet is less prone to decrease its velocity. Thus, since the water droplets will accelerate and deaccelerate slower than the control particles, it is likely that their velocities are less variant.

Another difference between the seeds was in the trajectories of the particles. There was a significant number of water droplet dashes that exhibited an angle of declination. It was found that 14% of the water droplets measured had an angle of declination greater than 15 degrees. These descending particles are the heaviest water droplets of the distribution. They are influenced by the force of gravity as they travel downstream, forcing them to display a projectile-like trajectory. Photograph 5.5 shows two water droplets traveling with an angle of declination of approximately 15 degrees.

Whereas the control particles exhibited instantaneously uniform velocity profiles, the water droplets did not. A typical frame reveals a wide variance in the velocities of the individual particles. A typical frame of water droplets reveals 169.2 cm/s, 151.6 cm/s, 132.7 cm/s, 159.2 cm/s, and 147.4 cm/s, resulting in

**Photograph 5.5: Water Droplets with 200 Hz Laser Chop; Angle of Declination of 15 Degrees**

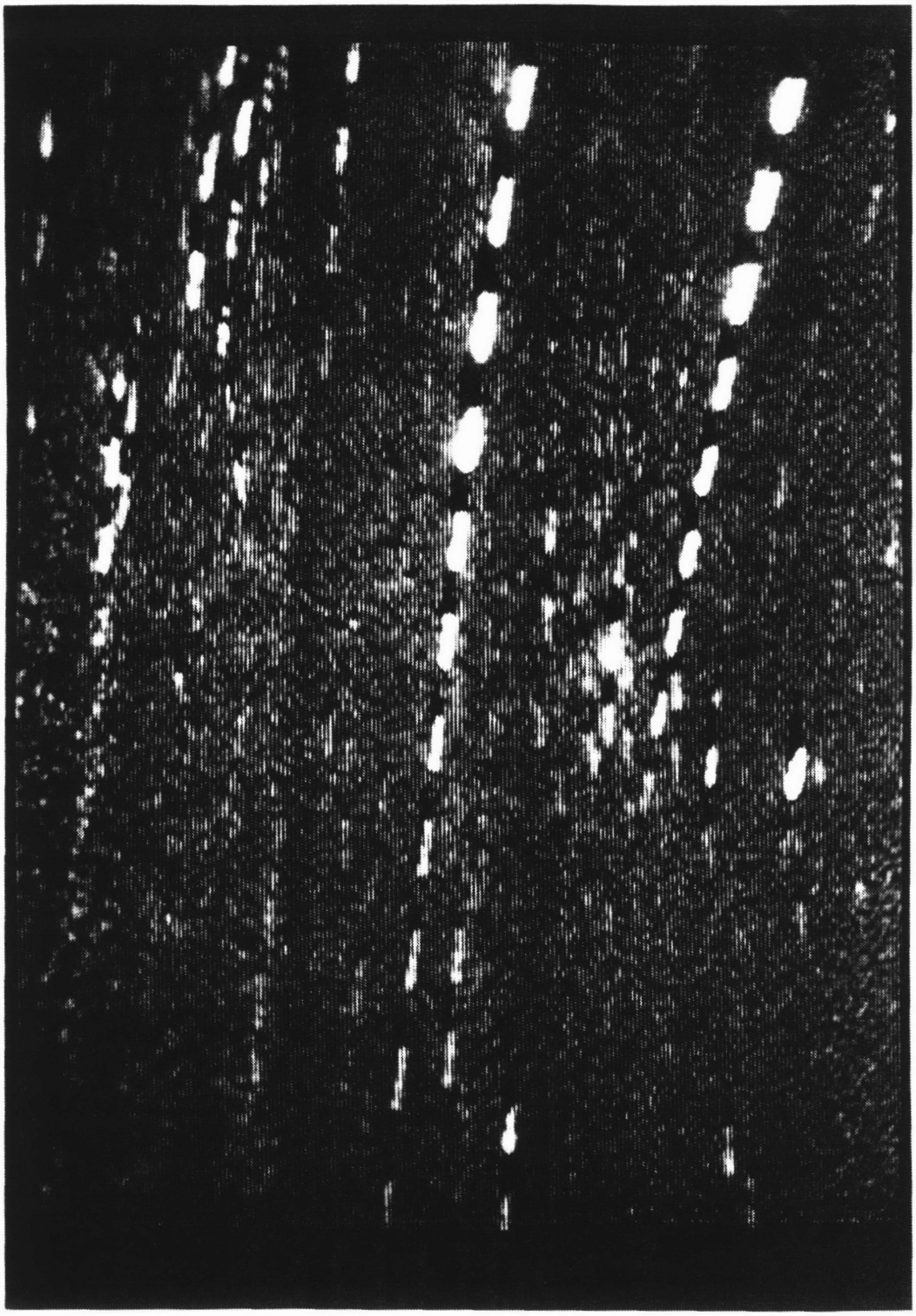

a velocity range of 36.5 cm/s within a field of view that is approximately 10 x 8 cm. This range seems to be due to the various sizes of the water droplets entrained in the flow. In Section 5.5, these findings will be used with the findings at 77 Hz to draw implications of the downstream particle velocity data, and provide a background for the understanding of the vortex data.

## 5.4: Downstream Flow Measurements at 75 Hz

Figures 5.7 - 5.9 show data for the particles traveling downstream in a sheet chopped at 75 Hz. Photograph 5.6 shows a set of water droplets traveling downstream with the 75 Hz chop. As was done for the 204 Hz data, the range and average velocities for each particle type are given below:

Control Particles
- Fastest Particle: 207.68 cm/s
- Slowest Particle: 97.07 cm/s
- Average Particle Velocity: 148.42 cm/s

Water Particles
- Fastest Particle: 214.38 cm/s
- Slowest Particle: 110.64 cm/s
- Average Particle Velocity: 158.83 cm/s

The similarity between the data at 204 Hz and 77 Hz shows the consistency of the LSV measurements. Figures 5.7, 5.8, and 5.9, are histograms of the control particles, water particles, and both particles, respectively. These histograms of the 77 Hz data, which provides a greater spatial resolution (1 pixel = 2.58 cm/s) shows histogram peaks with narrower widths than for 204 Hz. The control particle histogram (Figure 5.7) has a width of 50 cm/s (65% of the velocities fall within this width) and agrees very well with the width of the data at 204 Hz. The water droplet velocity histogram has a width of 35 cm/s, with 71% of all the particles falling within this range.

**Figure 5.7**

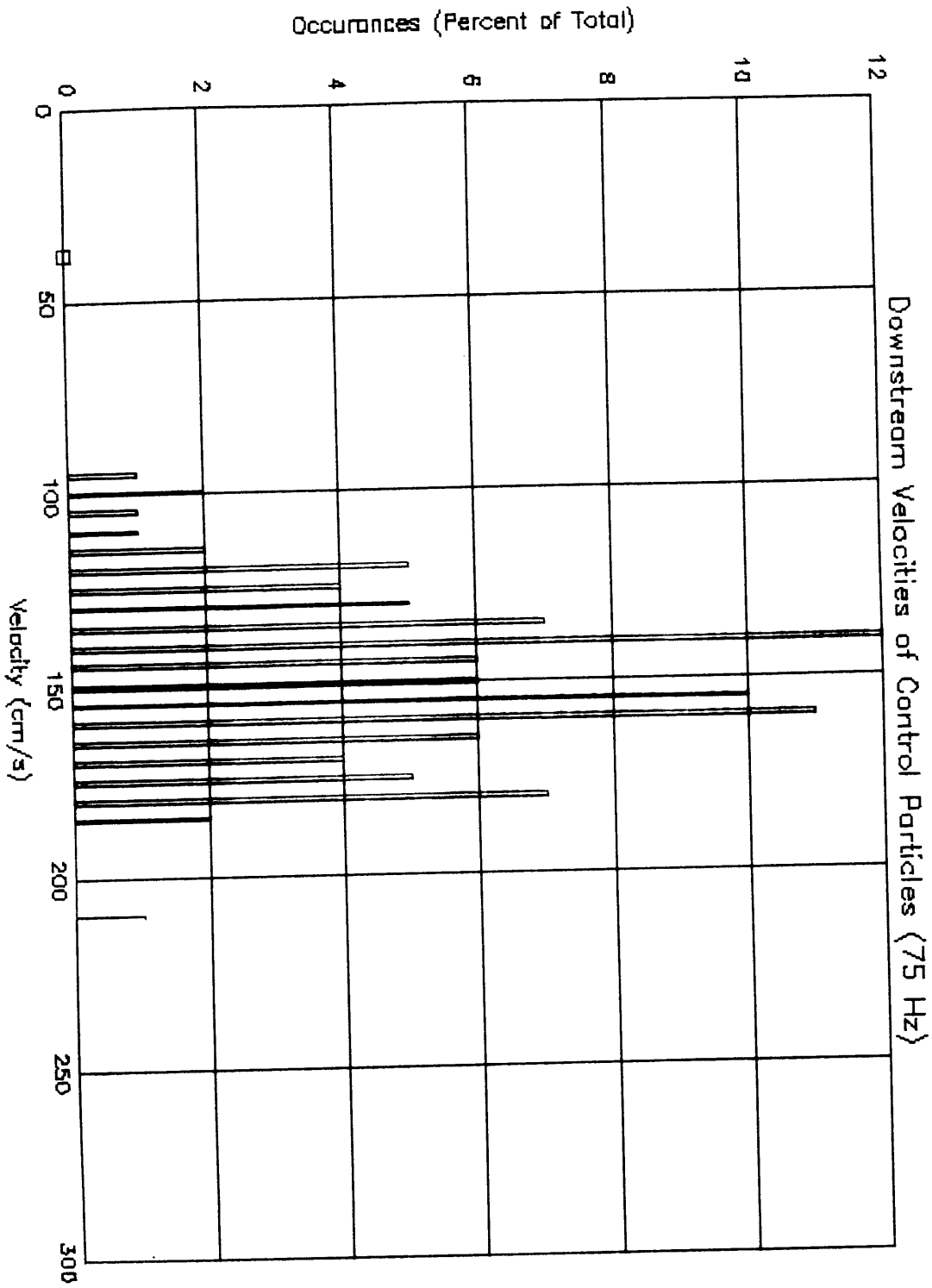
Occurances (Percent of Total)
0
2
4
6
8
10
12
Velocity (cm/s)
0
50
100
150
200
250
300
Downstream Velocities of Control Particles (75 Hz)

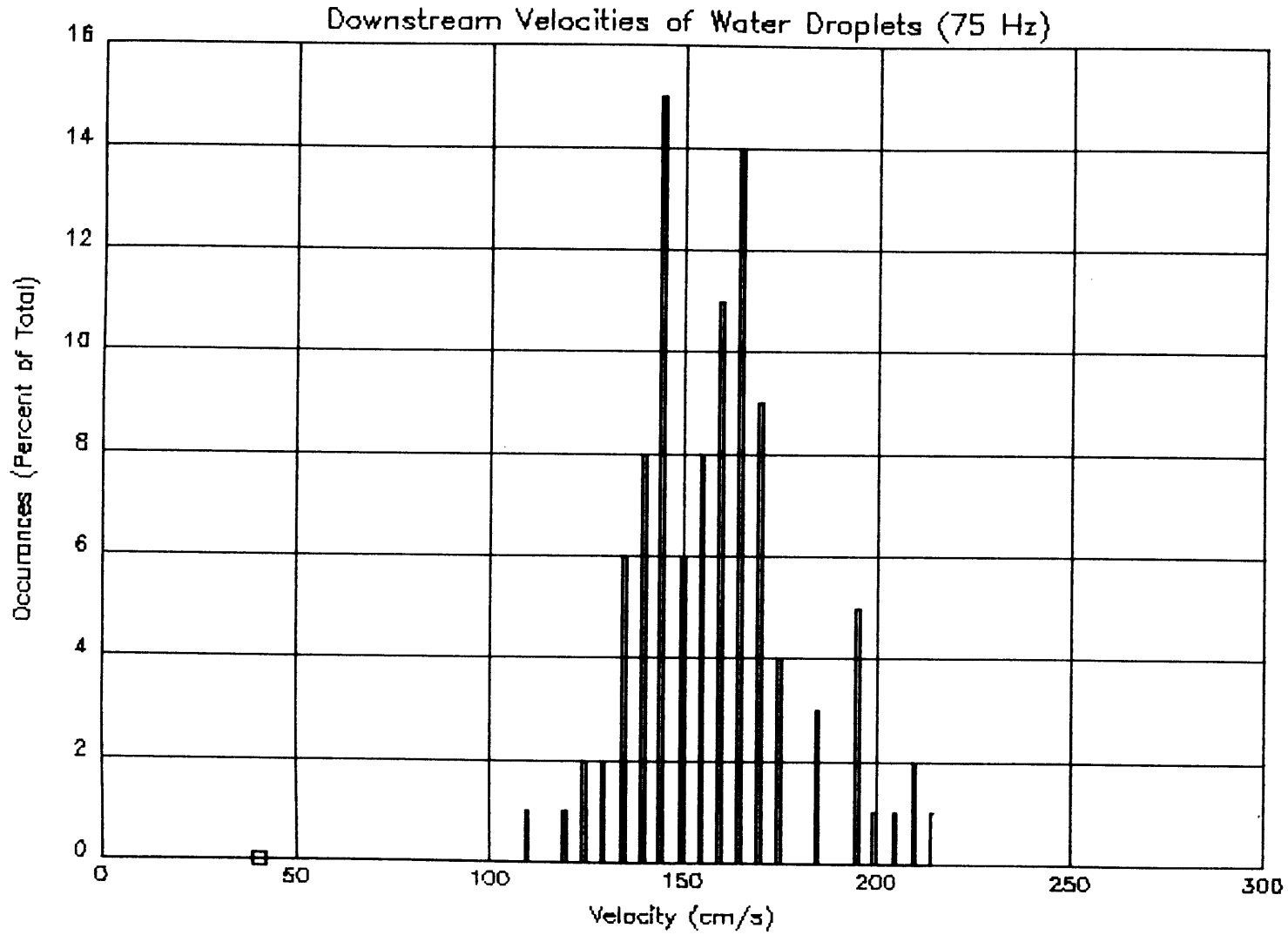
Downstream Velocities of Water Droplets (75 Hz)
Occurances (Percent of Total)
0
2
4
6
8
10
12
14
16
0
50
100
150
200
250
300
Velocity (cm/s)

**Figure 5.8**

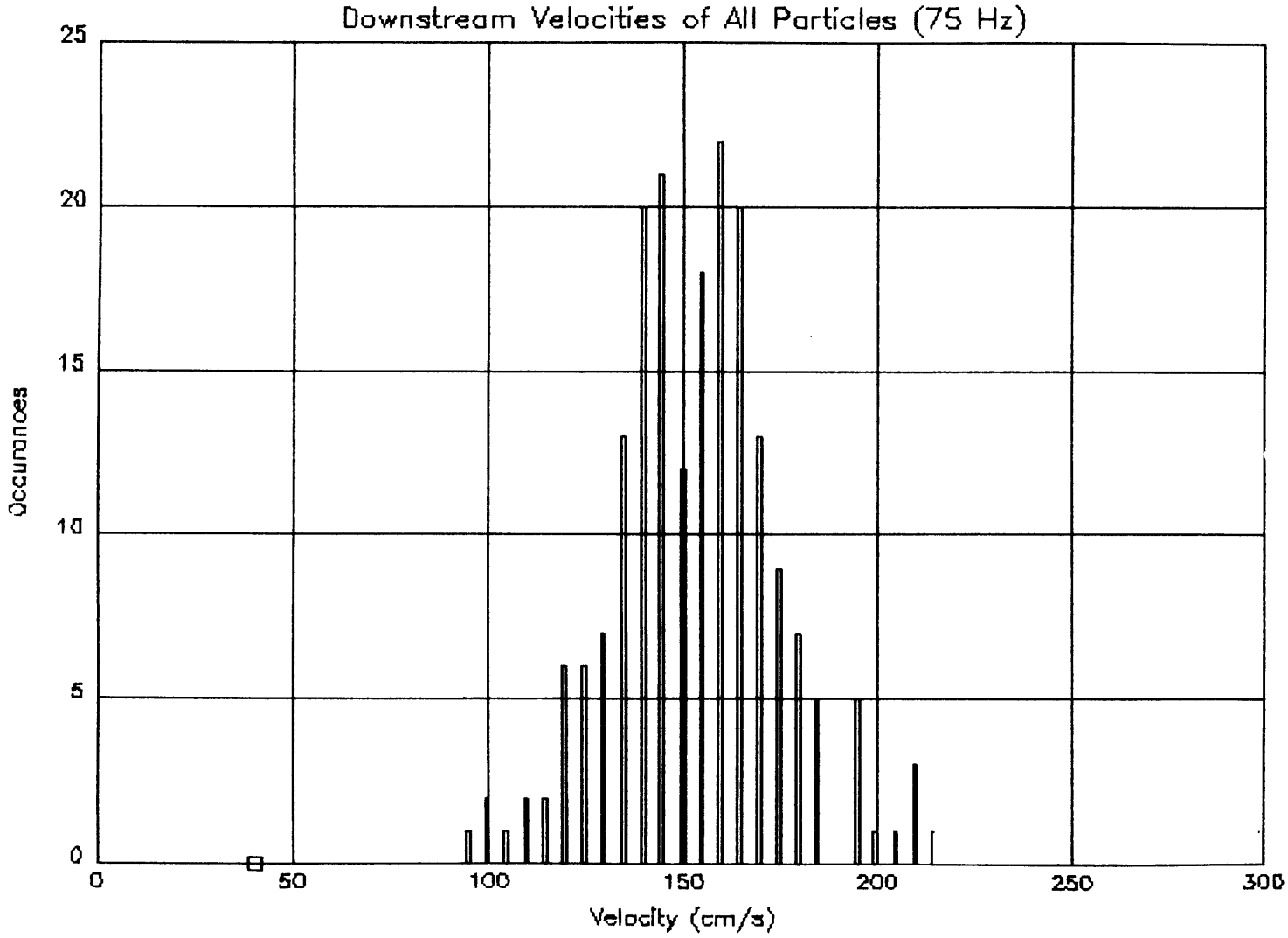
Downstream Velocities of All Particles (75 Hz)
Occurrences
25
20
15
10
5
0
0
50
100
150
200
250
300
Velocity (cm/s)

Figure 5.9

**Photograph 5.6: Water Droplets with 75 Hz Laser Chop**

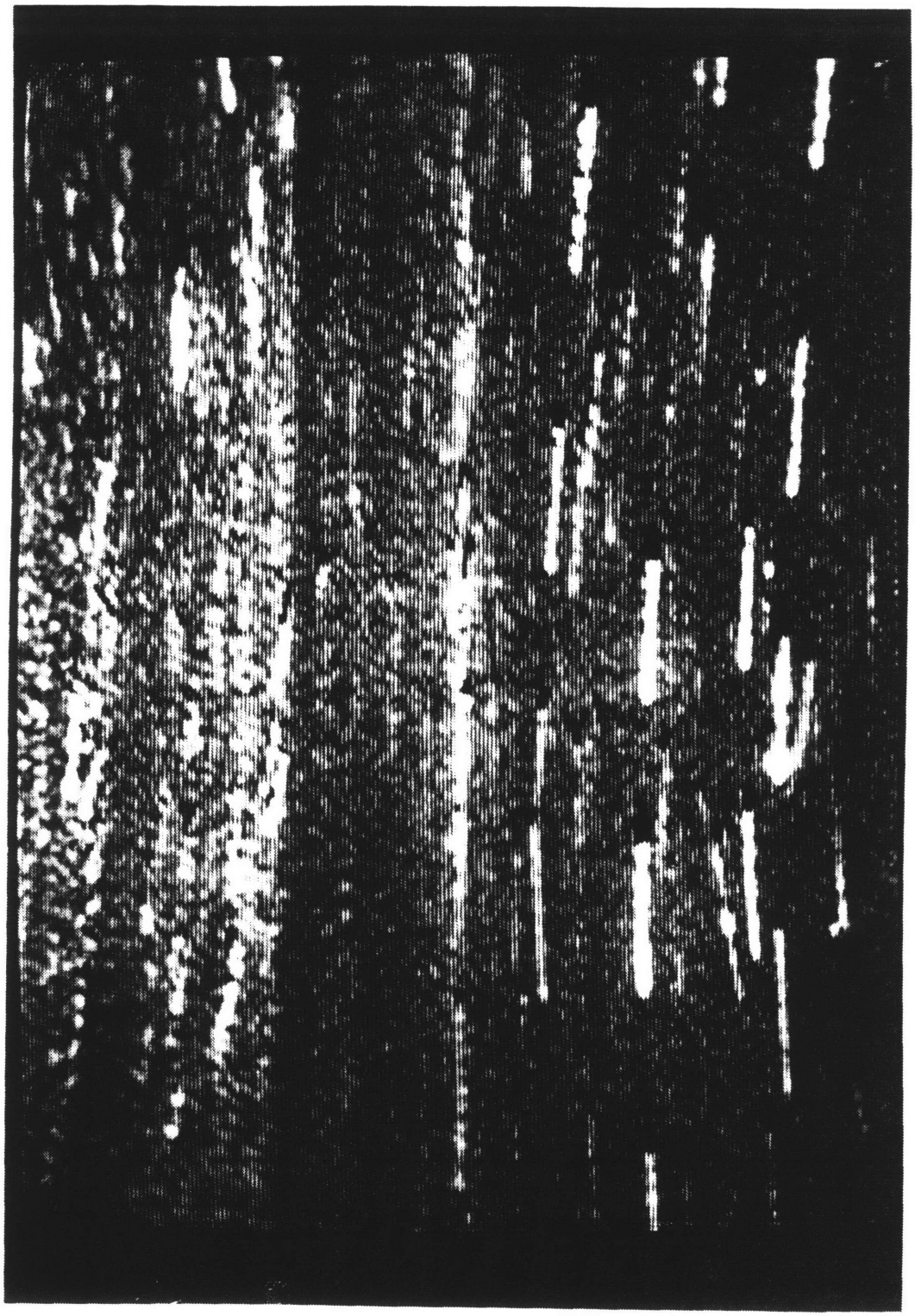

Here, the ratio between the widths of the control particles and water droplets are the same as the widths measured with the 200 Hz chop. This confirms that the water droplets tend to travel at velocities that vary less than the control particles as they travel downstream. The nonuniformity was also evident here. The differences associated with the angle of declination are much less however. According to the data from the 75 Hz chopping, only 7% of the water droplets have an angle greater than 15 degrees and even 3% of the control particles were found to have comparable angles of declination.

## 5.5 Consequences of Downstream Observations

The downstream velocity data provides very valuable information for our understanding of the wind tunnel flow. To gain more insight into the effect of the downstream flow, we recall the derivation of wing-tip vortex tangential velocities of Chapter 2. Recall that theoretical tangential velocity of the air,

$$w_\theta = (\Gamma_o/2\pi r), \text{ for } r \geq r_c, \qquad [2.11b]$$

where again, $\Gamma_o$ is the circulation constant, r is the radius of the velocity, and the radius of the core ($r_c$), is defined as the location of the maximum velocity. In order to obtain the circulation constant we also recall Equation [2.10], which defines the dimensionless lift distribution ($\gamma$) as

$$\gamma(\eta) = \Gamma(y)/(bw_a),$$

where

$w_a$ is the downstream air speed,

and

b is the wing span.

From the downstream data, we select a typical value of 150 cm/s as our downstream air speed. Since the wing span is 12 cm and the dimensionless lift distribution is 0.26, we solve for the circulation

$$\Gamma_o = 468.$$

Thus for a radius of 2 cm we find the tangential velocity

$$w_\theta = 468/(2\pi(2)) = 37.24 \text{ cm/s.}$$

As has been discovered, the downstream velocity exhibits a significant variation over time. Using 210 cm/s to 95 cm/s as the range of downstream velocities, the corresponding circulation constants and tangential velocities are as follows

For $w_\theta = 210$ cm/s,

$$\Gamma_o = 655$$

and

$$w_\theta = 52.12 \text{ cm/s.}$$

For $w_\theta = 95$ cm/s,

$$\Gamma_o = 296$$

and

$$w_\theta = 7.56 \text{ cm/s.}$$

From these observations it can hypothesized that a vortex will form, but not remain stable. If the variation is not too sudden, the vortex will not become completely unstable, but it will change its structure and velocity profile.

The downstream velocity data and the results that are inferred from it provide predictions for the vortex velocity profiles. The consistency in the data shows a reliable and accurate measurement technique for the measurement of particle flow. Although the variance in the velocities is a primary concern, the uniform velocity profiles give reason to believe that vortices will be generated with ordered velocity profiles. The results and

analysis of the vortex measurements presented in the next chapter will test the analytical expectations.

# Chapter 6: Vortex Measurements & Analysis

Now that the wind tunnel downstream motion has been characterized, observations and measurements of particles entrained in vortices remain as the final topic of this investigation. The approach to the understanding of the vortex and the response of the two particle types that are entrained within it will begin with general observations on the vortex. Here the vortex will be studied from a flow visualization point of view; that is, the motivation here will be to note aspects of the vortex's structure without measuring velocities of entrained particles. Of key interest here will be observing the stability of the vortex to determine whether it responds in a manner consistent with the results presented for the downstream flow. Once the general observations have been made, the velocity data will be presented as tabular data for each particle type. From these data, calculations will be made and presented which will allow a comparison with the predictions of Chapter 2. Finally, the response of the water droplets entrained in the vortex will be compared to the response of the eccospheres.

## 6.1: General Observations

In order to express the results of the vortex analysis with confidence, the vortex must have enough stability to allow measurement. From the results of Chapter 5, there is reason to suggest that a stable vortex can be formed with temporary stability. This prediction proved to be true. In addition, a cursory observation reveals that both the control particles and the water droplets respond as expected to the vortex.

Photographs 6.1 and 6.2 are flow visualization images of counter clockwise rotating vortices generated by the test wing and wind tunnel. They are seeded by different concentrations of control particles. Photograph 6.2 is a result of low concentration of particles and a chop rate of 100 Hz, used to make the particles appear as short streaks. No velocity data are extracted from these

**Photograph 6.1: Vortex with Eccospheres, No Chop**

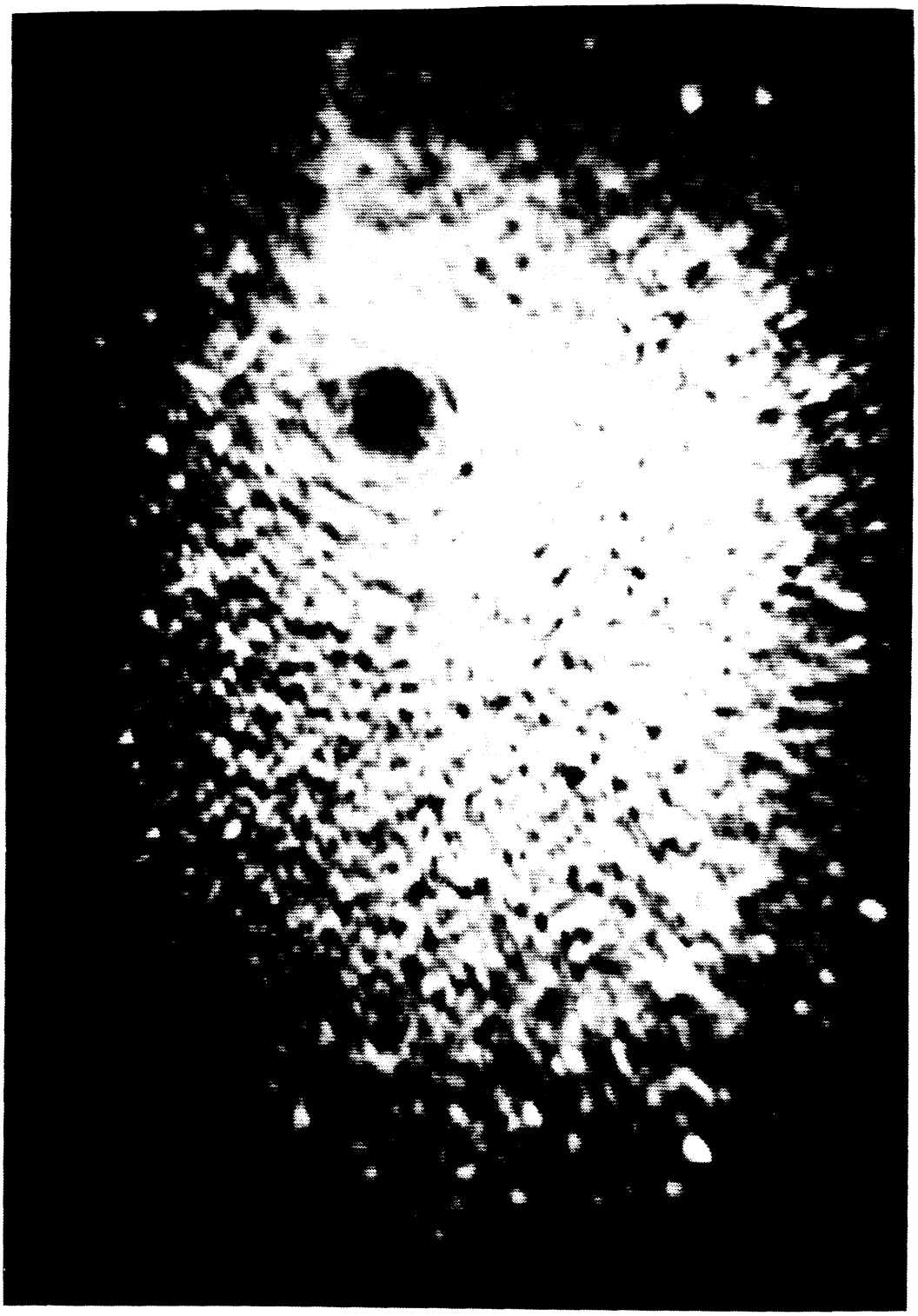

**Photograph 6.2: Vortex with Eccospheres, 100 Hz**

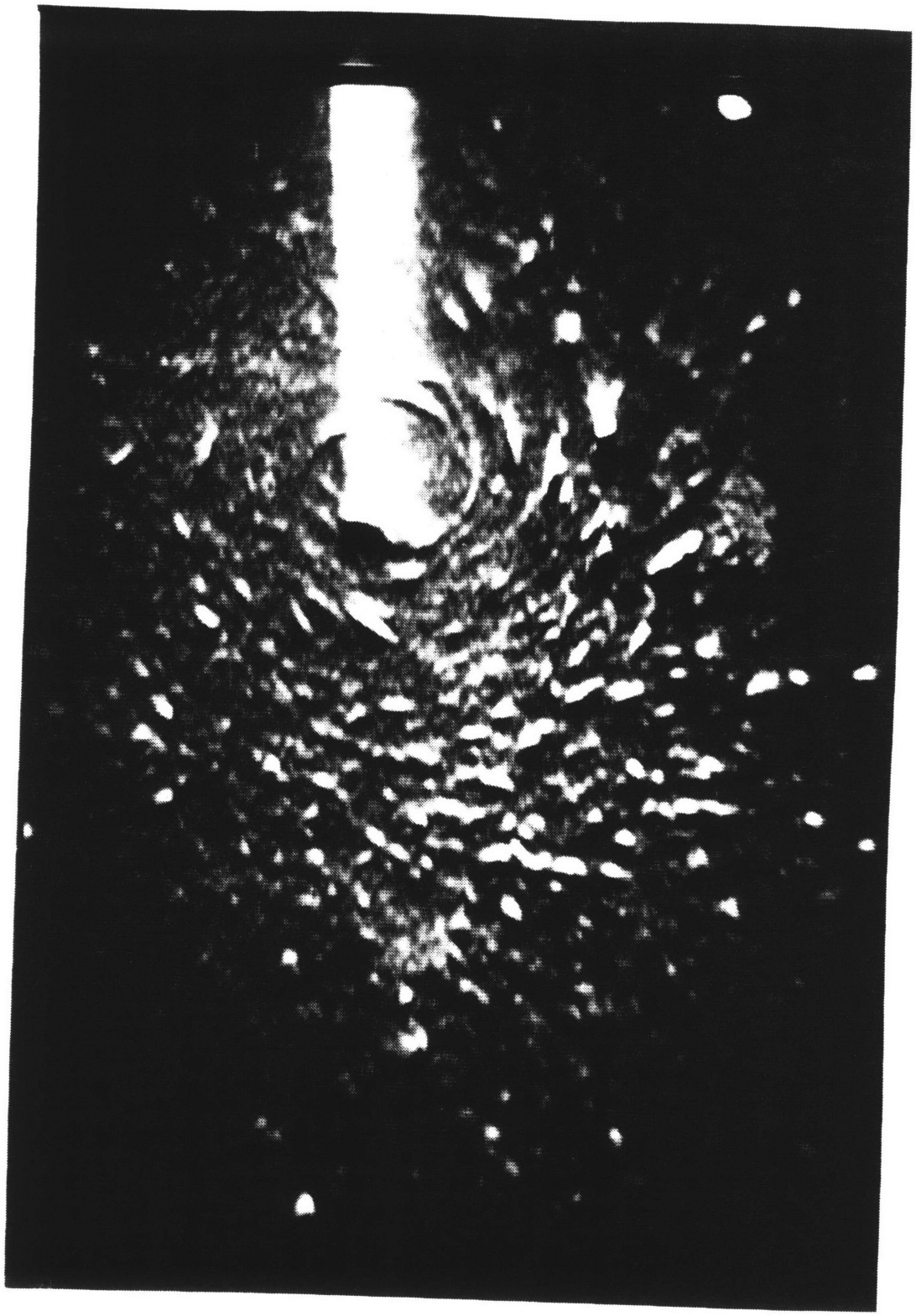

images. The vortex core is clearly defined as the area with no particles. The reason why there are very few particles in the vortex core (here or for any wing-tip vortex) is that the velocity within the core is great enough to cause all of the particles that respond to the flow to be quickly spun out of the core. It was found with the vortices measured in the investigation that slight variations existed in core positions due to the instability of the downstream flow. However, the vortex core maintained a radius of approximately 1 cm (from 0.85 cm to 1.2 cm).

From the motion of the core, it was possible to note the degree of the vortex instability. It was observed that the vortex would form at the wing-tip, but then "dance" around in an area of about 4 to 5 $cm^2$. The "dancing" was not periodic so modeling the instability was not pursued. In describing the motion of the core (and thus the entire vortex), the core typically remained centered on the wing-tip for a few seconds, then "danced" around within the area for an indefinite amount of time (but still on the order of seconds), most of the time being drawn toward the center of the wing and dancing in that region before returning to the wing-tip. The consequences of this instability are that it is not possible to measure the vortex if the laser volume and imaging plane are too far downstream from the wing. Attempts to measure the vortex at a distance two wing spans downstream from the wing proved to be fruitless. Instead, it was necessary to measure the vortex at a distance about one wingspan downstream from the wing. At this point the vortex repeatedly remained stable at the wing-tip for a few seconds. Although this may not be thought a substantial amount of time, when one considers that there are 60 fields scanned per second, there is a sufficient amount of data for analysis for just the short period of time that the vortex is stable (the video cassette recorder used advances field by field).

When the vortex "danced" it was apparent that the motion favored a region towards the middle of the wing. Closer inspection reveals that a shearing flow to the left (in-wing) of the wing-tip vortex existed because it was an area where the wing-tip vortex and a counter vortex (likely caused by the intersection of

the wing with the tunnel wall) met and combined their strengths. The counter vortex was much more unstable however. When it did exist, it gave rise to the observed "dancing", especially the jittering motion that pulled the core of the wing-tip vortex from the wing-tip to about 2.3 cm toward the center of the wing.

The shearing force also had a secondary effect on the wing-tip vortex. This region of high velocity tended to deform the circular shape of the vortex to one which was more elliptical. This altered vortex structure was difficult to define specifically, but was always present to some degree throughout the measurements, whether or not the vortex core was "dancing".

## 6.2: Data Analysis

Given the intermittent stability of the vortex, it is necessary for the data to be analyzed using a methodology that minimizes the ambiguities. This methodology must include criteria for deciding what constitutes valid data. It is easiest to summarize the methodology in the form of ground rules for making measurements:

1. Select only the vortices that are at the wing-tip and have a recognizable core. A vortex that is experiencing the motion of instability should not be considered for measurement. Although an image of such a vortex can be digitized and analyzed, there is no longer the ability to claim results that correspond to the equations of Chapter 2 which assume a well-behaved vortex. The center of the vortex was estimated on the basis of the image data. The accuracy of the estimation depends on how well the vortex is visualized.

2. The streaks from the entrained particles and the center of the vortex are to be initially expressed in terms of their pixel coordinates on the digitized image plane. Using these data, each particle's radial distance, tangential velocity, and radial velocity are calculated. The section of the vortex in

which the particle is measured is recorded by stating in which quadrant of a Cartesian coordinate grid, placed on top of the vortex, the particle is found (See Figure 6.1). Using this guide, it is possible to note how particles respond in the second and third quadrants (the quadrant closest to the shearing flow) when compared to particles in the first and fourth. See Photograph 6.3 for a picture of a control particle traveling from quadrant I to II, and being exposed to the chopped light sheet (75 Hz).

3. Since vortex flow within its core is not understood as well analytically, all streaks found to be less than 1 cm from the center will not be analyzed.

4. Knowing that the downstream flow varies, it follows that the vortex velocity data will not be constant from measurement to measurement. However, each individual measurement should follow the theoretical 1/r relationship between the velocity and the distance from the vortex center. Each vortex will be evaluated on the basis of individual frames. General conclusions will be based on the individual findings for each particle type.

Using these rules for measurement, the values for eight vortex frames are presented, four with control particles entrained (Table 6.1), four with water particles entrained (Table 6.2). The calculations are all based on pixel coordinates associated with the particles and the center of the vortex. The particle's radius is calculated by determining the number of pixels from the center of the vortex to the streak of the traveling particle. The pixel length is converted to centimeters by multiplying the pixel length by the scaling ratio, associated with the region of the scaling grid where the particle was measured. The streak's length in pixels is similarly converted to centimeters, then divided by the pulse width of the laser, 1/154th of a second (corresponding to the 75 Hz chop). This is the particle's total velocity, with two

Location of Measurements Guide

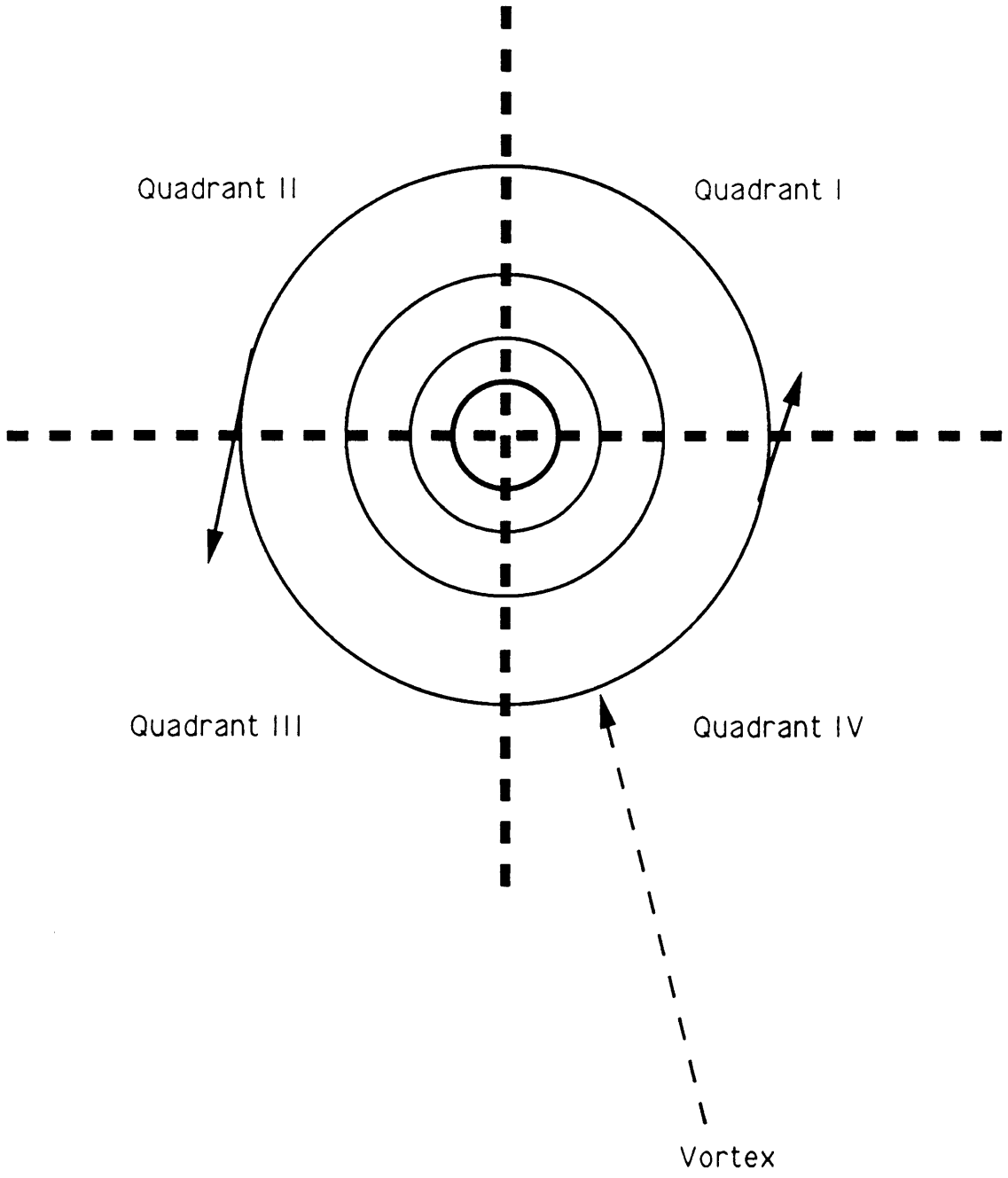


Figure 6.1

**Photograph 6.3: Vortex with Eccospheres, 75 Hz**

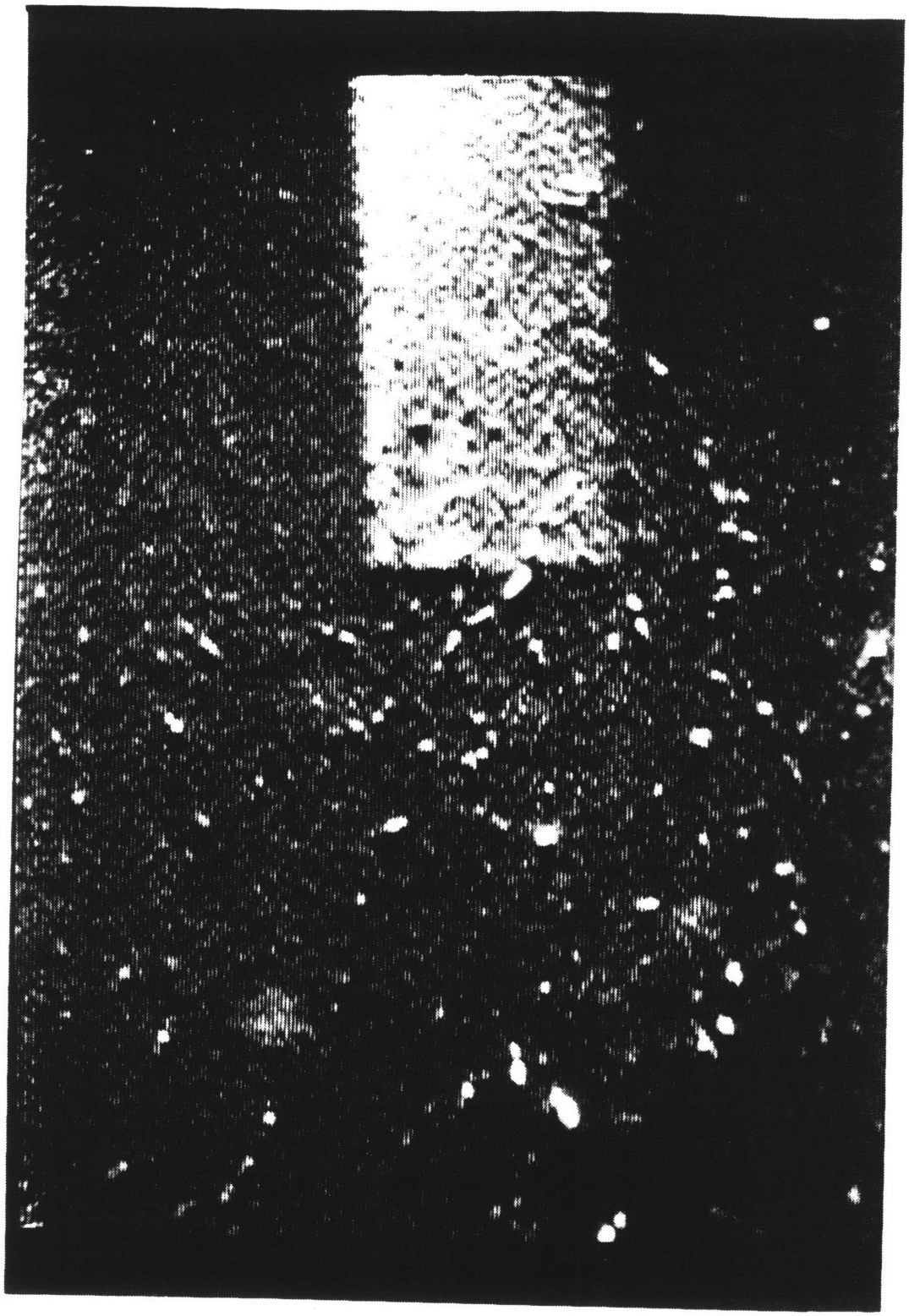

## Table 6.1: Vortex Velocity Measurements from Entrained Control Particles (Eccospheres)

Vortex CON1 (Units: cm, cm/s):

| Particle # | Radius | Tang. Velocity | Radial Velocity | Quad |
|---|---|---|---|---|
| 1 | 1.2084 | 53.060 | -0.65647 | IV |
| 2 | 1.9474 | 29.548 | -8.4237 | I |
| 3 | 2.6513 | 26.269 | -1.3068 | I |
| 4 | 2.6916 | 17.411 | -10.956 | I |
| 5 | 2.3960 | 32.022 | +21.913 | III |
| 6 | 2.8896 | 39.226 | -9.4336 | IV |
| 7 | 4.1413 | 18.840 | -8.2619 | IV |
| 8 | 2.4164 | 25.791 | -18.765 | I |
| 9 | 1.7207 | 25.206 | +7.5115 | I |

Vortex CON2 (Units: cm, cm/s):

| Particle # | Radius | Tang. Velocity | Radial Velocity | Quad |
|---|---|---|---|---|
| 1 | 1.9418 | 61.124 | +27.050 | II |
| 2 | 2.1195 | 30.638 | +2.3078 | IV |
| 3 | 1.1218 | 38.060 | +0.0000 | IV |
| 4 | 2.1026 | 22.279 | +20.574 | IV |
| 5 | 2.0175 | 28.096 | -0.11814 | I |
| 6 | 2.6080 | 24.633 | +9.2170 | I |
| 7 | 3.3766 | 24.538 | -0.36077 | I |

Vortex CON3 (Units: cm, cm/s):

| Particle # | Radius | Tang. Velocity | Radial Velocity | Quad |
|---|---|---|---|---|
| 1 | 1.2128 | 69.982 | +5.1155 | II |
| 2 | 1.7553 | 60.726 | -11.004 | I |
| 3 | 2.2252 | 50.089 | -9.7652 | I |
| 4 | 2.4549 | 34.414 | -22.548 | IV |
| 5 | 0.86492 | 68.360 | +9.7941 | IV |

Vortex CON4 (Units: cm, cm/s):

| Particle # | Radius | Tang. Velocity | Radial Velocity | Quad |
|---|---|---|---|---|
| 1 | 0.97866 | 76.759 | -0.21637 | II |
| 2 | 1.1480 | 45.676 | +12.960 | II |
| 3 | 1.3520 | 38.195 | +19.294 | IV |
| 4 | 0.76954 | 37.389 | -13.142 | IV |
| 5 | 1.6310 | 29.651 | +17.345 | IV |

## Table 6.2: Vortex Velocity Measurements from Entrained Water Droplets

Vortex WAT1 (Units: cm, cm/s):

| Particle # | Radius | Tang. Velocity | Radial Velocity | Quad |
|---|---|---|---|---|
| 1 | 1.1568 | 67.478 | +6.6983 | IV |
| 2 | 1.1951 | 38.191 | +19.301 | I |
| 3 | 1.8221 | 34.778 | +21.420 | I |
| 4 | 1.3948 | 37.800 | +18.582 | I |
| 5 | 2.2459 | 40.451 | +30.182 | I |
| 6 | 2.8443 | 32.550 | -6.8751 | IV |

Vortex WAT2 (Units: cm, cm/s):

| Particle # | Radius | Tang. Velocity | Radial Velocity | Quad |
|---|---|---|---|---|
| 1 | 2.2624 | 55.777 | +18.426 | I |
| 2 | 1.4506 | 49.484 | +11.452 | I |
| 3 | 0.8893 | 56.625 | +0.23851 | I |
| 4 | 2.9371 | 43.498 | -3.5038 | I |
| 5 | 2.7969 | 36.374 | +15.736 | I |
| 6 | 0.9594 | 66.080 | -20.060 | IV |
| 7 | 1.7556 | 36.105 | +27.037 | III |

Vortex WAT3 (Units: cm, cm/s):

| Particle # | Radius | Tang. Velocity | Radial Velocity | Quad |
|---|---|---|---|---|
| 1 | 0.9374 | 60.386 | -24.529 | IV |
| 2 | 1.1364 | 32.407 | -8.0436 | IV |
| 3 | 0.7934 | 63.734 | +18.460 | IV |
| 4 | 1.5516 | 37.459 | +24.305 | I |
| 5 | 1.3342 | 55.039 | -2.5062 | II |
| 6 | 1.9596 | 39.109 | -21.358 | I |
| 7 | 2.0188 | 36.844 | -5.1016 | I |
| 8 | 1.1229 | 27.337 | +29.256 | I |
| 9 | 1.7031 | 28.651 | -9.9368 | IV |
| 10 | 2.1067 | 66.535 | +5.7343 | IV |

Vortex WAT4 (Units: cm, cm/s):

| Particle # | Radius | Tang. Velocity | Radial Velocity | Quad |
|---|---|---|---|---|
| 1 | 1.3878 | 69.183 | +24.354 | III |
| 2 | 1.9472 | 45.989 | -0.97789 | I |
| 3 | 3.0720 | 48.354 | -4.6849 | IV |
| 4 | 4.3524 | 36.869 | -12.094 | IV |
| 5 | 1.3459 | 54.168 | +10.066 | II |
| 6 | 1.5916 | 51.474 | +19.646 | II |
| 7 | 1.9885 | 39.624 | +8.5932 | I |

components, the tangential and radial. Given both ends of a dash in pixel coordinates, the difference between the distance of each end of the dash to the center of the vortex is called the radial displacement. From this radial displacement, the radial velocity is calculated, once again dividing by the pulse width. The tangential component is caculated by a vector subtraction of the radial component from the total velocity.

The Tables 6.1 and 6.2 show each particle's distance from the vortex center, its tangential and radial velocities, and the quadrant the particle was measured in. The vortices, as individual frames of data, are identified as CON1, CON2, CON3, and CON4 for those with eccospheres entrained and WAT1, WAT2, WAT3, and WAT4 for the vortices with water droplets entrained. The vortex frames presented in the tables are the subset of all of the vortex frames measured that had the greatest number of measurable particles. Each of the selected vortex frames has between five and ten particles at various radii. From these data, comparison to the analytical predictions will be made. Through these comparisons the response of the control particles to the vortex will be compared to that of the water droplets.

## 6.3: Comparison to Analytical Predictions

It is very difficult to compare the radial displacements and velocities measured to analytical values. The accuracy with which one can determine the radial velocity is extremely sensitive to knowing precisely where the center of the vortex is located. Also, negative radial velocity values in the first and fourth quadrants, and positive values in the second and third quadrants are more likely due to the elliptical nature of the vortex. There are, however, some values that cannot be explained by an elliptical structure. The only explanation for these values is either an error in measurement or an error in the location of the center of the vortex. Take note that only a slight error in locating the center will have a more significant effect on the radial velocity than the tangential. If the center is off 5 pixels, or a little less than a

millimeter, the effect on the radial velocity, which is directly related to the distance from the center of the vortex, will result in a 14.3 cm/s change. The tangential velocity, however, will experience a maximum difference of 2 or 3 cm/s. Since the velocity resolution is 2.58 cm/s (one pixel) at the center of the field of view, this difference in the tangential velocity is negligible.

Therefore, the particles cannot be evaluated on the basis of their radial velocities. Radial velocities are presented for purposes of future research, with the intention that later LSV vortex studies can benefit from these findings. In addition, the negative values for the radial velocity (the positive ones are expected) may also be an indication of the amount of error made in locating the center of the vortex. For instance, particle 4 of vortex CON3 in Table 6.1 has a radial velocity of -22.548 cm/s. It is possible that this is a function of the elliptical structure of the vortex. However, assuming it is not, this value may indicate an error of 1.46 millimeters in the location of the center of the vortex. Nevertheless, it is concluded that the radial measurements must be treated with a high degree of skepticism.

## Equivalent Circulation and Downstream Velocity

From the measurements on the downstream velocities of the particles in the tunnel (Chapter 5), it was found that the center of the histogram peaks, which corresponds to the average downstream velocity, was approximately 150 cm/s for all four experiments. Using this value, the circulation ($\Gamma_o$) was calculated to be 468 $cm^2/s$, and, from this, the tangential velocity was found to be 37.24 cm/s for a radius of 2 cm. It was also shown that the downstream velocity varies with time. Thus, it is not sensible to expect the vortex data to agree with predictions that are based on a single value for the downstream velocity. In fact, it is best not not assume any one value and rather derive an equivalent circulation and downstream velocity from the tangential velocity measured from the vortex. By averaging the particle tangential

velocities from all the particles in a vortex frame, an average circulation value can be obtained and used as the theoretical expectation. How well the particle velocities follow the theoretical values based on this average circulation will provide us with a measure of particle entrainment in the vortex. For each particle tangential velocity measured at a certain radius, we recall that Equation [2.11b],

$$w_\theta = \Gamma_o/(2\pi r), \quad \text{for } r \geq r_c,$$

can be used to calculate the circulation constant necessary to produce the tangential velocity. In addition, Equation 2.10

$$\gamma(0) = \Gamma_o/(bw_a),$$

or

$$0.26 = \Gamma_o/(12w_a),$$

shows the relationship between the circulation and the downstream velocity that gives rise to it. Thus it is possible to also present the equivalent downstream velocity necessary to give rise to the measured tangential velocity. Chapter 5 also presented observations that the circulation and downstream velocities are bounded such that

$$296 < \Gamma_o < 655 \text{ cm}^2/\text{s},$$

and

$$95 < w_a < 210 \text{ cm/s}.$$

## Theoretical vs. Measured Tangential Velocities

Not every measured tangential velocity will be used in the circulation constant averaging. Any particle that is inside the core (radius less than 1 cm) and any particle with an equivalent circulation value outside of the range presented above and in Chapter 5 will not be considered candidates in the calculations. For

example, for vortex CON1, each particle's radius, velocity, and quadrant can be presented with their equivalent circulation ($\Gamma_o$):

Vortex CON1 (Units: cm, cm/s):

| Particle # | Radius | Tang. Velocity | Quad | $\Gamma_o$ |
|---|---|---|---|---|
| 1 | 1.2084 | 53.060 | IV | 402.87 |
| 2 | 1.9474 | 29.548 | I | 361.55 |
| 3 | 2.6513 | 26.269 | I | 437.60 |
| 4 | 2.6916 | 17.411 | I | 294.45 |
| 5 | 2.3960 | 32.022 | III | 482.07 |
| 6 | 2.8896 | 39.226 | IV | 712.18 |
| 7 | 4.1413 | 18.840 | IV | 490.21 |
| 8 | 2.4164 | 25.791 | I | 391.58 |
| 9 | 1.7207 | 25.206 | I | 272.52 |

Particles 4, 6, and 9 have equivalent circulations that are out of the range indicated above. Their circulation values would imply simultaneous downstream velocities of 94.38 cm/s, 228.26 cm/s and 87.35 cm/s. This cannot be true. If the other six equivalent circulations are averaged, the result is 428 $cm^2/s$. Figure 6.2 shows all of the tangential velocities plotted against a theoretical tangential velocity curve based on a circulation constant of 428 $cm^2/s$. The six particles used in the average circulation, show tangential velocities that vary little from the theoretical velocity values. Figure 6.2 also shows that as expected, the three particles not included in the averaging have tangential velocities furthest from the theoretical curve.

One may argue that the data are biased to agree with the theoretical curve by excluding those particles that fall out of the range of the stated criteria. Although a certain amount of agreement is achieved when the average circulation constant is calculated, the degree of agreement is subject to the remaining particles (all remaining by the same criteria that their equivalent circulations fall within the acceptable range), which have no obligation to agree to the average circulation. To be more direct, once the appropriate data are excluded, the evaluation of the remaining particles becomes an analysis of how many have a significant deviation from the theoretical value which was based

**Figure 6.2**

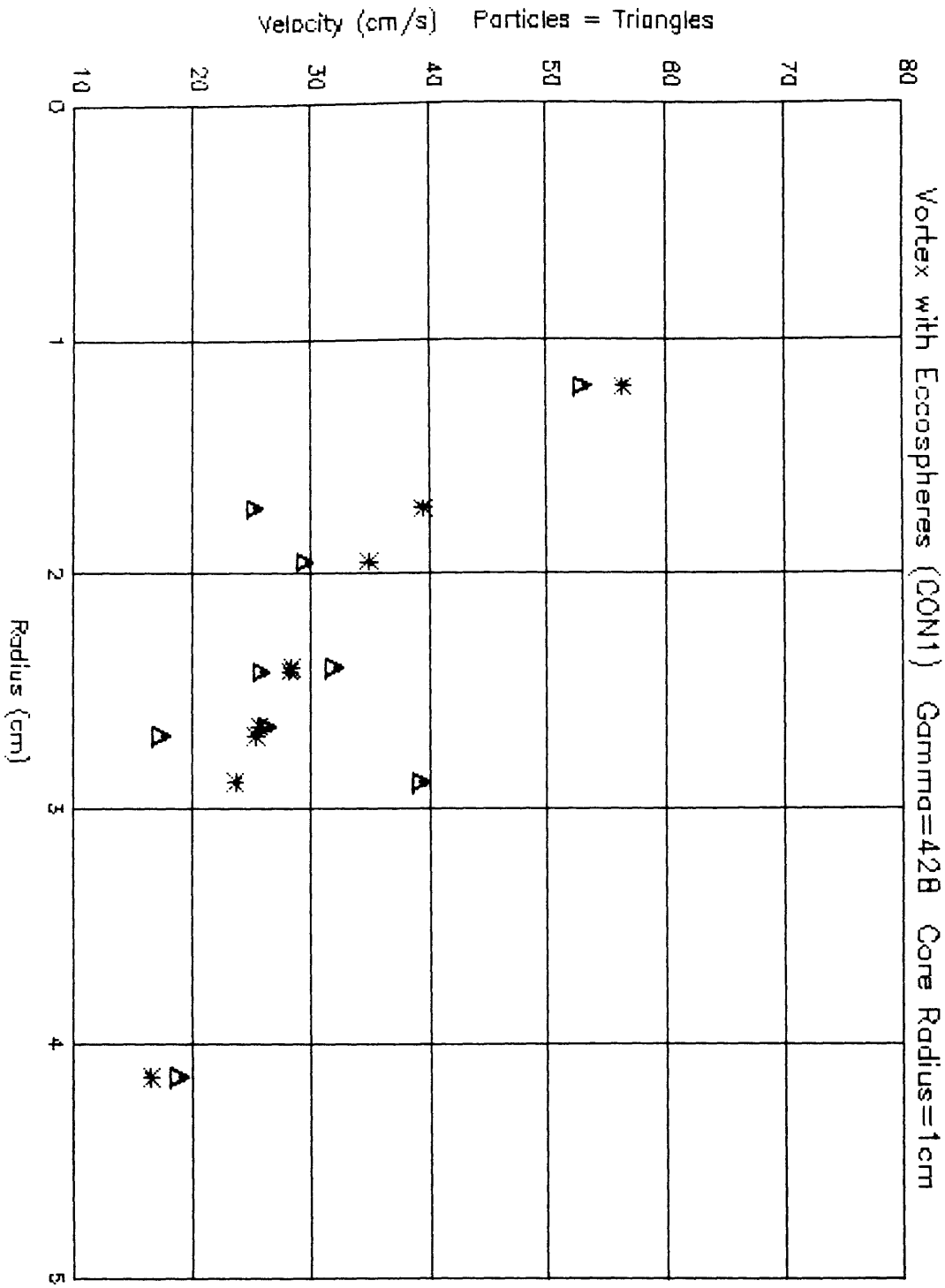
Velocity (cm/s) Particles = Triangles
10
20
30
40
50
60
70
80
0
1
2
3
4
5
Radius (cm)
Vortex with Ecospheres (CON1) Gamma=428 Core Radius=1cm

on an average. The deviation of the measured velocities from the theoretical velocities is expressed as the percent difference and the absolute difference.

Vortex WAT1 displays a set of measured velocity data that, even after one particle is excluded because of an out of range circulation constant, reveals remaining particles that show a greater deviation from the theoretical velocities. The average absolute difference and the percent difference are 10.01 cm/s and 21.62% respectively, but the corresponding values for vortex CON1 are 2.94 cm/s and 9.9%. The particles of vortex WAT1 deviate from the theoretical expectations over twice as much as do the particles of CON1.

The analysis of each of the vortex frames is approached just as vortex CON1 and WAT1 were presented above. The data used in this analysis begins with Tables 6.1 and 6.2. The comparisons between theory and measurements are represented in both tabular and graphical form. The graphs display the values of the measured tangential velocities (represented by triangles) as they compare to the theoretical values (the asterisks) which are based on the average circulation constant. Figures 6.2 through 6.9 are the graphs for the eight vortex frames analyzed. The average circulation values and their associated tangential velocities for each vortex frame are presented in Tables 6.3a, 6.3b, 6.4a and 6.4b to assist in the interpretation of the graphical data. In addition to presenting the theoretical and measured velocities, the tables give the absolute and fractional difference between the velocities. Velocities that correspond to particles with equivalent circulation values outside of the acceptable range, and the velocities that are from particles that are within the core of the vortex are presented italics with a '*'. They are not used in any of the calculations.

## 6.4: Comparison: Control vs. Water

Using Tables 6.3 and 6.4 in association with Figures 6.2 through 6.9, an evaluation can be made as to the ability of each of

## Table 6.3a: Theoretical vs. Measured Vortex Tangential Velocities for Entrained Control Particles (Eccospheres)

**Vortex CON1, Figure 6.2**

**Average Circulation: 428**

**Equivalent Downstream Velocity: 137.2 cm/s**

Units: cm, cm/s

| Radius | Theoretical Vel. | Measured Vel. | Difference | %Difference |
|---|---|---|---|---|
| 1.2084 | 56.324 | 53.060 | 3.264 | 5.8% |
| *1.7207** | *39.554* | *25.206* | *14.348* | |
| 1.9474 | 34.949 | 29.548 | 5.401 | 15.5% |
| 2.3960 | 28.406 | 32.022 | 3.616 | 12.7% |
| 2.4164 | 28.166 | 25.791 | 2.375 | 8.4% |
| 2.6513 | 25.67 | 26.269 | 0.596 | 2.0% |
| *2.6916** | *25.286* | *17.411* | *7.875* | |
| *2.8896** | *23.553* | *39.226* | *15.673* | |
| 4.1413 | 16.434 | 18.840 | 2.406 | 14.6% |
| Average Difference: | | | 2.943 | 9.9% |

**Vortex CON2, Figure 6.3**

**Average Circulation: 422**

**Equivalent Downstream Velocity: 135.3 cm/s**

Units: cm, cm/s

| Radius | Theoretical Vel. | Measured Vel. | Difference | %Difference |
|---|---|---|---|---|
| *1.1218** | *59.886* | *38.060* | *21.826* | |
| *1.9418** | *34.597* | *61.124* | *26.527* | |
| 2.0175 | 33.299 | 28.096 | 5.203 | 15.6% |
| *2.1026** | *31.951* | *22.279* | *9.672* | |
| 2.1195 | 31.696 | 30.638 | 1.058 | 3.3% |
| 2.6080 | 25.759 | 24.633 | 1.126 | 4.4% |
| 3.3766 | 19.896 | 24.538 | 4.642 | 23.3% |
| Average Difference: | | | 4.3402 | 11.7% |

## Table 6.3b: Theoretical vs. Measured Vortex Tangential Velocities for Entrained Control Particles (Eccospheres)

**Vortex CON3, Figure 6.4**

**Average Circulation: 532**

**Equivalent Downstream Velocity: 170.5 cm/s**

Units: cm, cm/s

| Radius | Theoretical Vel. | Measured Vel. | Difference | %Difference |
|---|---|---|---|---|
| *0.86492** | *73.241* | *68.360* | *4.8814* | |
| 1.2128 | 69.822 | 69.982 | 0.1600 | 0.2% |
| *1.7553** | *48.242* | *60.726* | *12.484* | |
| *2.2252** | *38.055* | *50.089* | *12.034* | |
| 2.4549 | 34.494 | 34.414 | 0.0803 | 0.2% |
| Average Difference: | | | 0.1202 | 0.2% |

**Vortex CON4, Figure 6.5**

**Average Circulation: 353**

**Equivalent Downstream Velocity: 113.1 cm/s**

Units: cm, cm/s

| Radius | Theoretical Vel. | Measured Vel. | Difference | %Difference |
|---|---|---|---|---|
| *0.76954** | *43.234* | *37.389* | *5.845* | |
| *0.97866** | *54.983* | *76.759* | *21.776* | |
| 1.1480 | 48.940 | 45.676 | 3.264 | 6.7% |
| 1.3520 | 41.554 | 38.195 | 3.359 | 8.1% |
| 1.6310 | 34.446 | 29.651 | 4.795 | 13.92% |
| Average Difference: | | | 3.806 | 9.5% |

## Table 6.4a: Theoretical vs. Measured Vortex Tangential Velocities for Entrained Water Droplets

**Vortex WAT1, Figure 6.6**

**Average Circulation: 449**

**Equivalent Downstream Velocity: 143.9 cm/s**

Units: cm, cm/s

| Radius | Theoretical Vel. | Measured Vel. | Difference | %Difference |
|---|---|---|---|---|
| 1.1568 | 64.393 | 67.478 | 3.085 | 4.8% |
| 1.1951 | 59.815 | 38.191 | 21.624 | 36.15% |
| 1.3948 | 51.255 | 37.800 | 13.455 | 26.30% |
| 1.8221 | 39.232 | 34.778 | 4.454 | 11.35% |
| *2.2459** | *31.831* | *40.451* | *8.62* | |
| 2.8443 | 25.134 | 32.550 | 7.416 | 29.50% |
| Average Difference: | | | 10.01 | 21.62% |

**Vortex WAT2, Figure 6.7**

**Average Circulation: 496**

**Equivalent Downstream Velocity: 159.1 cm/s**

Units: cm, cm/s

| Radius | Theoretical Vel. | Measured Vel. | Difference | %Difference |
|---|---|---|---|---|
| *0.8893** | *70.201* | *56.625* | *13.576* | |
| *0.9594** | *75.738* | *66.080* | *9.658* | |
| 1.4506 | 54.419 | 49.484 | 4.935 | 9.1% |
| 1.7556 | 44.965 | 36.105 | 8.860 | 19.7% |
| *2.2624** | *34.893* | *55.777* | *20.884* | |
| 2.7969 | 28.224 | 36.374 | 8.150 | 28.9% |
| *2.9371** | *26.877* | *43.498* | *16.621* | |
| Average Difference: | | | 7.315 | 19.2% |

## Table 6.4b: Theoretical vs. Measured Vortex Tangential Velocities for Entrained Water Droplets

**Vortex WAT3, Figure 6.8**

**Average Circulation: 416**

**Equivalent Downstream Velocity: 133.3 cm/s**

Units: cm, cm/s

| Radius | Theoretical Vel. | Measured Vel. | Difference | %Difference |
|---|---|---|---|---|
| *0.7934** | *52.505* | *63.734* | *11.225* | |
| *0.9374** | *62.037* | *60.386* | *1.651* | |
| *1.1229** | *58.937* | *27.337* | *31.60* | |
| *1.1364** | *58.237* | *32.407* | *25.83* | |
| 1.3342 | 49.603 | 55.039 | 5.436 | 11.0% |
| 1.5516 | 42.653 | 37.459 | 5.194 | 12.2% |
| 1.7031 | 38.859 | 28.651 | 10.208 | 26.3% |
| 1.9596 | 33.774 | 39.109 | 5.335 | 15.8% |
| 2.0188 | 32.782 | 36.844 | 4.062 | 12.4% |
| *2.1067** | *31.414* | *66.535* | *31.121* | |
| Average Error: | | | 6.047 | 15.5% |

**Vortex WAT4, Figure 6.9**

**Average Circulation: 527**

**Equivalent Downstream Velocity: 169.0 cm/s**

Units: cm, cm/s

| Radius | Theoretical Vel. | Measured Vel. | Difference | %Difference |
|---|---|---|---|---|
| 1.3459 | 62.352 | 54.168 | 8.184 | 13.1% |
| 1.3878 | 60.469 | 69.183 | 8.714 | 14.4% |
| 1.5916 | 52.727 | 51.474 | 1.253 | 2.4% |
| 1.9472 | 43.098 | 45.989 | 2.891 | 6.7% |
| 1.9885 | 42.203 | 39.624 | 2.579 | 6.1% |
| *3.0720** | *27.318* | *48.354* | *21.036* | |
| *4.3524** | *19.281* | *36.869* | *17.588* | |
| Average Error: | | | 4.72 | 8.54% |

**Figure 6.3**

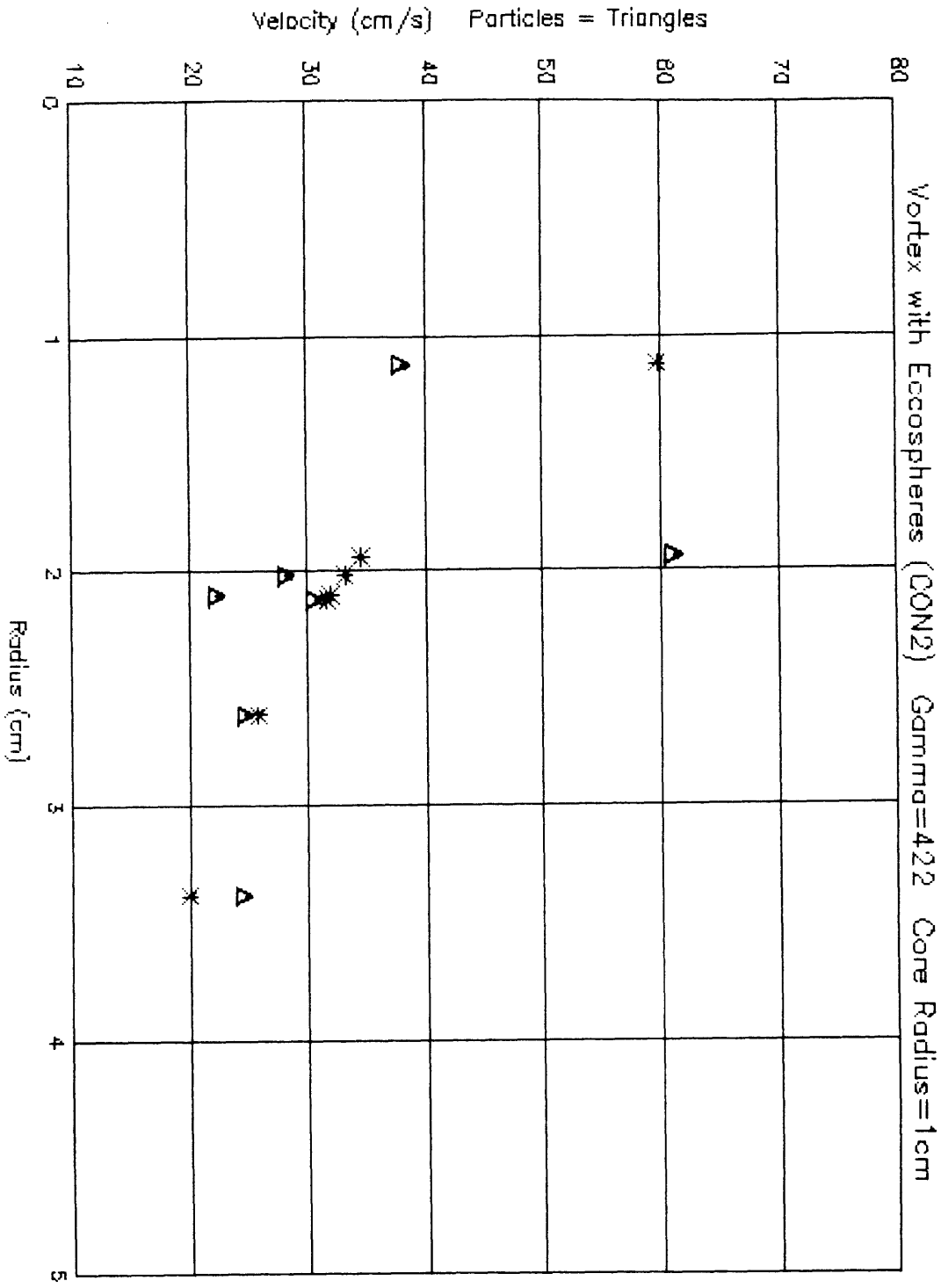
Velocity (cm/s) Particles = Triangles
10
20
30
40
50
60
70
80
0
1
2
3
4
5
Radius (cm)
Vortex with Ecospheres (CON2) Gamma=422 Core Radius=1cm

**Figure 6.4**

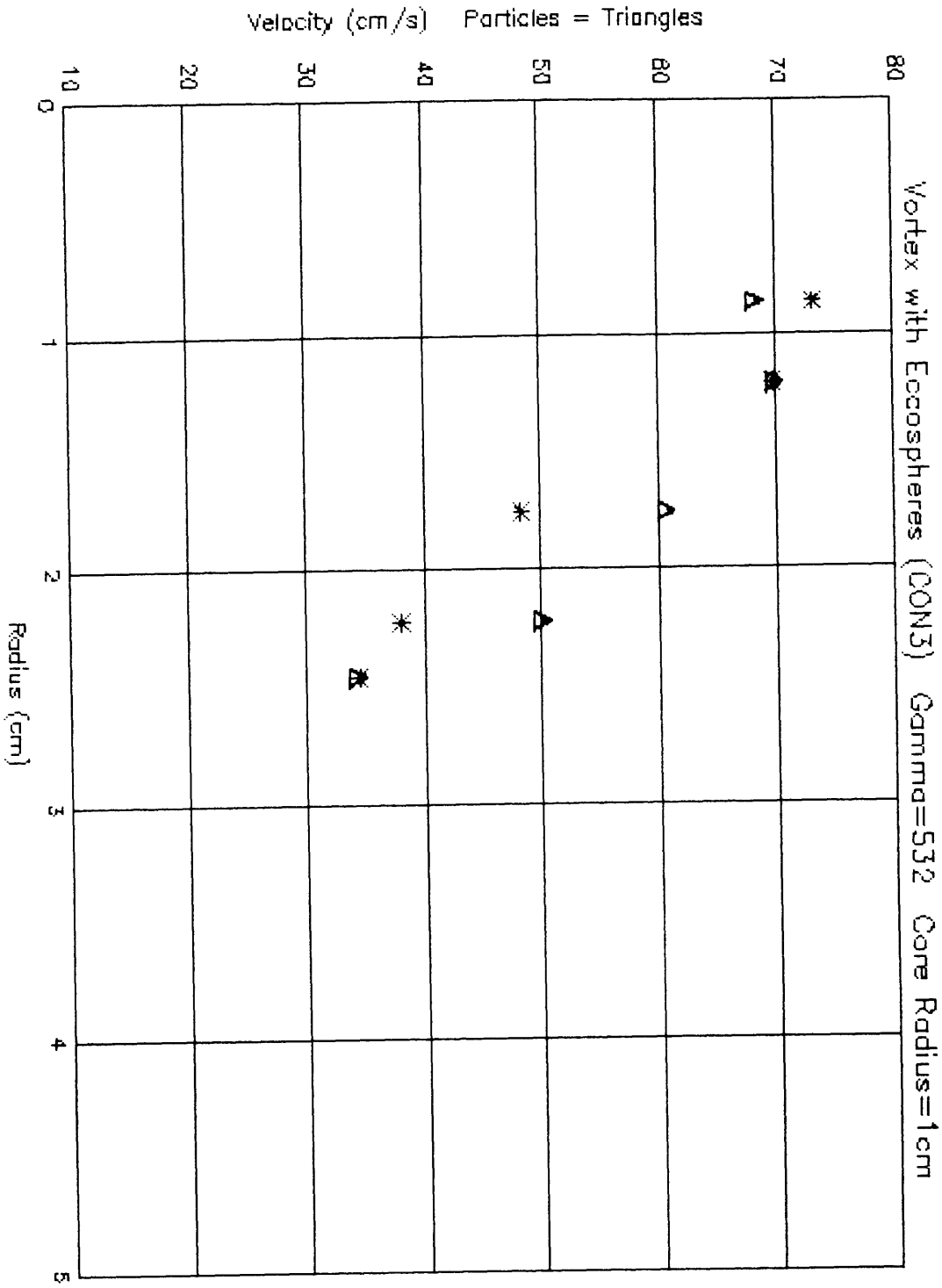
Velocity (cm/s) Particles = Triangles
10
20
30
40
50
60
70
80
0
1
2
3
4
5
Radius (cm)
Vortex with Eccospheres (CON3) Gamma=532 Core Radius=1cm

**Figure 6.5**

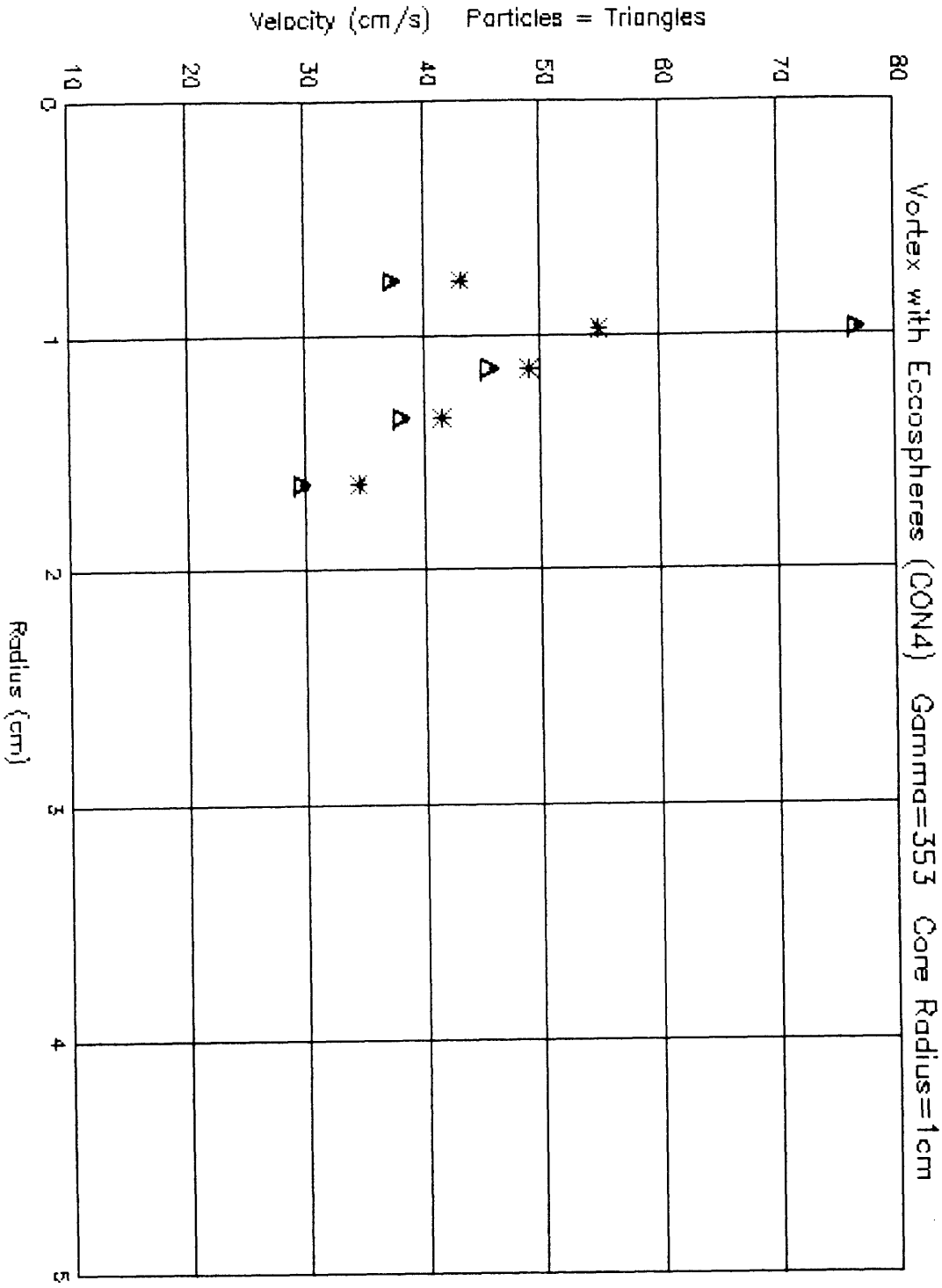
Velocity (cm/s) Particles = Triangles
10
20
30
40
50
60
70
80
0
1
2
3
4
5
Radius (cm)
Vortex with Ecospheres (CON4) Gamma=353 Core Radius=1cm

**Figure 6.6**

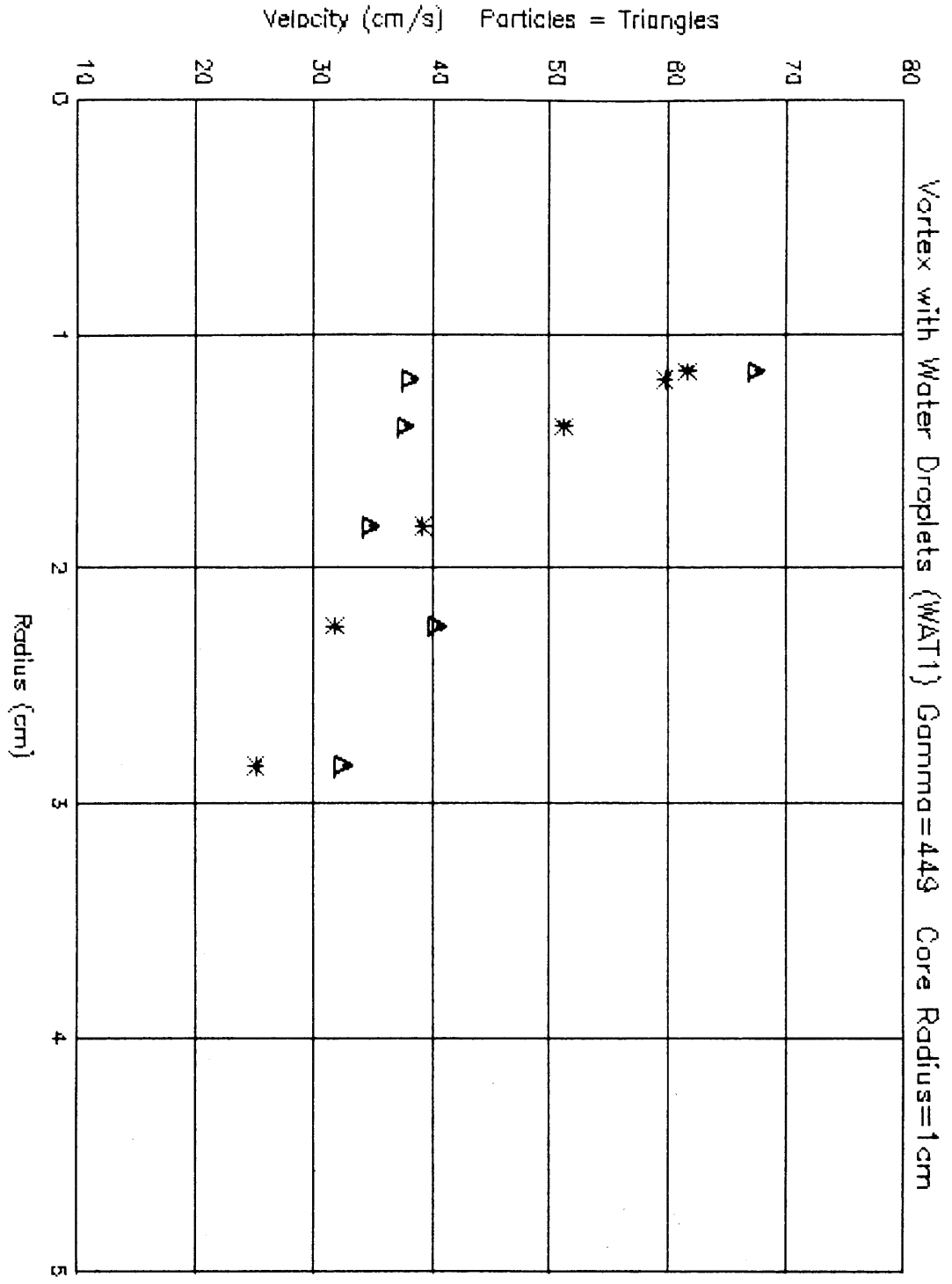
Velocity (cm/s) Particles = Triangles
10
20
30
40
50
60
70
80
Radius (cm)
0
1
2
3
4
5
Vortex with Water Droplets (WAT1) Gamma=449 Core Radius=1cm

**Figure 6.7**

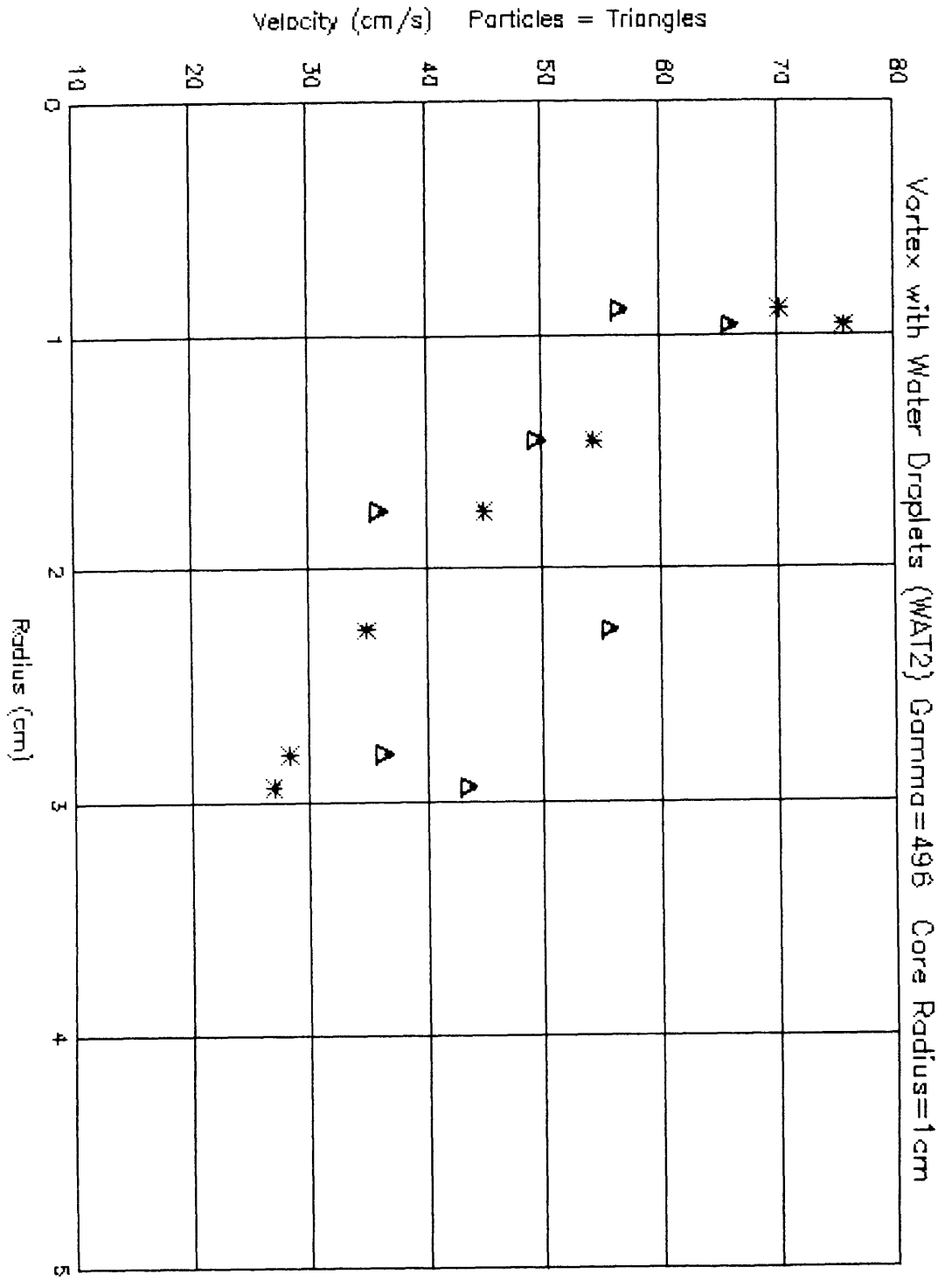
Velocity (cm/s) Particles = Triangles
10
20
30
40
50
60
70
80
0
1
2
3
4
5
Radius (cm)
Vortex with Water Droplets (WAT2) Gamma=496 Core Radius=1cm

**Figure 6.8**

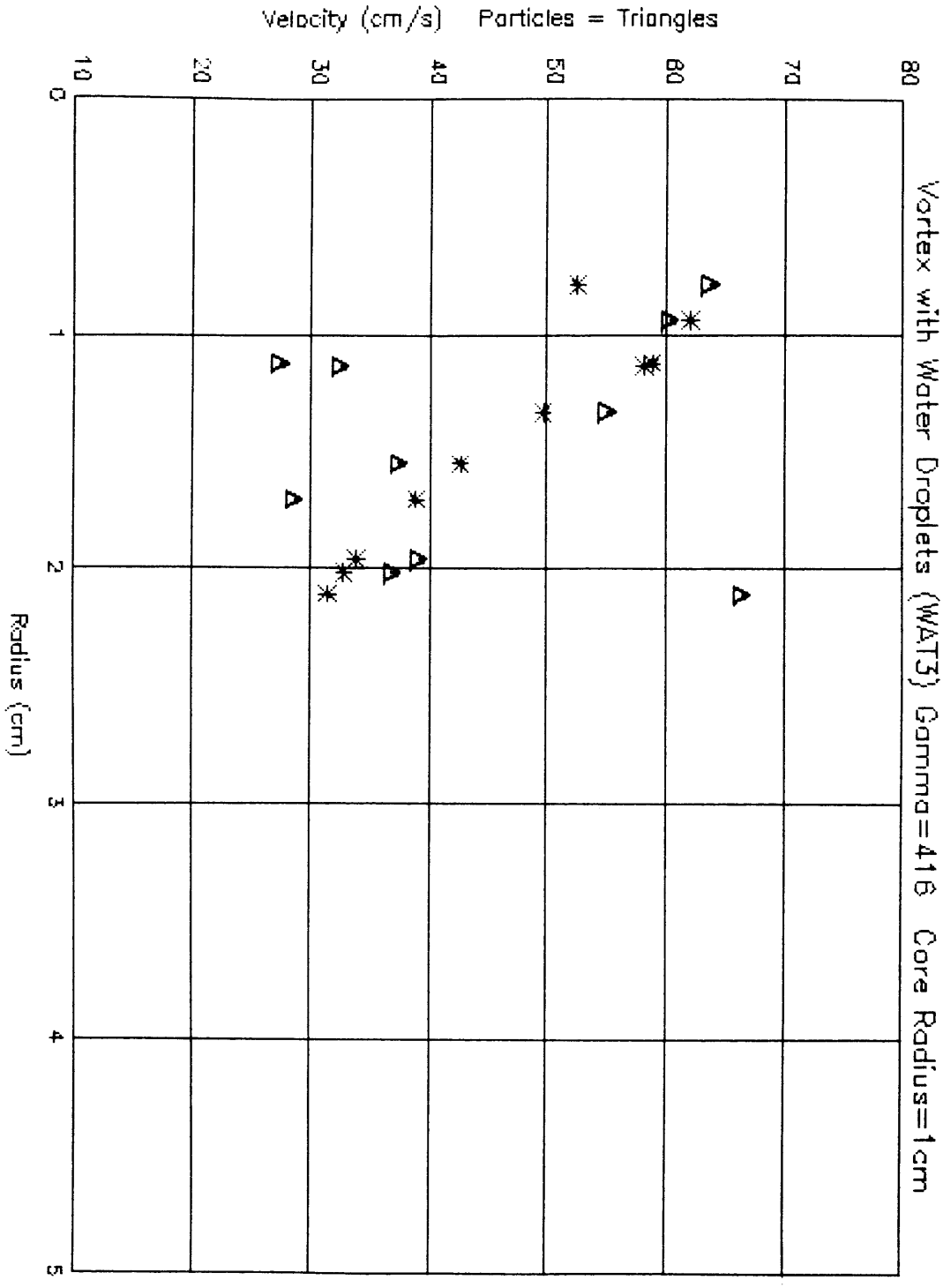
Velocity (cm/s) Particles = Triangles
10
20
30
40
50
60
70
80
0
1
2
3
4
5
Radius (cm)
Vortex with Water Droplets (WAT3) Gamma=416 Core Radius=1cm

**Figure 6.9**

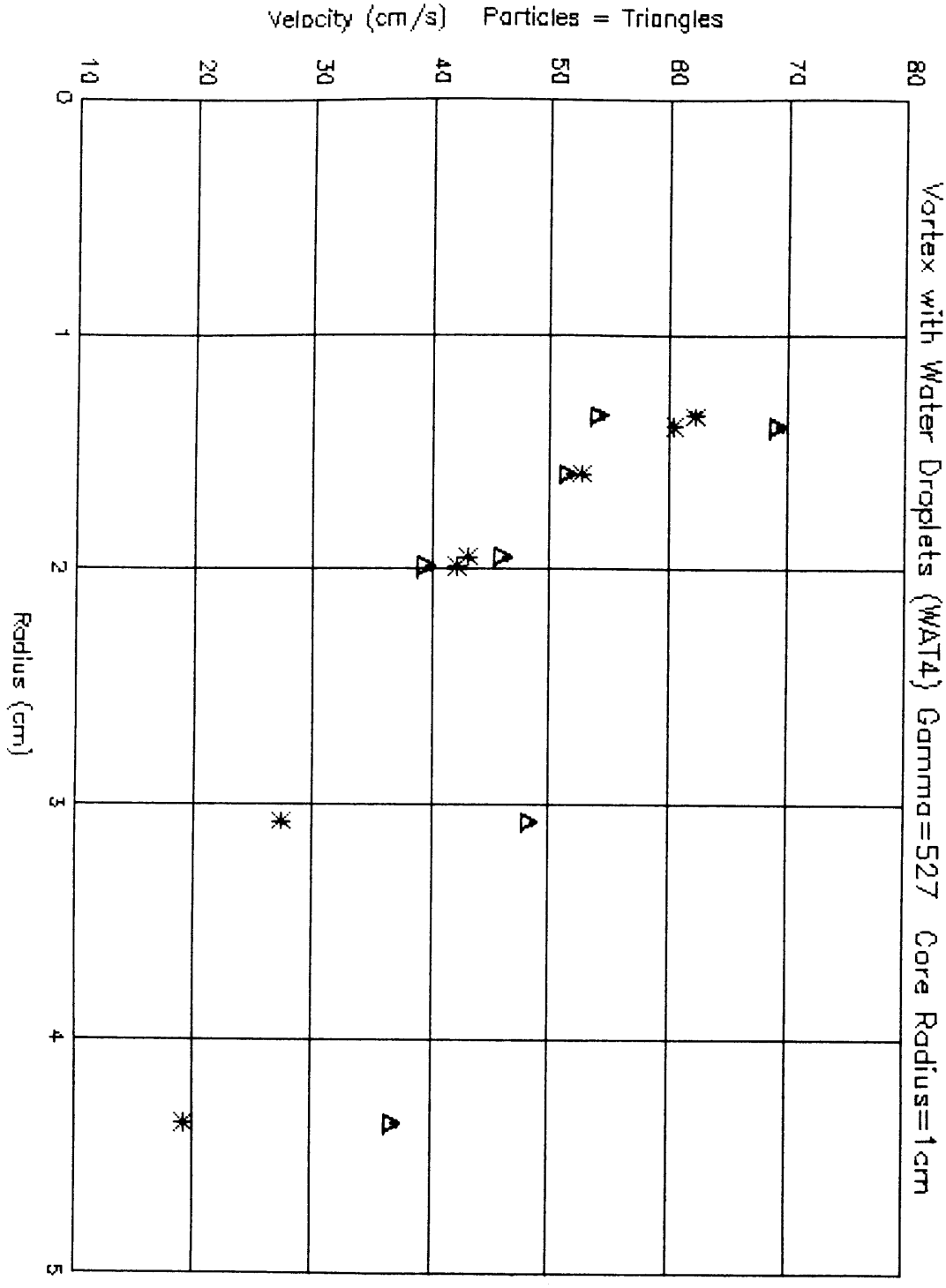
Velocity (cm/s) Particles = Triangles
10
20
30
40
50
60
70
80
0
1
2
3
4
5
Radius (cm)
Vortex with Water Droplets (WAT4) Gamma=527 Core Radius=1cm

these particles to follow the flow of a vortex. As a metric for this evaluation, the difference between the theoretical and measured values and the percent differences are used. Each of these will provide a different perspective on the variation of the particle's velocity from the predicted velocity. First the percent difference will be discussed.

The percent difference was calculated as

$$\left[ \, | \text{ Theory - Measured } | \, / \, \text{ Theory} \right] \text{ x } 100.$$

From analyzing the percent difference, it is seen that the measured tangential velocities of the eccospheres were seldom more than 15% different from the theoretical value with three-quarters of all the eccospheres having less than a 10% percent difference. The average percent difference for all of the control particle entrained vortex frames is 8.98%. This implies that those particles that did follow the flow (since the suspect particles were not included) followed it rather well.

There are many possible explanations for the velocity differences of the control particles. It is likely that there were some errors made during the measurement process, and since the differences do not seem to have any correlation (e.g. if all of the velocity errors were a result of the particles lagging behind the air flow) this error source is a strong candidate. However, since it has been determined that the vortices may have some degree of instability, the measurement results may reflect the actual velocity profile of an unstable vortex. Nevertheless the graphical data show that the eccospheres responded reasonably and consistently to the vortices.

There is no consistency in the percent difference for each of the water particle-entrained vortex frames. Whereas vortex WAT4 in Table 6.4b (expressed graphically in Figure 6.9) seems to have fairly well behaved particles, vortices WAT1 and WAT2 (Table 6.4a) show much less agreement between the theoretical

distributions and the measurements. Vortex WAT1 (Table 6.4a) , discussed earlier, shows the greatest differences, with an average percent difference of 21.62%. The average percent difference for all of the water droplet entrained vortex frames is 16.84%, twice that of the average control particle percent difference.

Presenting the absolute difference between the theoretical velocity and the measurement gives rise to another tool for analysis. The percent difference values provide a fractional difference, while the absolute difference can be compared directly to the velocity resolution. Recall in Chapter 5, Section 5.2, that the temporal resolution provided with the chop rate of 75 Hz (which was the rate used for all of the vortex measurements), combined with the spatial resolution results in a velocity resolution of

(1 pixel) x (1.3/70) / (6.51 ms) = 2.8528 cm/s.

The differences in velocity can be expressed in terms of resolution cells, equivalent to spatial pixels. For instance, vortex CON1 of Table 6.3a has six candidate control particles, three of which have velocity differences below the limiting resolution, or less than one pixel. The other three have differences of less than two pixels. This means that the first three particles are traveling very close to the theoretical speed, within the measurement error. Even the greatest velocity difference in vortex CON1 (5.401 cm/s) implies that spatially, the measured length was less than two pixels (each pixel is about a fifth of a millimeter) from what the theory predicted. The measurements can be reviewed from this perspective. Below a table presents the maximum, minimum and average difference in velocities for both particle types (not including any suspect particles):

<u>Control Particles</u>

| | |
|---|---|
| Maximum Difference in Velocity: | 5.401 cm/s |
| Minimum Difference in Velocity: | 0.0803 cm/s |
| Average Difference in Velocity: | 2.76 cm/s |

Water Droplets

| | |
|---|---|
| Maximum Difference in Velocity: | 21.264 cm/s |
| Minimum Difference in Velocity: | 1.253 cm/s |
| Average Difference in Velocity: | 7.40 cm/s |

Thus, we have more evidence that the water droplets undergo a greater deviation from theoretical expectations, for the water droplet average difference is over two and a half times greater than the average for the control particles. Also, the range of differences for the water droplets (from 21.264 to 1.253) is much greater than the range for the control particles (5.401 to 0.0803).

For the control particles, there are no velocities measured that are greater than two pixel lengths from the expected value (except for the discarded measurements). The greatest difference is 5.401 cm/s (which resulted in a 15.5% difference). However, the data for the water particles reveal that many of the particles with smaller percent difference than this had velocity differences that were much higher, as high as 21.624 cm/s for vortex WAT1 in Table 6.4a.

Both methods of error analysis allow one to come to the same conclusions. Once the particles most closely associated with instabilities of the vortex and the region within the core are eliminated, it is found that the control particles follow the vortex flow consistently well with variations that can partially be traced to the limiting resolution, but also to the possibility that not all of the errors due to the instability of the vortex environment have been removed. It is clear that the water particles do not respond as consistently. In terms of percent difference and absolute difference between the theoretical and measured velocities, the water droplets varied from the theory more often and with greater magnitude. Although there are examples of agreement between the water droplet tangential velocities and the theoretical values, these occurrences are sporadic, and do not present convincing evidence of following the vortex flow as well as the eccospheres.

The differences in the responses of each of the particles were first seen in the downstream flow analysis of Chapter 5. In this analysis it was found that instantaneous velocity profiles lacked uniformity, and many of the heavier particles were observed to be descending as they traveled downstream. Therefore, a random size distribution of a relatively dense particle cannot follow a unidirectional or a vortex flow as well as particles of a specified size distribution and much lower density.

# Chapter 7: Conclusions

The purpose of this investigation was to determine whether water droplets follow the flow in a vortex as well as well-behaved particles do. The motivation is to provide some insight to the field of detection and measurement of wing-tip wake vortices, that must contend with measuring various types of naturally occuring particles in the airport environment. These include soot, exhaust and other debris, as well as snow, rain, and mist or fog. Given each of these randomly-sized scattering sources, the objective was to recreate the response of water droplets in a small scale vortex experiment. After a brief analytical background was established, the measurement system (LSV) was introduced, along with the modifications necessary to make the vortex measurements. The experimental procedures were outlined, and after the data were taken, the results and analyses were presented and discussed.

It was found that the water droplets produced in the experiments do indeed respond differently than the control particles, called eccospheres, which have a density about one-third of the water particles. This difference was detected despite an unsteady flow that gave rise to a vortex that could not maintain its structure and stability for any length of time. Laser Streak Velocimetry allowed an understanding of the velocity of particles via flow visualization with a two-dimensional field of view. Modifications to the technique allowed for low light detection with spatial resolution on the order of fractions of a millimeter. This resulted in the imaging and measurement of vortex velocity profiles that showed that the control particles followed the flow well. The water droplets did not agree as well with the theoretical expectations.

Because of the small-scale of the wind tunnel, and consequent smaller velocities and wing geometry, it is difficult to make a quantitative comparison to an actual system. However, the implications can be assessed qualitatively. The results suggest that an actual wing-tip vortex detection system should question the velocity data it receives when the vortex measured

has been seeded with water droplets, in the form of rain or mist, or any other flow seeds that have densities greater than or equal to that of water. In the airport environment, an average percent difference on the order of 16% to 17% would not be acceptable, since, in reality, tangential velocities can reach 100 m/s. Velocity measurement for the purposes of hazard warning may be hindered by this uncertainty. The measurements will ultimately depend on what size water droplets are being measured. Below a certain size threshold, all of the water droplets will follow the flow equally well. However, any particles larger than the threshold will be prone to variance from the true airspeed and, if the detection system is a lidar system that relies on scattered radiation, may dominate the return signal.

The results here do motivate the need for future study for both the purposes of confirmation and clarification. It is hoped that this research, the techniques used, and the findings are useful contributions to the field of aeronautics.

# Chapter 8: Recommendations for Future Work

The completion of the analysis of the vortex data marks the end of this investigation. However, before continuing the research in order to confirm the results of this study, one should first keep in mind some limitations that were discovered in this investigation, as well as possible new directions that this research could take. Certain factors arose that complicated the process of evaluating the water droplets in a vortex. Although these complications were overcome, their existence presented delays and unnecessary digressions from the actual investigation.

Future work should consider the value of using a more uniform and consistent downstream flow that generates the vortex. The instabilities of the flow provided an added factor that had to be understood, in addition to the trajectories and velocities of the particles in the vortices. Vortex velocity profiles are very sensitive to fluctuations in the downstream air flow. The video-based LSV system (operating at 60 fields a second) proved to be capable of analyzing the vortices despite these inconveniences. However, if other methods of vortex measurements are used, the problem of vortex instability should be immediately addressed. If the same type of tunnel used in this experiment were to be used again, the flow quality may benefit from a vacuum-based, instead of a blower-based, wind generation system.

The fact that it was discovered that the flow was not perfect revealed another effective use of the video-based LSV system. It should be relatively easy to convert the measurement system that measures downstream flow and vortices to one of flow mapping in general. In these experiments the ISIT camera was focused at one plane. However, one could also acquire excellent data with experiments that scanned and mapped an entire wind tunnel, whether the tunnel is the apparatus used in the present investigations, or one that is larger and more stable. The LSV measurement system makes an excellent flow quality inspection tool. However, the measurements need not be confined to wind tunnels. A similar measurement system has been previously

utilized for measuring flow in an automobile engine [14]. But flow through a volume that can be viewed with a camera could benefit immensely from this velocity measurement technique.

The availability of an automated control particle dispersion device, similar to the atomizer for the water droplets, would have eased some of the experimentation process. This would have allowed a continuous flow of control particles through the wind tunnel and into the test section to be visualized. The water droplet dispersion system could also be improved. It could have been adjustable so that the amount of particles being released into the flow could be controlled. Also, the release of the water droplets was not continuous, it was characterized by an occasional burst of droplets, followed by a relatively constant spray.

All of the experiments used a rectangular wing with an angle of attack of 35 degrees. This consistency allowed for the reduction of variables. It would be interesting to continue the vortex analysis by first varying the angle of attack, and then by using a different wing (e.g. a delta wing), or another object (like a cylinder) that has a unique response to being immersed in one dimensional flow. By varying the angle of attack and measuring the changes, useful information can be extracted, like the effective lift of the wing, to compare the flow and wing geometries to theoretical expectations. If a cylinder is placed in the flow, von Karman vortices can be observed and compared with theory [6], to give a further understanding of the flow, as well as the capabilities of the video-based LSV system.

Preliminary measurements were taken of the downstream wind tunnel flow with the wing. The laser sheet was propagated parallel to the axis of the tunnel, normal to the wing. When the sheet was oriented just off the wing tip, the vortex rollup could be observed two-dimensionally. The angle of rollup decreased as the speed of the air increased. There could be valuable information obtained from establishing experiments to further understand the rollup of the wing-tip vortex, and how it relates to the angle of the wing and the speed of the downstream air.

# References


[1] Barber, M.R. and Tymczyszyn, J.J., "Techniques for Early Demise of Vortices - A Pilot's View.", Proceedings of the Aircraft Wake Vortices Conference, March 15-17, 1977.

[2] Burnham, D. C., "Review of Vortex Sensor Development Since 1970," Proceedings of the Aircraft Wake Vortices Conf., FAA-RD-77-68, June 1977.

[3] Meng, J. C. S. and Thomson, J. A. L., " Simulation and Data Analysis of a Scanning Laser Doppler Velocimeter System for Sensing Aircraft Wake Vortices.", Proceedings of the Aircraft Wake Vortices Conf., FAA-RD-77-68, June 1977.

[4] Back, L. H., "Optical and Physical Requirements for Fluid Particles Marking Trailing Vortices from Aircraft," Journal of Aircraft, Vol. 13, No. 7, July 1976.

[5] Lutchen, K. R., "Strategic Detection of Subsonic Aircraft Wakes: A Theoretical Assessment." Personal Communications, Lexington, MA: MIT Lincoln Laboratory.

[6] Sparks, Jr., G. W. and Ezekiel, S., "Laser Streak Velocimetry for Two-Dimensional Flows in Gases", AIAA Journal, Vol. 15, #1, 1976.

[7] Merzkirch, Wolfgang, Flow Visualization, 2nd ed., New York: Harcourt Brace Jovanovich, 1987.

[8] Bilanin, A. J., and Donaldson, C. duP., "Estimation of Velocities and Roll-up in Aircraft Vortex Wakes", J. Aircraft, Vol12, #7, 1974,

[9] Donaldson, C. duP., Snedeker, R. S., and Sullivan, R.d D., "Calculation of Aircraft Wake Velocity Profiles and Comparison with Experimental Measurements", J. Aircraft, Vol 11, #9, 1974

[10] Brown, Clinton E., "Aerodynamics of Wake Vortices", AIAA Journal, Vol. 11, #4, April 1973.

[11] Bofah, K. K., "Some Remarks on Aircraft Wake Vortex Analysis", Proceedings of the Aircraft Wake Vortices Conference," March 1977.

[12] Schlichting, H., Aerodynamics of the Airplane, New York: McGraw-Hill, Inc., 1979.

[13] Gouesbet, Gerard, and Grehan, Gerard, "Proceedings of an International Symposium on Optical Particle Sizing: Theory and Practice", Plenum Press, 1988

[14] Rimai, Li, Adamczky, Klick, and Marko, "Flow Velocity Field Mapping by Video Recording of Coded Seed Track Images", Proceeding of the 4th International Symposium on Flow Visualization, Paris, 1986.

[15] Freymuth, Finaish, and Bank, "Visualization of Wing Tip Vortices in Accelerating and Steady Flow", J. of Aircraft, Vol. 23, No. 9, 1985.

# Bibliography


Allario, F., *et. al.*, "Laser Remote Sensing Supports Aviation Safety", Laser Focus World, Vol. 28., #4, April, 1992

Bazin, M. F., "Trajectory of a Particle Released in the Wake of an Aircraft", M. S. Thesis, MIT Department of Mechanical Engineering, 1982.

El-Ramly, Rainbird, and Earl, "Wind Tunnel Measurements of Rolling Moment in a Swept-Wing Vortex Wake", J. of Aircraft, Vol. 13, # 12, 1976.

Harrison, J. Michael, Brownian Motion and Stochastic Flow Systems, John Wiley and Sons, New York, 1985.

Horowitz and Hill, The Art of Electronics, 2nd Ed., Cambridge University Press, Cambridge, 1989.

Kuethe, A. M., and Chow, C., Foundations of Aerodynamics, John Wiley & Sons, New York, 1986.

Kuhn, G. D., and Nielsen, J. N., "Analytical Studies of Aircraft Trailing Vortices", Proceedings of the AIAA 10th Aerospace Meeting, 1972.

Kundu, P. K., Fluid Mechanics, Academic Press, Inc., Harcourt Brace Jovanovich, San Diego, 1990.

Neuhauser, Robert G., "Lag Reduction and Lag Characteristics of Television Camera Tube Signals", TP-115 Camera Tubes, Burle Technologies, 1989.

Saffman, P. G., "The Lift on a a Small Sphere in a Shear Flow, J. Fluid Mechanics, Vol. 22, (1965)

Sparks, Jr., G. W., "Laser Streak Velocimeter For Two-Dimensional Flows in Gases", Thesis, Department of Aeronautics and Astronautics, Massachusetts Institute of Technology, 1976.

Stockham, John, D.& Fochtman, Edward, G., Particle Size Analysis, Ann Arbor, MI: Ann Arbor Science, 1979.

Sullivan, J. P., and Ezekiel, S., "A Two-Component Laser Doppler Velocimeter For Periodic Flow Fields.", Journal of Physics, Vol. 7, 1974.

Yang, Wen-Jei, Handbook of Flow Visualization, Hemisphere Publishing Corporation, New York, 1989.

CRC Handbook of Chemistry and Physics, 67th Ed.

RCA ISIT Camera Specifications, Model TC1040/H, 1986.